ISTANBUL TECHNICAL UNIVERSITY ★ GRADUATE SCHOOL OF SCIENCE ENGINEERING AND TECHNOLOGY

THE EFFECT OF POSTWELD HEAT TREATMENT ON THE MECHANICAL PROPERTIES OF TIG WELDED INCONEL 718 ALLOY

M.Sc. THESIS

Ece Canan KOŞMAZ

Department of Materials Science and Engineering

Materials Science and Engineering Programme

AUGUST 2015

ISTANBUL TECHNICAL UNIVERSITY ★ GRADUATE SCHOOL OF SCIENCE ENGINEERING AND TECHNOLOGY

THE EFFECT OF POSTWELD HEAT TREATMENT ON THE MECHANICAL PROPERTIES OF TIG WELDED INCONEL 718 ALLOY

M.Sc. THESIS

Ece Canan KOŞMAZ
(521121007)

Department of Materials Science and Engineering

Materials Science and Engineering Programme

Thesis Advisor: Prof. Dr. Hüseyin ÇİMENOĞLU

AUGUST 2015

İSTANBUL TEKNİK ÜNİVERSİTESİ ★ FEN BİLİMLERİ ENSTİTÜSÜ

KAYNAK SONRASI ISIL İŞLEMİN TIG İLE KAYNAK YAPILMIŞ INCONEL 718 ALAŞIMININ MEKANİK ÖZELLİKLERİNE ETKİSİ

YÜKSEK LİSANS TEZİ

Ece Canan KOŞMAZ
(521121007)

Malzeme Bilimi ve Mühendisliği Anabilim Dalı

Malzeme Bilimi ve Mühendisliği Programı

Tez Danışmanı: Prof. Dr. Hüseyin ÇİMENOĞLU

AĞUSTOS 2015

Ece Canan KOŞMAZ, a M.Sc. student of ITU Graduate School of Science Engineering and Technology student ID 521121007, successfully defended the thesis entitled **"THE EFFECT OF POST WELD HEAT TREATMENT ON THE MECHANICAL PROPERTIES OF TIG WELDED INCONEL 718 ALLOY",** which she prepared after fulfilling the requirements specified in the associated legislations, before the jury whose signatures are below.

Thesis Advisor : **Prof.Dr. Hüseyin ÇİMENOĞLU**
İstanbul Technical University

Jury Members : **Assoc.Prof.Dr. Murat BAYDOĞAN**
İstanbul Technical University

Assoc.Prof.Dr. Erdem ATAR
Gebze Technical University

Date of Submission : 29 July 2015
Date of Defense : 14 August 2015

To the memory of my father,

FOREWORD

I would like to express my deepest gratitude to my advisor Prof. Dr. Hüseyin ÇİMENOĞLU for his guidance, encouragement and support throughout this study. I also want to express my sincere thanks to Research Assistants M.Sc. Faiz MUHAFFEL and M.Sc. Onur TAZEGÜL for their guidance and help during experimental studies.
I would like to declare my deep thanks to Ms. Bilkay GÜLAÇTI and Mrs. Rabia GÜNAY at the Department of Structural Engineering, TEI Tusas Engine Industries Inc., for giving me the opportunity to start this project. Thanks are also to my collegues at Materials and Processes Leadership, especially PhD. Ceylan KUBİLAY ERDEM, M.Sc. Ezgi KOTAN and Techn. Cengiz KOCALAR for their technical support and help for laboratory work in the completion of the thesis.
I would like to thank my family and friends for their continued support throughout doing my master's degree, especially my mother for her moral support, guidance and trust.
Finally, a very special thanks to Mete KARABASTIK for his existence, understanding, patience, encouragement and unconditional love and support.
This thesis is dedicated to the memory of my father, Mustafa Cengiz KOŞMAZ, who always believed in me and motivated me to achieve better in life.

August 2015

Ece Canan KOŞMAZ
(Materials & Processes Engineer)

TABLE OF CONTENTS

Page

ABBREVIATIONS

GTAW	**:** Gas Tungsten Arc Welding
TIG	**:** Tungsten Inert Gas
EBW	**:** Electron Beam Welding
PWHT	**:** Post-weld Heat Treatment
FCC	**:** Face Centered Cubic
BCT	**:** Body Centered Tetragonal
HCP	**:** Hexagonal Closed Packed
BCC	**:** Body Centered Cubic
TCP	**:** Topologically Closed Packed
TTT	**:** Time-Temperature-Transformation
HAZ	**:** Heat Affected Zone
PMZ	**:** Partially Melted Zone
FZ	**:** Fusion Zone
BM	**:** Base Material
IPM	**:** Inch per minute
CFH	**:** Cubic feet per hour
AMS	**:** Aerospace Materials Standard
ISO	**:** International Standards Organization
NDT	**:** Non-destructive Testing
FPI	**:** Fluorescent Penetrant Inspection
SEM	**:** Scanning Electron Microscobe
XRD	**:** X-Ray Diffraction
EDS	**:** Energy Dispersive X-Ray Spectroscopy

LIST OF TABLES

Page

LIST OF FIGURES

Page

THE EFFECT OF POST WELD HEAT TREATMENT ON THE MECHANICAL PROPERTIES OF TIG WELDED INCONEL 718 ALLOY

SUMMARY

Superalloys have been mostly utilized in gas turbine technology with regards to their advantages of high temperature resistance characteristics. Superalloys readily satisfy the requirements including corrosion resistance, high strength at elevated temperatures, good fatigue and creep resistance which are demanded for both aerospace and land based power generation applications.

The components manufactured for those fields mostly require combination of varios conventional and special processes in terms of machining, forming and joining. Tungsten Inert Gas (TIG) welding is one of the common joining processes that is applicable to superalloys.

Superalloys are grouped as iron-nickel, nickel and cobalt based depending on the main alloying elements inside their structure. Each of the superalloys have face-centered cubic (FCC) matrix combined with secondary strengthening phases. Inconel 718 is a member of iron-nickel based superalloys group. Precipitation hardening is the main strengthening mechanism of Inconel 718 which is primarily strengthened by gamma double prime (γ") precipitate. Slow hardening response of gamma double prime (γ") enhance the weldability of Inconel 718 such that producing a relatively low strength and high ductility heat affected zone (HAZ) as this phase cannot form during weld cycles. This also provides adequate time for the alloy to reach desired hardness level and complete stress relief prior to hardening via precipitation of gamma double prime (γ"). However, segregation of microalloying elements particularly niobium (Nb) and formation of brittle Nb-rich Laves $(Ni,Fe,Cr)_2(Nb,Mo,Ti)$ phase is still an issue due to nonequilibrium solidification conditions during welding. Laves phase is known to be detrimental to mechanical properties. Thus, post weld heat treatments (PWHTs) are recommended for dissolving Laves phase in order to have homogenized structures and regain material properties.

The aim of this study was to evaluate the influence of the type of PWHT (direct aging or solutionizing and aging) on the microstructure and mechanical properties of TIG welded Inconel 718 sheets. In this study, Inconel 718 sheets were utilized with two different thicknesses: 2 and 3,2 mm. Material was supplied in solution treated condition (between 950-990°C) per the AMS 5596 specification. Each group of specimens were welded by TIG method. Automatic welding equipment preferred for repeatitive weld joint quality. Square butt weld joint design and single V-groove butt weld joint design employed for 2 and 3.2 mm thick specimens, respectively. Constant welding paramaters applied to each group depending on the workpiece thickness. Weld joints were controlled with non-destructive test (NDT) methods including FPI and X-Ray. No remarkable welding defects have been identified by NDT methods.

In order to enlighten the effect of PWHT, the welded specimens subjected to different heat treatment programs. One group was subjected to solution heat treatment at 980°C ±10° for 1 hour and subsequent aging heat treatment at 720°C±10°C for 8 hours and 620 °C±10 °C for 8,5 hours in an inert atmosphere industrial vacuum furnaces. Second group was subjected to direct aging heat treatment at 720°C±10°C for 8 hours and 620 °C±10 °C for 8,5 hours in an inert atmosphere industrial vacuum furnaces. The last group is stayed as welded to represent the weld tensile properties without heat treatment and check the influence of selected heat treatment cycles. It is to be noted that those heat treatment cycles also performed to original Inconel 718 specimens together with welded specimens in order to compare the properties of base material with its welded state.

Initially, base material microstructure of Inconel 718 were examined for following conditions: as-received with no PWHT, solution (980°C) treated+aged and direct aged under optical microscope and scanning electron microscope (SEM). The grain size measurements revealed that these post-weld heat treatments did not much change the grains and 2 mm thick specimens have finer grains in all conditions. It was also observed that secondary particles were present in the austenite matrix in solution condition and could not be dissolved after subsequent heat treatments. These particles were thought to be MC type carbides. In addition, The post-weld solution heat treatment at 980°C resulted in needle-like secondary particles precipitation which is suggested to be delta (δ) in the literature. Vickers microhardness test were conducted on three groups of specimen and concluded that both post-weld heat treatments increase the hardness in same magnitude. This hardness increase is attributed to gamma prime (γ') and gamma double (γ") precipitation during aging heat treatment. However, these precipitates could not be detected during XRD analysis due to their lower volume fraction.

After base material characterization, structural features of weld regions were characterized with macro and micro examinations. Weld cross sections of 2mm and 3,2 mm thick specimens in all conditions showed that weald bead size developed by amount of heat input. Heat input per unit length for 2 mm thick specimens is calculated 192 J/mm and for 3.2 mm thick specimens is calculated 419 J/mm. Thus, 3,2 mm thick specimen is all conditions represent more elongated weld pool shape.

Microstructure of weld transverse section consist of dendritic fusion zone, HAZ and unaffected base material. The weld microstructure examined through the fusion zone, fusion boundary and HAZ regions. HAZ includes two subzones namely coarse grained HAZ and partially melted zone (PMZ). The dendrites in the weld fusion zone was appeared to be equiaxed while columnar dendrites were seen close to the fusion boundary. For further microstructural examination, SEM was utilized. Irregular shaped secondary particles were detected in interdendritic regions. It is suggested to be Laves phase in litetarure which further confirmed with spot EDS analysis. Laves phase was distinguished with its higher niobium concentration. However, these secondary particles could not be detected during XRD analysis due to their lower volume fraction. Laves phase formation is beacause of segragation of niobium during weld solidification. Once this phase is formed in weld metals, post weld heat treatment is critical to dissolve this undesired phase and homogenize the structure with uniform niobium distribution. According to SEM images, Laves phase was readily formed in fusion zone of the as welded and direct aged specimens. However, solution heat treatment at 980°C±10°C resulted in partially dissolution of Laves phase and subsequently formation of needle-like delta phase (δ) around nearly

dissolved Laves phase. Solution heat treatment at 980°C did not achieve the free of Laves phase microstructure.
The effect of PWHT on the mechanical properties of welded specimens were investigated by conducting microhardness and room temperature tensile testing. Fracture surfaces of samples failed from fusion zone further examined via stereomicroscope and SEM. Below conclusions were made accordingly;

- Post weld heat treatments nearly double the hardness levels of all three zones: fusion zone, HAZ and base material. The hardness levels are identical in HAZ and base material while fusion zone is approximately 5% softer.
- Comparable hardness results in fusion zone, HAZ and base material in as-welded condition could reflect that precipitation of gamma double prime (γ") and gamma prime (γ') did not occur during weld metal cooling.
- Tensile testing was performed to original samples and welded samples. It is obtained that both post-weld heat treatments increased the yield strength up to 150%, ultimate tensile strength up to 60% wheras decreased the ductility down to 140%.
- The yield strength and ductility of solution+aged and direct aged welded samples are almost in the same range. The differences between yield strength and ductility are found to be lower than 5%. However, almost identical tensile strength values were obtained from the solution+aged and direct aged specimens.
- When the mechanical properties of welded samples and original samples in 2 mm thick samples are compared, It was concluded that the difference of yield strength, tensile strength and ductility in same heat treatment conditions are negligible. Deformation was started from any region away from fusion zone so that almost identical yield points were obtained with original samples and welded samples.
- When the mechanical properties of welded samples and original samples in 3,2 mm thick samples are compared, It was concluded that the difference of yield strength and ductility in same heat treatment conditions is more than 10%, while tensile strength is lower than 5%. Deformation was started from fusion zone where hardness is lower than the base material. This is consistent with inferior tensile properties (10% reduction in yield point) compared to base material.
- Two samples as-welded (2 mm thick sheet) and solution+aged (3,2 mm thick sheet) conditions fractured from fusion zone. Fracture zones were further examined and found that microvoids were initiated at the Laves/matrix interface.

KAYNAK SONRASI ISIL İŞLEMİN TIG İLE KAYNAK YAPILMIŞ INCONEL 718 ALAŞIMININ MEKANİK ÖZELLİKLERİNE ETKİSİ

ÖZET

Uçak ve uzay endüstrisinde yaygın olarak kullanılan gaz türbinli motorlarda uygulanabilir malzemelerden olan süperalaşımlar, yüksek çalışma sıcaklıklarında yüksek performans gereklilikleri üstün korozyon direnci, yüksek mukavemet değerleri, sahip oldukları yorulma ve sürünme direnci karakteristikleri ile karşılamaktadır.

Havacılık alanında kullanılan parçaların, işleme, form verme ve birleştirme gibi imalat operasyon aşamalarında konvensiyonel metodlar yanı sıra birok özel proseste kullanılmaktadır. Tungsten inert gaz (TIG) kaynağı, süperalaşım malzemelerin imalatında tercih edilen özel proseslerdendir.

Süperalaşımlar, yapısında bulundukları temel alaşım elementlerine bağlı olarak demir-nikel, nikel ve kobalt esaslı olarak sınıflandırılır. Tüm süperalaşım sınıfları yüzey merkezli kübik (YMK) matris içerisinde mukavemet artırıcı ikincil fazları içerir. Demir-nikel bazlı süperalaşımlar grubuna dahil olan Inconel 718, çökelti sertleştirmesi ile mukavemet özellikleri geliştirilen bir alaşımdır. Üstün mekanik özellikleri, uygun ısıl işlem koşullarında yapısında büyük oranda gamma iki üssü (γ'') çökelmesi ile açıklanır. Bunun yanı sıra bu fazın varlığında yavaş yürüyen sertleştirme mekanizması Inconel 718 alaşımınının kolay kaynaklabilirliğini sağlamaktadır. Kaynak işlemi süresince ısıdan etkilenen bölgede (ITAB), bu fazın çökelememesi ile düşük mukavemet ve yüksek süneklik değerleri gözlenir. Yavaş yürüyen sertleştirme mekanizması sayesinde, alaşımın gerilim giderme ve istenen sertlik değerlerine ulaşması sağlanır. Ancak kaynak sırasında söz konusu dengesiz katılaşma sebebiyle özellikle niobyum gibi yüksek konsantrasyonlu refrakter elementlerin dendritler arası bölgelere segregasyonu sonucu yapıda istenmeyen kırılgan Laves $(Ni,Fe,Cr)_2(Nb,Mo,Ti)$ fazı oluşumu gözlenmektedir. Bu fazın sahip olduğu morfoloji nedeniyle malzemelerin mekanik özelliklerine negatif etkisi bilinmektedir. Bu fazın oluşmasının önüne geçilemediği durumlarda, yapının tekrar homojen hale getirilmesi ve mekanik özelliklerin geri kazanılması için kaynak sonrası ısıl işlem yapılması tavsiye edilmektedir.

Bu çalışmanın amacı, kaynak sonrası uygulanan ısıl işlem tipinin (doğrudan yaşlandırma ya da çözeltiye alma ve yaşlandırma) TIG ile kaynak yapılmış Inconel 718 alaşımının mikroyapısında, ve buna bağlı olarak mekanik özelliklerinde yol açtığı etkileri değerlendirmektir. Bu çalışma kapsamında, 2mm ve 3,2 mm olarak iki farklı kalınlıkta seçilen AMS 5596 standardında çözeltiye alma ısıl işlemi uygulanmış (950-990 °C) Inconel 718 saclar belirli uzunluklarda temin edilmiştir. Kaynak işlemleri, kaynağın tekrarlanabilir kalitede olması için Jetline otomatik kaynak tezgahında gerçekleştirilmiştir. 3,2 mm kalınlığındaki numunelere kaynak ağzı açılırken, 2 mm kalınlığındaki numunelere kaynak ağzı açılmadan alın alına ve tüm kaynaklar hadde yönüne dik olacak şekilde yapılmıştır. Ana malzeme kalınlığına bağlı olarak, kaynak parametreleri sabit tutulmuştur. Kaynak sonrası tüm numuneler penetrant ve radyografik muayene metodları uygulanarak kaynak dikişindeki

indikasyonlara karşı kontrol edilmiştir. Penetrant ve radyografik muayenelerde herhangi bir indikasyona rastlanmamıştır. Kaynak sonrası ısıl işlemin etkilerini gözlemlemek için, kaynaklı numuneler vakum fırınlarında inert atmosfer altında farklı ısıl işlem programlarına tabi tutulmuştur. İçerisinde iki farklı kalınlıktaki numuneleri barındıran bir gruba 980°C ±10°C sıcaklığında 1 saat süreyle çözeltiye alma, ardından 720°C±10°C sıcaklıkta 8 saat ve 620 °C±10 °C sıcaklıkta 8,5 saat kalacak şekilde iki kademeli yaşlandırma ısıl işlemi uygulanmıştır. İkinci grup numuneler 720°C±10°C sıcaklıkta 8 saat ve 620 °C±10 °C sıcaklıkta 8,5 saat kalacak şekilde doğrudan yaşlandırma ısıl işlemine tabi tutulmuştur. Kaynak mekanik özelliklerinin tespit edileceği ve ısıl işlemin etkilerinin karşılaştırmalı olarak kontrol edileceği referans grup olarak tanımlanabilecek son grupta ise kaynak sonrası herhangi bir ısıl işlem yapılmamıştır. Kaynak metali özelliklerinin orijinal Inconel 718 ile karşılaştırılabilmesi için, kaynaklı numunelerin yanında orijinal Inconel 718 numunelerde aynı ısıl işlem programlarına tabi tutulmuştur.

İlk olarak uygulanan bu ısıl işlemlerin ana malzeme özelliklerine etkisinin incelenmesi için optik mikroskop ve taramalı elektron mikroskobu çalışmaları yapılmıştır. Mikroyapı incelemeleri sırasında gerçekleştirilen tane boyutu ölçümü sonucunda, çözeltiye alma (980°C) & yaşlandırma ve doğrudan yaşlandırma ısıl işlemlerin tane boyutu üzerinde belirgin bir etkisinin olmadığı ve 2 mm kalınlıktaki sacların tüm koşullarda daha ince tane yapısına sahip olduğu belirlenmiştir. Çözeltiye alınmış durumdaki Inconel 718 mikroyapısında östenitik matris içerisinde ikincil partiküllerin varlığı belirlenmiştir ve bahsi geçen ısıl işlemler ile bu partiküllerin yapıda çözülemediği tespit edilmiştir. Literatürde bu ikincil partiküllerin MC tipi karbürler olduğu belirtilmektedir. Bunun yanı sıra, 980°C ‘de uygulanan çözeltiye alma ısıl işleminin iğnemsi formda ikincil bir fazın çökelmesine neden olduğu tespit edilmiştir. Literatürde bu yapı delta (δ) fazı olarak geçmektedir.

Mikroyapı incelemeleri sonrasında, çözeltiye alınmış, çözeltiye alma ve yaşlandırma ısıl işlemi uygulanmış ve doğrudan yaşlandırma ısıl işlemi uygulanmış numunelere Vickers mikrosertlik testi yapılmıştır. Bu testlerin sonucunda, çözeltiye alma&yaşlandırma ve doğrudan yaşlandırma ısıl işlemlerin ana malzeme sertliğini aynı oranda arttırdığı belirlenmiştir. Inconel 718 sertlik artışı literatüde gamma üssü (γ’) ve gamma iki üssü (γ”) fazlarının yaşlandırma ısıl işlemi sırasında çökelmesi ile açıklanmaktadır. Ancak yapılan XRD çalışmalarında bu çökelti fazlara rastlanmamıştır. Bunun nedeni olarak bu fazların yapıda hacimsel olarak az miktarda bulunmaları düşünülmektedir.

Ana malzemenin karakterizasyonu sonrasında kaynak bölgesi makro ve mikro incelemeleri gerçekleştirilmiştir. 2 mm ve 3,2 mm kalınlığındaki sacların kaynak kesitlerinden alınan makroyapı görüntüleri ile kaynak genişliğinin, kaynak sırasında uygulanan ısı girdisiyle ilişkili olduğu düşünülmüştür. 2 mm kalınlığındaki saclarda uygulanan kaynak parametreleri sonucu hesaplanan ısı girdisi : 192 J/mm iken 3,2 mm kalınlığındaki saclarda bu değer 419 J/mm olarak belirlenmiştir. Bu nedenle, 3,2 mm kalınlığındaki numuneler tüm ısıl işlem koşullarında daha geniş kaynak havuzuna sahiptir.

Kaynak bölgesi kesiti mikroyapısı incelendiğinde, dendritik formda ergime bölgesi, ısı tesiri altında kalan bölge (ITAB) ve ısıdan etkilenmeyen ana malzeme bölgeleri gözlemlenmiştir. Ergime bölgesi, ergime sınırı ve ITAB ayrıca incelemeye tabi tutulmuştur. ITAB, kaba taneli ITAB ve kısmi ergime bölgesi olarak iki alt bölgeye ayrılmaktadır. Ergime bölgesindeki dendritler eş eksenli yapıda iken ergime sınırına doğru eş eksenliden sütunsal dendritik formda oldukları görülmüştür. Detaylı mikroyapı incelemeleri için taramalı elektron mikroskobu kullanılmıştır. Bu

çalışmalarda ergime bölgesinde, düzensiz şekilli ikincil partiküllern varlığı tepit edilmiştir. Literatür incelemeleri bu partiküllerin niobyumca zengin Laves fazı olabileceğinden bahsetmektedir. Partikülere yapılan enerji dağılımlı X-ışınları (EDS) analizlerinde 25%'ler seviyesindeki niobyum miktarı literatür ile uyumlu olduğundan Laves fazı olduğu ihtimalini güçlendirmişir. Ancak X-ışınları difraksiyon (XRD) analizlerinde bu fazlar hacimsel oranlarının düşük olması sebebiyle gözlemlenememiştir.

Kaynak katılaşma esnasında segregasyon sonucu oluşan Laves fazının giderilmesi ve yapının tekrar kimyasal homojenliğini sağlaması için kaynak sonrası ısıl işlem yapılması önem teşkil etmektedir. Taramalı elektron mikroskobu (SEM) ve enerji dağılımlı X-ışınları (EDS) çalışmaları ile, Laves fazının kaynak edilmiş ve kaynak sonrası doğrudan yaşlandırma ısıl işlemine tabi tutulmuş numunelerin kaynak dikişinde var olduğu belirlenmiştir. Ancak, 980°C±10°C sıcaklığında 1 saat süreyle yapılan çözeltiye alma ısıl işlemi Laves fazının kısmen çözülmesine ve bu yapının etrafında delta fazının (δ) çökelmesini sağlamıştır. Çözeltiye alma sıcaklığı olarak seçilen 980°C±10° Laves fazının tamamen çözünmesini sağlayamamıştır.

Kaynak sonrası ısıl işlemin, kaynaklı numunelerin mekanik özelliklerine etkisi için mikosertlik ve oda sıcaklığı çekme testleri yapılmıştır. Çekme testleri sonrasında kaynak dikişinden kopan numuneler steromikroskop ve taramalı elektron mikroskobu (SEM) ile detaylı incelemeye tabi tutulmuştur. Bu çalışmada elde edilen bulgular şu şekildedir :

- Kaynak sonrası ısıl işlemler, ergime bölgesi, ITAB ve ana malzeme sertlik değerlerini yaklaşık iki katı kadar arttırmıştır. ITAB ve ana malzeme benzer sertlik değerlerine sahip iken ergime bölgesi yaklaşık 5% daha yumuşaktır.
- Çözeltiye alınmış halde ölçülen sertlik değerleri sonucunda ergime bölgesi, ITAB ve ana malzemede benzer sonuçlar tespit edilmiştir. Bu sonuçlara göre kaynak metali soğuma sırasında herhangi bir mukavemet artırıcı çökeltinin gamma üssü ve gamma iki üssü (γ' ve γ") oluşmadığı düşünülmektedir.
- Orijinal Inconel 718 numunelere ve kaynaklı numunelere çekme testi yapılmıştır. Çekme testleri sonucunda kaynak sonrası yapılan her iki ısıl işlemin akma mukavemetini 150%, çekme mukavemetini 60% arttırdığı bununla birlikte sünekliği 140% oranında düşürdüğü tespit edilmiştir.
- Çözeltiye alma & yaşlandırma ve doğrudan yaşlandırma ısıl işlemlerinin kaynaklı numunelerin akma mukavemetine ve sünekliğe etkisi aynı mertebelerdedir. Isıl işlemsiz numuneler ile kıyaslandığında farkın 5% den daha az olduğu görülmüştür. Ancak, çekme mukavemetleri karşılaştırıldğında neredeyse aynı sonuçlar görülmüştür ve ısıl işlemin belirgin bir etkisi tespit edilememiştir.
- 2 mm kalınlığındaki saclardan elde edilen kaynaklı numunelerin çekme test sonuçları orijinal numuneler ile kıyaslandığında, aynı ısıl işlem koşullarındaki akma mukavemeti, çekme mukavemeti ve süneklik özellikleri arasındaki farkın göz ardı edilebilir olduğu belirlenmiştir. Çekme testi sonrası yapılan mikroyapı incelemelerinde deformasyonun kaynak dikişinden başlamadığı, ITAB ya da ana malzemeden başlamış olabileceği bu nedenle orijinal numuneler ile kaynaklı numunelerin benzer akma noktalarına sahip olacağı düşünülmektedir.
- 3,2 mm kalınlığındaki saclardan elde edilen kaynaklı numunelerin çekme test sonuçları orijinal numuneler ile kıyaslandığında, aynı ısıl işlem koşulunda akma mukavametinin ve süneklik değerleri arasındaki farkın 10% dan fazla olduğu bununla birlikte çekme mukavemeti arasındaki farkın

5%'den düşük olduğu tespit edilmiştir. Çekme testi sonrası yapılan mikroyapı incelemelerinde deformasyonun ana malzemeden daha yumuşak olan kaynak dikişinden başladığı, ana malzeme ile kıyaslandığında kaynaklı numunelerde görülen akma noktasındaki 10% 'luk düşüşün bununla ilişkili olacağı düşünülmektedir.

- Çekme testi sonrası 2 mm kalınlığındaki ısıl işlemsiz gruptan bir tane ve 3,2 mm kalınlığındaki çözeltiye alma & yaşlandırma ısıl işlemine tabi tutulmuş gruptan bir tane numunenin kaynak dikişinden koptuğu tespit edilmiştir. Kırılma yüzeyleri incelemeleri sonrasında Laves/matrix arayüzeyinde mikroboşlukların oluştuğu gözlemlenmiştir.

1. INTRODUCTION

Superalloys are mainly used in fields such as aerospace and nuclear industries for components of power generating turbines and aeroengines in where required mechanical properties shall be satisfied and maintained during high operating temperatures.

In those engines, higher operating temperatures are also associated with efficieny increase, which in turn provides energy efficiency considering economical and environmental issues [1].

Superalloys have been introduced in the mid 20^{th} century, since that time high demand for superalloys and in particular, the precipitation hardening Ni-based superalloys are increasing due to their superior properties such as corrosion resistance, creep resistance and high strength at elevated temperatures [2].

They can be used efficiently up to temperatures 0.9 T_M (melting point). The elevated temperature mechanical properties of these alloys are unique and cannot be challenged by any other alloy system. This is also the major reason why they are preferred as the cost is not in their favor, at least not when compared to steel in terms of high temperature mechanical properties [3].

The main elements of superalloys are group VIIIB elements (Fe, Ni, and Co). Based on this fact, three major types as iron-nickel based, nickel based and cobalt based are present. Secondary elements in their alloy sytem can also be listed as W, Zr, B, Mo, Ta, Nb, Re, Ti, Al, C, Hf, and Cr. The material properties of super alloys particulary depend upon the quantity of those secondary elements [4].

Inconel alloys introduced in nickel-based superalloys group which are extra-alloyed with Al, Ti, Nb, Co, Cu and W to enhance mechanical and corrosion resistance for severe environments. Fe can be ranged in amounts 1–20%, as well [5].

Several alloys with different compositions and characteristics have been developed up to now. One of the most well-known is Inconel 718 (IN718) whose trademark rights belongs to the Special Metals Corporation, New Hartford, NY.

Inconel 718 is a precipitation hardenable alloy consisting of considerable amounts of Fe, Nb, and Mo. Al and Ti are also present in relatively less content. It contains both gamma double prime (γ") in the form of Ni_3Nb and gamma prime (γ') in the form of Ni_3(Al,Ti,Nb) phases, however strengthened primarily by gamma double prime (γ").

Inconel 718 shows good corrosion resistance, creep resistance and high mechanical properties up to 650°C as well as outstanding weldability. They are mostly selected for elevated temperature critical applications in space and aero engines [5].

Structural components in aero engines can be manufactured by either forging, casting or fabrication methods [6]. Designs are moving forward to the fabrication of substructures and welding them together to avoid cost and transportation of large cast structures. Thus, components genarally requires to combine different fabrication methods like machining, forming and joining. Most common joining methods for aerospace assemblies are fusion welding processes such as Tungsten Inert Gas Welding (TIG) and Electron Beam Welding (EBW) [7].

Inconel 718 has been reputed to show good weldability and good resistance to weld solidification cracking whereas sensitive to heat input due to wide range of elements and precipitated phases under heating conditions resulting with segregation of B/Nb and formation of brittle intermetallic Laves phase $(Ni, Cr, Fe)_2(Nb, Mo, Ti)$ [8,9].

Welding process generates residual stresses and changes the microstructure of the material, which in turn adversely effect the mechanical properties of the component. Thus, a post weld heat treatment is recommended to restore the microstructure and reduce the residual stresses [6].

Precipitation-hardened nickel alloys are recommended to weld in the solution treated state and undergone post weld solution and aging heat treatments for precipitation hardening [9].

It is imperative that microsructural and mechanical effects of welding considered in component design. Therefore, welding and subsequent heat treatment trials are required to perform and resulting mechanical properties associated with different microstructures monitored.

The objective of this thesis is to characterize the weld joint by means of microstructure, phases and microhardness and understand the effects of post weld

heat treatment by conducting solution+aging and direct aging heat treatment cycles on tensile properties of TIG welded Inconel 718 specimens.

The difference in material properties between base material and welded part is determined for reliable design input.

2. SUPERALLOYS

2.1 General Characteristics of Superalloys

Superalloys consist of group VIIIB elements (Fe, Ni, and Co) of periodic table and also include secondary alloying elements such as W, Zr, B, Mo, Ta, Nb, Re, Ti, Al, C, Hf, and Cr [4]. Superalloys cover nickel, iron-nickel and cobalt base alloys, which can operate at above temperatures of 540°C (1000°F) until below their melting points given at approximately 1204 °C to 1371 °C (2200°F to 2500°F) [4,10].

Super alloys show high strength at elevated temperatures; resistance to aggressive environments including nitridation, carbonization, oxidation and sulfadation; outstanding creep resistance, stress-rupture strength, toughness and metallurgical stability; favorable thermal expansion behavior; and resistance to thermal corrosion and fatigue [10].

The iron-nickel base superalloys have come after stainless steel technology and wrought in general. On the other hand, cobalt base and nickel base super alloys can be cast or wrought based on chemical composition and the application [4].

Generally, the usage of wrought nickel and iron-nickel base alloys has limitations at temperetures about 816 °C (1500°F). Thus, cast alloys generally preferred above those temperatures. The majority of superalloys are strengthened by initiation of secondary phases (precipitates), and the operating temperature restriction for alloys depends on basis alloying element, the volume/type ratio of precipitate and the form either cast of wrought [4].

The common ranges of major alloying elements in superalloys are summarized in Table 2.1.

The strength properties of superalloys are not just depend on chemistry of the alloy, but also melting techniques, forging or working processes and casting procedures. Besides, subsequent heat treatment after forming, forging or casting considerably

affects the final properties [4]. Superalloys generally treated such a way that particulary desired property optimized. Cast and wrought products may be subjected to different heat treatments regardless of having same chemical composition. The processes may also vary to improve one property over others for superalloys in the same product form [4].

Table 2.1 : Common ranges of major alloying elements in superalloys [3].

	Range (%)	
Element	**Fe-Ni and Ni Base**	**Co Base**
Cr	5-25	19-30
Mo, W	0-12	0-11
Al	0-6	0-4,5
Ti	0-6	0-4
Co	0-20	Balance
Ni	Balance	0-22
Nb	0-5	0-4
Ta	0-12	0-9
Re	0-6	0-2

Iron, nickel and cobalt are face centered cubic (FCC) austenite in crystal structure as long as they are the major elements of superalloys [4]. In superalloys based on iron and cobalt, the FCC stabilized forms of these elements due to generally by addition of alloying elements, in particular nickel to gain the best properties. It is to be noted that room temperature structures of iron and cobalt are not FCC [4].

Superalloys were first introduced to use in aircraft piston engine turbosuperchargers and their development along the last 60 years has been accelerated by the demand of improving gas turbine engine technology [10]. Superalloys in particular nickel based alloys have been implemented to turbines for both aerospace applications and land-based power generation that operates under relatively high temperatures and require high corrosion, creep and fatigue resistance [10].

Today, both military and civil aircraft gas turbines support the advance of superalloys. In accordance with that, 75% of all group of superalloys are applying to aviation gas turbines as seen in Figure 2.1, remaining 25% is shared with power-genaration gas turbines, chemical industry, medical applications, petrochemical equipment, space ships, rocket engines, nuclear reactors, submarines, high temperature industrial furnaces [11].

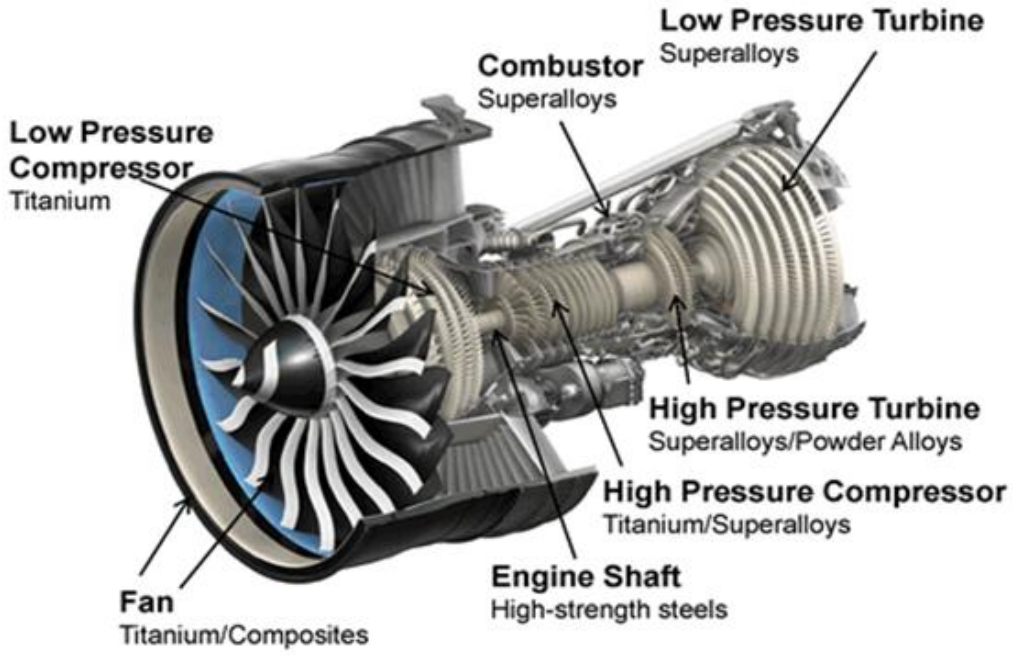

Figure 2.1 : Applications of superalloys for the modules of aircraft engine [12].

The high-temperature strength of all superalloys is associated with the basis of a stable face centered cubic (FCC) matrix combined with either precipitation strengthening and/or solute-solution hardening. Superalloys generally exhibit austenitic (γ-phase) matrix and have different type of secondary phases. The most common secondary phases are metal carbides (MC, $M_{23}C_6$, M_6C and M_7C_3) and the ordered FCC strengthening phase gamma prime (γ ′) in the form of $Ni_3(Al,Ti)$ that is available in iron-nickel and nickel-base superalloys. The primary strengthening phase is gamma double prime (γ") that is a body centered tetragonal (BCT) phase for the alloys having niobium or niobium and tantalum. Cobalt base superalloys can form some precipitation strengthening phases from carbides, but none of intermetallic-phase strengthening equal to the gamme prime (γ') strengthening in nickel-base alloys has been found in cobalt-base superalloys [10]. The function of alloying elements are given in below Table 2.2.

Other phases, mostly undesirable, may be initiated because of composition variations, processing, or subjected to high temperatures. Those undesirable phases can be listed as orthrombic delta (δ) phase in the form of (Ni_3Nb), σ-phase, Laves and the hexagonal close packed (HCP) η-phase (Ni_3Ti). Furthermore, nitrides can be available in strcutures as well as borides in some alloys [10]. The physical metallurgy of those alloys is not as simpler as other alloy systems.

Table 2.2 : Function of alloying elements in superalloys [13].

Effect	Iron Base	Cobalt Base	Nickel Base
Solid solution strengtheners	Cr, Mo	Nb, Cr, Mo, Ni, W, Ta	Co, Cr, Fe, Mo, W, Ta, Re
FCC matrix stabilizer	C, W, Ni	Ni	-
Carbide form			
MC	Ti	Ti	W, Ta, Ti, Mo, Nb, Hf
M_7C_3	-	Cr	Cr
$M_{23}C_6$	Cr	Cr	Cr, Mo, W
M_6C	Mo	Mo, W	Mo, W, Nb
Carbonitrides: M(CN)	C, N	C, N	C, N
Promotes general precipitation of carbides	P	-	-
Forms γ' Ni_3(Al,Ti)	Al, Ni, Ti	-	Al, Ti
Retards formation of hexagonal η(Ni_3Ti)	Al, Zr	-	-
Raises solvus temperature of γ'	-	-	Co
Hardening precipitates and/or intermetallics	Al, Ti, Nb	Al, Mo, Ti, W, Ta	Al, Ti, Nb
Oxidation resistance	Cr	Al, Cr	Al, Cr, Y, La, Ce
Improve hot corrosion resistance	La, Y	La, Y, Th	La, Th
Sulfidation resistance	Cr	Cr	Cr, Co, Si
Improves creep properties	B		B, Ta
Increases rupture strength	B	B, Zr	B
Grain boundary refiners	-	-	B, C, Zr, Hf
Facilitates working	-	(Ni3Ti)	-
Retard γ' coarsening	-	-	Re

2.2 Groups of Superalloys

Superalloys are grouped based on the major alloying elements in their structure with the three base metals such as iron, nickel and cobalt. Each group of superalloy exhibit the common microstructure that is a FCC matrix with a number of dispersed secondary strengthening phases. Nickel is the only base metal of superalloys having FCC structure in elemental form at room temperature. Cobalt is hexagonally closed packed (HCP) at room temperature but exhibits a transformation to FCC at 417 °C (783°F). In elemental form, iron has a body centered cubic (BCC) structure at room temperature but exhibits a transformation to FCC austenite at 912 °C (1647°F). In

both iron and cobalt base superalloys, addition of nickel maintain the FCC crystal structure during relatively high operating temperatures [14].

Superalloys include number of elements with in combination to achieve required properties. Some elements introduce into solid solution to gain following properties: strength by molybdenum, tantalum, tungsten and rhenium, oxidation resitance by chromium and aluminium, hot corrosion resistance by titanium, phase stability by nickel and increased volume fraction of favorable secondary precipitates by cobalt. Other elements are added to form hardening precipitates such as gamma prime γ' (by aluminium and titanium) and gamma double prime γ'' (by niobium) [4].

Early iron-nickel base superalloys, such as 16-25-6 alloy consisting of 16% Cr, 25 %Ni, 6% Mo and the first Nimonic and Inconel series of nickel base superalloys were solid solution strengthened [4].

2.2.1 Iron-nickel based alloys

Iron-nickel based superalloys are the initially raised superalloy group and adapted from austenitic stainless steels. These alloys consist of 25-60 % nickel and 15-60 % iron. The first alloys were developed wih addition of titanium to high chromium content austenitic stainless steels to achieve age hardening capability. There are examples such as German Tinidur and very known American A-286 alloy. These alloys include considerably high amount of iron with less amount of precipitates. They required a minimum of 25 % nickel to maintain FCC austenitic matrix. These alloys are cost-effective and exhibits improved forgeability due to their high amount of iron content. However, oxidation and corrosion resistance is moderate accordingly [11]. Iron-based superalloys have identical solid solution strengthening mechanism with nickel-based alloys. Mo and Cr are used to achieve solid solution hardening. It is to be noted that W may also substitute for Mo regardless of cost and density disadvantage. As well as hardening, Cr provides oxidation and sulfidation resistance during operating temperatures. Carbon, boron and nitrogen element with small atomic radius also supports solid solution hardening with interstitial placement in FCC lattice.

Ti is added to the matrix to form coherent gamma prime (γ') precipitation hardener phase like Ni-based superalloys.

Al addition is limited comparing with nickel-based alloys because of the nature of

iron which results with the formation of metastable structure of gamma prime (γ') and subsequently transforms to not desirable or detrimental stable phases under working conditions.

Thus, main function of Al in iron-nickel based alloys is deoxidizing agency. The lattice parameters of FCC matrix increase with increasing amount of iron. To replace Al with Ti generates the same effect on gamma prime (γ') phase. Based on this fact, high amount of Ti makes reduction in γ/γ'lattice misfit. Ni provides to stabilize FCC austenite matrix and to form gamma prime γ' (Ni_3Ti-Al). This group also form gamma double prime γ" (Ni_3Nb) precipitates. This phase exhibits BCT structure that improves the mechanical properties. However, the effective temperature of gamma double prime γ"is low, just nearly 650°C, which in turn limits the service temperure of iron-nickel based superalloys. They exhibit high strength at intermediate-temperature regime [11].

Grain boundary carbides such as $Cr_{23}C_6$ improve grain boundary strength. However, undesired MC carbides of thick continuos morphology form on grain boundaries and introduce brittle nature in alloys like A-286 and Incoloy 901.

Iron nickel based superalloys generally categorized into four subgroups as following gamma prime strengthened alloys γ' (identical to Nickel-based superalloys), primarily gamma double prime γ" strengthened alloys, solid solution alloys and low-expansion alloys.

γ' strengthened alloys: This group of iron-nickel based alloys has been modified from austenitic stainless steel with Ti addition. Thus, formerly raised alloys exhibit iron-rich matrix while later alloys include more nickel than iron. The popular examples of iron-rich alloys are A-286, Tinidur, Discaloy and V-57. Those mentioned alloys contain less solid solution and lower volume fractions of precipitate strengtheners than nickel-rich alloys. They can be used up to 650°C. Nickel rich iron-nickel base superalloys can perform under relatively high temperature and stress levels compared to iron-rich alloys. The well-known examples of this subgroup are alloy 901 and Inconel X-750.

γ" strengthened alloys: This group of materials mainly preferred in gas turbine industry. Inconel 718 is the most reputable alloy from this group, which was found in the 1950s and having considerably high production rate.

Member of nickel-rich group and form both gamma prime γ' and gamma double γ" precipitates. This alloy is widely used for components of gas turbines operate under high stresss and moderate temperatures such as rear stages of compressor blades and vanes, shafts, supports, cases and etc.

Solid Solution alloys: This group has lower strength but good oxidation resistance associated with very little or no precipitates. The examples of this solid solution strengthend iron riched alloys can be listed as 19-9 DL, Alloy N-155 (Multimet). They usually preferred for applications requiring low strength in highly oxidizing environments such as combustion chambers and flame holders in gas turbines.

Low expansion iron-nickel based alloys: Low expansion characteristic is due to absence of ferrite stabilizers like Cr and Mo. Since Cr is not available in the structure, this group of materials can easily be oxidized above 550°C. Regardless of poor oxidation resistance, low expansion iron-nickel based alloys such as Incoloy 903 and Pyromet CTX-1 preferred in components of gas turbines where tight clearance control is higly requested between rotating and static parts. These iron rich alloys includes Co and form gamma prime γ'and sometimes η (Ni_3Ti) precipitates resulting high strength characteristic up to 650°C [11].

2.2.2 Nickel based alloys

Nickel base superalloys have significant role among all superalloys in terms of their strength and temperature capability [11]. Nearly, the 50% weigtht of advanced aircraft engines are consisting of nickel based alloy components such as high and low pressure turbine blades, vanes and disks [10]. The fundematal strengthening mechanism is precipitation hardening, which is also the origin of better mechanical properties. Precipitation hardening is the most effective mechanism at elevated temperatures and nickel based alloys strengthened by this mechanism via gamma prime γ' phase precipitates. They can be available both cast and wrought fom, but it is to be noted that the cast one exhibit better strength properties at elevated temperatures including stress rupture and creep life rather than wrougt one [11].

The major alloying elements available in nickel base alloys are shown in Figure 2.2. The height of the element blocks associated with the amounts present in the structure [10].

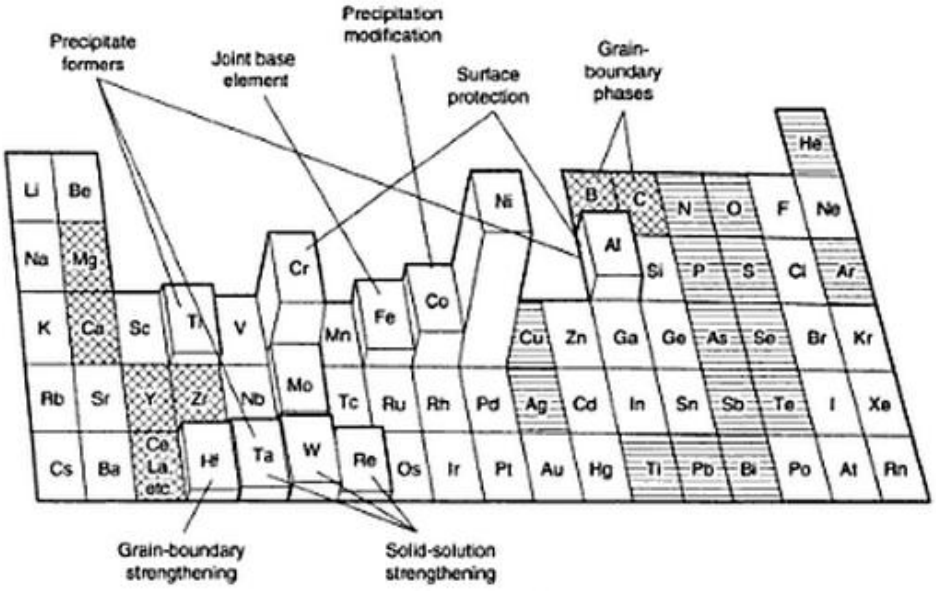

Figure 2.2 : Alloying elements in nickel base alloys (Beneficial trace elements and harmful trace elements shown with cross hatching and horizontal line hatching, respectively) [10].

Nickel-base high temperature alloys are mainly grouped in three types: solid solution strengthened, precipitation hardenable and oxide-dispersion strengthened (ODS). The solid solution alloys include little or no aluminium, titanium, or niobium, while the precipitation hardenable alloys include considerable amount of aluminium and titanium and little substitutional niobium. The ODS alloys manufactured by powder metallurgy methods also include small percent of fine oxide particles (0.5 to 1 % Y_2O_3). The age-hardenable alloys are strengthened by γ' precipitation as well as the addition of aluminum and titanium, by carbide and by solid solution alloying. γ' is the significiant phase to develop high temperature properties. The weight percent of aluminium and titanium as well as aluminium/titanium ratio have great importance to control the high temperature properties. The high temperature properties are increasing with the increase of aluminium/titanium ratio. Further attention need to be paid on the volume fraction, size and spacing of γ'.

As stated in Figue 2.3, precipitation hardened alloys exhibit higher strength rather than the solid solution strengthened alloys. In general, γ'-strengtened alloys are selected for their capability to withstand high temperatures with no loss on their strenghth wheras solid solution strengthened alloys are preferred for moderete operating temperatures due to their ease of fabrication, in particular their weldability [10].

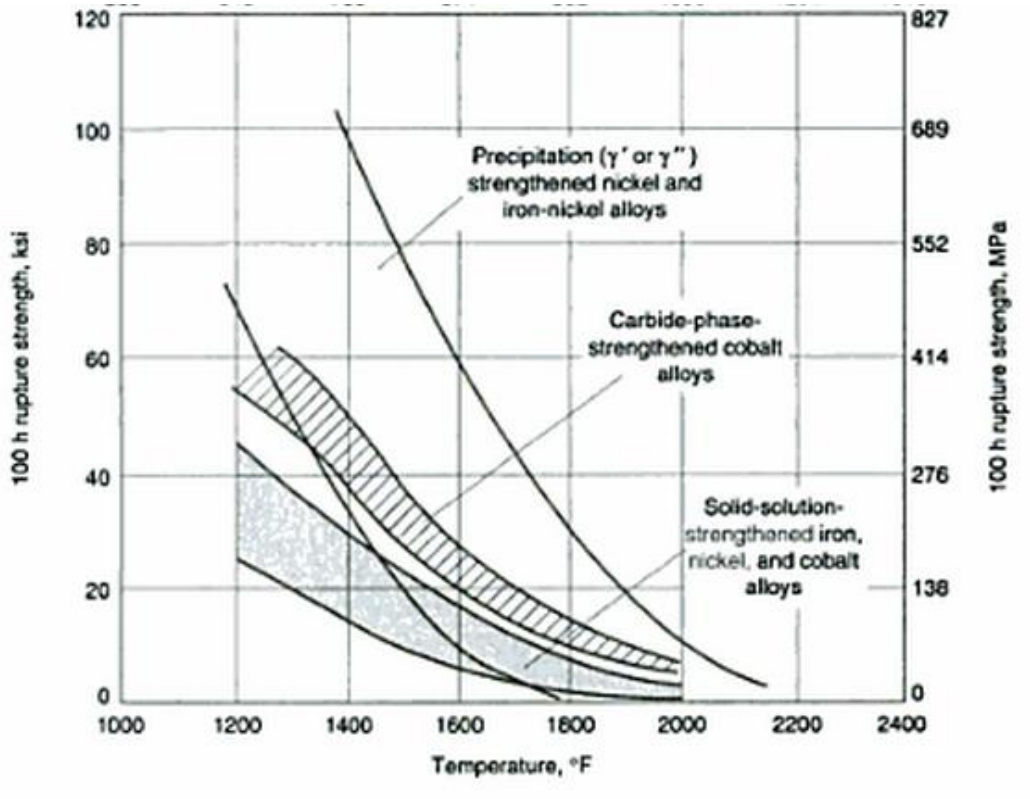

Figure 2.3 : Stress-rupture characteristics of wrought superalloys [10].

Taking into consideration the microstructure of nickel based superalloys, the principal phases that can be constitued in nickel based alloys are listed in Table 2.3.

Gamma Matrix (γ): is an FCC nickel-base nonmagnetic phase that frequently constitute considerably high amount of solid solution elements such as cobalt, iron, chromium, molybdenum and tungsten. This phase is present in all nickel base alloys as the continuous matrix. The lattice sites in the γ-phase are almost equal to each other and the atoms constituting the solid solution being distributed randomly [15].

Table 2.3 : Common phases available in wrought Ni-based superalloys [3].

Phase	**Crystal structure**	**Typical Formula**
γ	FCC	Ni (Cr, Fe, Mo)
γ'	FCC	Ni_3(Al, Ti)
γ''	BCT	Ni_3Nb
δ	Orthorombic	Ni_3Nb
MC	FCC	TiC, NbC
$M_{23}C6$	FCC	$(Cr, Fe, W, Mo)_{23}C_6$
M_6C	Cubic	Fe_3Mo_3C

Gamma Prime (γ'): precipitates coherently with the austenitic gamma matrix in which aluminium and titanium are needed in structure to precipitate FCC γ' (Ni_3AlTi). Other elements like niobium, tantalum and chromium also involves in γ'. This phase is essential for high temperature strength and resistance to creep. In the γ′-phase $Ni_3(Al,Ti)$ the nickel atoms locate at the face-centers and the aluminium or titanium atoms locate at the corners, shown in Figure 2-4 [15].

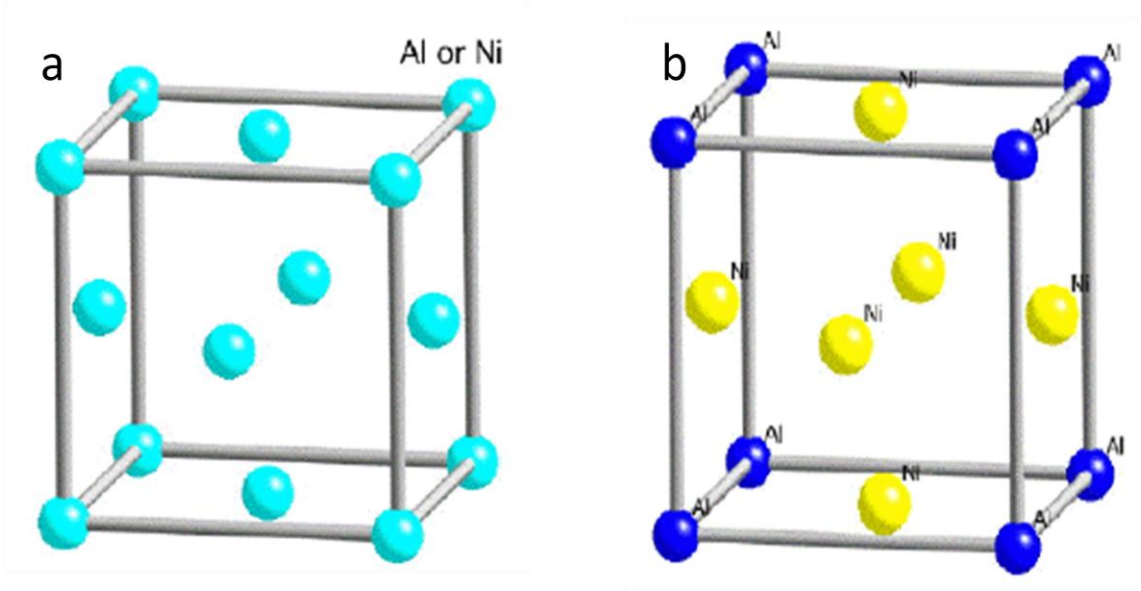

Figure 2.4 : Crystal structures of **(a)** Gamma and **(b)** Gamma prime [15].

Gamma double prime (γ"): is coherent with gamma matrix in which nickel and niobium combines in the presence of iron to precipitate BCT (Body centered tetragonal) γ" Ni_3Nb. This precipitate is present in nickel-iron base alloys such as Inconel 706 and Inconel 718 providing high strength at moderate temperatures since it is unstable at temperatures higher than 650°C (1200°F). In the absence of iron, or at temperatures and times indicated in the Figure 2.5 TTT (Time-Temperature-Transformation) diagram of an iron-containing alloy, an orthorhombic precipitate of the same Ni_3Nb composition (delta phase) forms instead. Delta phase is incoherent and adversly affect the mechanical properties as long as available in increased amount. Heat treatment of this alloy requires special care to avoid delta phase formation instead of desired gamma double prime γ".

Grain boundary γ': is a film along the grain boundaries induced by heat treatments and service exposure. Rupture properties are positively affecting due to presence of this phase along the grain boundaries.

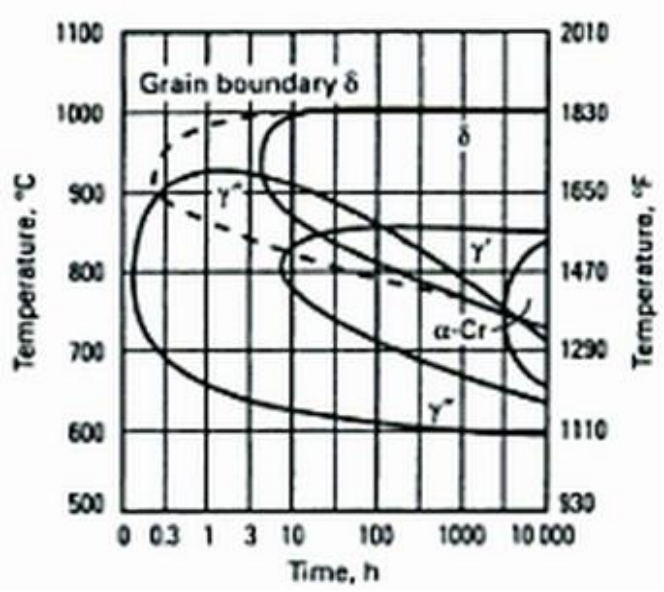

Figure 2.5 : TTT diagram of vacuum melted and hot forged Inconel 718 bar [10].

Carbides: in particular, metal carbides form in the presence of 0.02 to 0.2 wt % carbon linked with reactive elements such as titanium (Ti), tantalum (Ta), hafnium (Hf) and niobium (Nb). MC carbides attempt to decompose and form other carbides such as $M_{23}C_6$ and/or M_6C during the heat treatment and operating conditions. The later generated carbides tend to introduce in grain boundaries. Carbides having the nature of solid solution alloys may introduce after extended operating temperetures.

Figure 2.6 illustrates the microstructural modificiations of substantital phases in nickel base superalloys depending on the chromium content

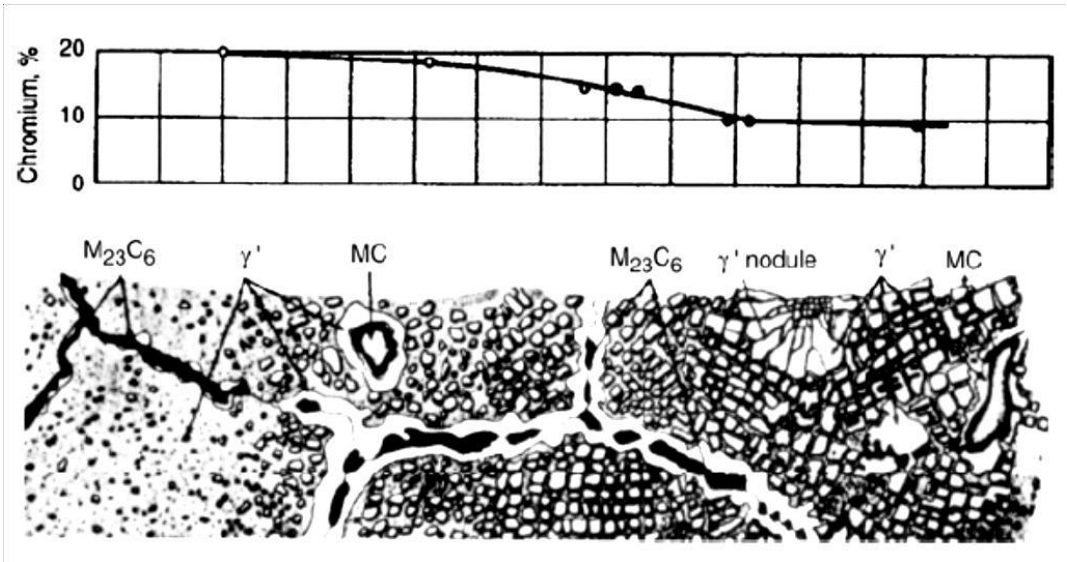

Figure 2.6 : The modification of microstructure in nickel-base alloys depending on chromium content [4].

As long as $M_{23}C_6$ is formed in the grain boundaries, the amount of chromium in the matrix is decreased and the solubility of γ′ is increased in these zones. All these carbides exhibit FCC crystal structure and improve the rupture strength at elevated temperatures. Examples of common carbides are given in Figure 2.7 [15].

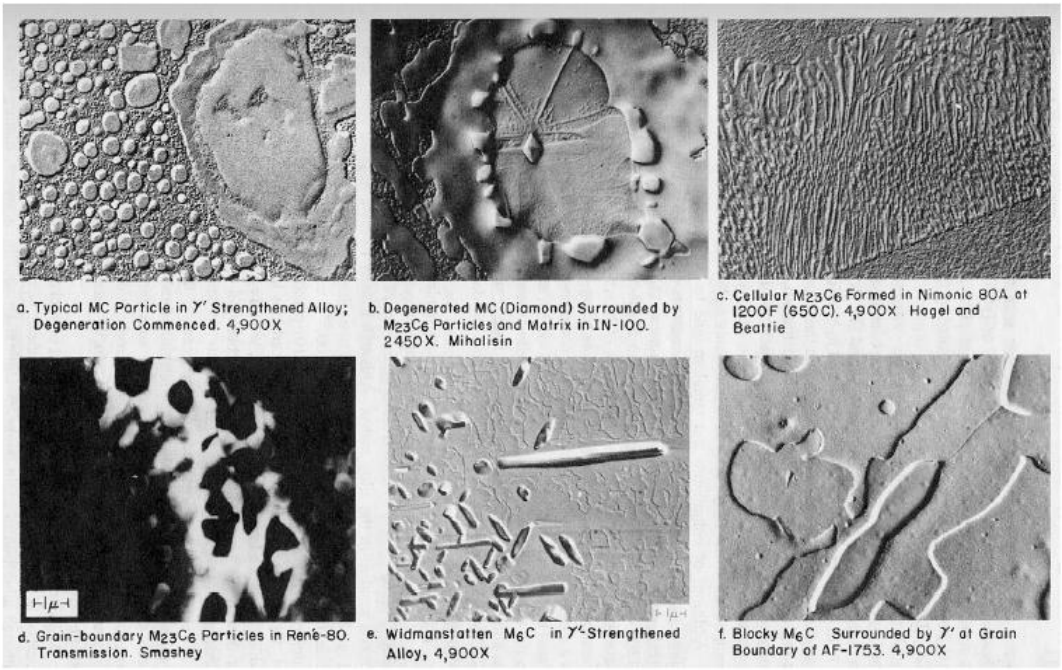

Figure 2.7 : Form of carbides [15].

Borides: in fact, only relatively low density of boride particles can be generated as long as boron segregates to grain boundaries.

Topologically close-packed (TCP) type phases: in which cover plate-like or needle-like phases such as σ, μ and Laves. Those undesirable phases that cause reduction of ductility and rupture strength may form under certain conditions with particular composition. Alloy including a high amount of BCC transition metals (tantalum, niobium, chromium, tungsten and molybdenum) are inevitably prone to TCP formation [4,15].

2.2.3 Cobalt based alloys

Cobalt base superalloys are different than other superalloys due to lack of strengthening mechanism by a coherent, ordered precipitate. There is no intermetallic phase exist in cobalt-based superalloys to form strengthening phases like gamma prime (γ ′) and gamma double prime (γ ″) which are available in iron-nickel and

nickel-based superalloys. Gamma is not stable at high temperatures in cobalt-based alloys.

The main strengthening mechanism of cobalt-based super alloys is solid solution alloying and carbide precipitation. Thus, cobalt base alloy constitue highest amount of C among other types of superalloys. M_6C, M_7C_3 and $M_{23}C_6$ are the common carbides in cobalt base superalloy similar to nickel-base alloys. As long as the main elements of M_6C (W and Mo) are in sufficient amount nearly %5 or more, this carbide can form. M_6C carbides may transform and precipitate on grain boundaries mainly as $Cr_{23}C_6$. Grain boundary carbides intercept the grain boundary sliding which in turn improve the creep rupture life. It is to be noted that these alloys suffer from embrittlement due to contain more carbides than other superalloys, particularly exposed to high temperatures for extended time. Cobalt crystallizes in the HCP structure below 417°C (780°F) and transfers to FCC as exposure to higher temperatures. All cobalt base alloys are alloyed with nickel to stabilize FCC matrix between room temperature and melting point due to eliminate the possibility of this transformation during service.

Cobalt base alloys are generally preferred for applications where hot corrosion is an major issue and/or low stress structural applications at moderate to high temperatures. Hot corrosion resistance characteristics are associated with considerably higher chromium content (20-30 %).

Cobalt base alloys shows better weldeability, good creep and stress rupture resistance at high tempeatures and and thermal-fatigue resistance compared with nickel base alloys. Moreover, they are capable to be melted in argon and air at low cost since their melt route does not require vacuum melting unlike nickel and iron-nickel base alloys that contain the reactive metals such as aluminium and titanium. However, they are more prone to precipitate harmful platelike σ, Laves and similar TCP phases. As an example, Laves phase formation (Co_2W) is an issue for very popular L-605 (Haynes 25) cobalt base alloy in both cast and wrought form [10,11].

2.3 Wrought and Cast Superalloys

The considerable progress of superalloys technology is not just associated with undestanding their microstructure and development of new alloys, but following

interest shall be given for improving the production and processing techniques of these alloys. Melting is the initial step regardless of next process such methods of casting, forging or powder metallurgy. Latest technological advances related with melting techniques utilize cleaner, more reliable and precise chemical compositions which in turn provide better reproducibility [11].

Superalloys can be found in cast or wrought forms which subsequently subjects to heat treatment and/or processing. A wrought superalloy in general originate in cast billets and post-processing with intermediate reheat treatments up to its finish form.

Wrought alloys are more homogenous than cast alloys which suffer from segregation during solidification of alloys. It is considered that wrought alloys are more ductile than cast alloys. Therefore, the mill products such as bars are in wrought form since they can be best produced by working which in turn generates optimal ductility for processing and further use. Forgings are also classified as wrought products and benefits considerable ductility to make certain larger shapes like gas turbine discs.

It is impratical to produce all alloys in wrought form. Some alloys require to fabricate and use in only cast forms, as well. Powder metallurgy (P/M) can be a method to process hard-to-work wrought alloys to prepare for final forging. Wrought or wought P/M alloys usually introduce to components of gas turbines at operating moderate temperatures [4].

Cast superalloys are generally applied for hot section parts of gas turbines such as turbine blades and vanes of airfoils. Common superalloy castings are pollycrystalline (PC) equiaxed, but there is alse directionally solidified (DS) versions. The PC castings constitute grains in different size depending on the component. While, DC casting may constitute multiplicty of grains all aligned parallel to each other (frequently parallel to the longitudional or airfoil axis of a turbine blade or vane component) as known columnar grain directionally solidified (CGDS) parts. There is also a sub-group of DS castings which have only one grain with an oriented crystal axis parallel to the airfoil main axis [4]. Single crystal superalloys exhibit no grain boundaries which in turn provides outsanding creep resistance.

The high temperature resistance of castings are better than forgings due to coarse grains constitute in castings rather than finer grained forgings. Moreover, composition of castings can be modified for elevated temperature durability which is

not an opportunity for others considering forgeabilty characteristics. In constistent with above explanation, for example, nickel base superalloy castings preferred for turbine blade applications which operates under high stress and high temperatures whereas forgings with fine-grain structure results with higher yield strength and superior low cycle fatigue (LCF) characteristic at moderate temperatures used for disk applications [4,11].

It is to be noted that melt route does not necessarily mean that it gives the final properties. Both wrought and casting superalloys require a combination of different manufacturing techniques to machine, join, form and so on to shape the final geometry and may have an impact on the properties.

3. INCONEL 718 ALLOY

3.1 General Characteristics of Inconel 718

Inconel 718 was first introduced by the International Nickel Company in the early 1960's and still demanded by wide range of applications in wrought, cast and powder forms [16]. Inconel 718 being a precipitation strengthened alloy particularly used for gas turbines, turbine blades, rocket engines, spacecraft, nuclear reactors, extrusion dies and containers with operating temperatures up to 650°C [5]. It combines high temperature tensile and creep properties, oxidation and corrosion resistance with easy fabrication. This alloy belongs to the iron-nickel (Fe-Ni) base superalloy group which exhibit austenitic matrix mainly strengthened by gamma double prime (γ") and supplemantary by gamma prime (γ') [16].

Inconel 718 is precipitation hardenable alloy constitutes considerable amount of iron (Fe), niobium (Nb), and molbydenum (Mo) with minor amounts of titanium (Ti) and aluminium (Al). Nominal composition of Inconel 718 is given in Table 3.1 [17,18].

Table 3.1 : Chemical composition of Inconel 718.

Element	% Weight
Nickel (plus Cobalt)	50-55
Chromium	17-21
Iron	Rest
Niobium (plus Tantalum)	4.75-5.50
Molybdenum	2.80-3.30
Titanium	0.65-1.10
Aluminium	0.20-0.80
Cobalt	1.00 max
Carbon	0.08 max
Manganese	0.35 max
Silicon	0.35 max
Phosphorus	0.015 max
Sulfur	0015 max
Boron	0.006 max
Copper	0.30 max

Inconel 718 has an austenitic FCC matrix with secondary phases which establish the particular behavior of the alloy. It is to be noted that niobium is the significiant

alloying element to form secondary phases and build the material characteristics, accordingly [17,19].

Nickel (Ni) and Chromium (Cr) assure the corrosion resistance of this material. Both elements crystallize in the form of FCC gamma (γ) phase [5]. Aluminium (Al) and chromium (Cr) generate the protective and impervious Al_2O_3 and Cr_2O_3 oxide films that gives resistance to corrosion in aggressive environments [19]. Niobium (Nb) contributes to form hardening precipitates such as gamma double prime (γ''). Titanium (Ti) and Aluminium (Al) act as initiating precipitates in the form of intermetallic gamma prime (γ'). Carbon (C) is also available to precipitate MC carbides (M refers to Ti or Nb). MC carbides precipitate at grain boundaries and prevent grain boundary sliding at elevated temperatures which in turn improve the creep resistance [18]. However, the C content shall be low enough to let Nb and Ti precipitation in the form of gamma prime (γ') and gamma double prime(γ''). Molybdenum (Mo) is another alloying element which contribute to increase the mechanical strength by solid solution hardening. During service conditions, delta phase δ may generate. It is an equilibrium particle with orthrombic lattice. All these mentioned particles precipitate along the gain boundaries of the gamma (γ) matrix which act to enhance the intergranular flow resistance of the alloy [5]. Furthermore, alloying elements including Fe, Cr, Mo, Al and Ti strengthen the alloy via solid solution mechanisms [18]. Figure 3.1 below shows the representative microstructure of wrought Inconel 718.

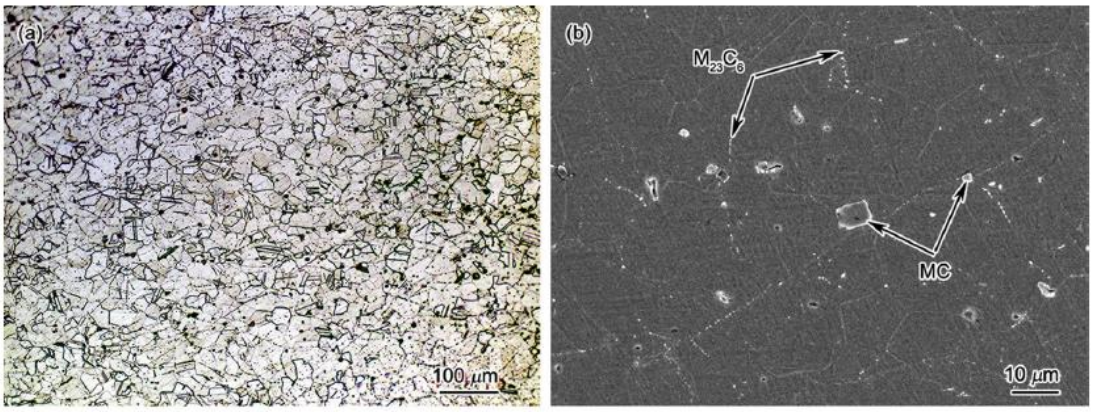

Figure 3.1 : Cold-rolled and annealed wrought Inconel 718 **(a)** Equiaxial grains in austenitic matrix **(b)** MC carbides at grain boundaries [20].

The FCC gamma prime (γ') phase as specified Ni_3(Al,Ti,Nb) precipitates in the form of ordered and coherent cubic or spherical particles, however this phase is not the

main strengthening mechanism unlike other nickel base superalloys. Gamma prime (γ') only covers the 10-20% of whole strengthening of the matrix [17]. The specified high strength of Inconel 718 is due to dispersion of gamma double prime (γ") in the matrix. Gamma double prime (γ") exhibit body-centered-tetragonal structure (BCT), ordered and coherent, precipitated in the form of plates with approximately %16 volume fraction. Gamma double prime (γ") generally precipitates at higher heat treatment temperatures (720°C) while gamma prime (γ') precipitates at slightly lower temperatures (620°C) [16,18,19]. As seen in the Figure 3.2, the precipitates such as δ,γ',γ" and carbides are observed in the Inconel 718 structure captured by high resolution field emission gun scanning electron microscope (FEG-SEM).

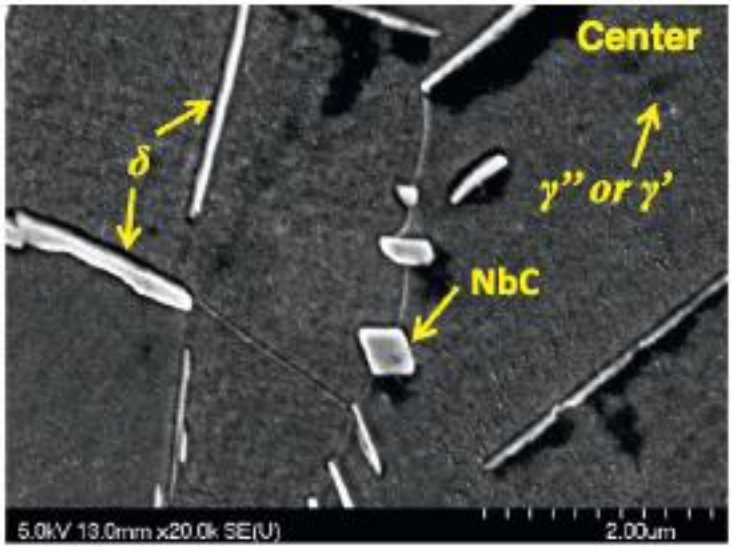

Figure 3.2 : γ', γ", δ, MC phases in the microstructure of forged Inconel 718 after heat treated (solution heat treatment at 954°C for 1 hour followed by air cooling, then double aging at 718°C for 8 h, followed by furnace cooling to 621 °C, second aging at 621 °C for 8 h, air cooling to room temperature) [18].

Gamma double prime (γ") phase is metastable thus under the long time exposure to temperatures higher than 650°C, it can tranform to delta (δ) phase Ni_3Nb having an orthorombic lattice not coherent. Delta (δ) phase formation during aging heat treatment is shown in Figue 3.3. The effects of delta (δ) phase is well established as detrimental to mechanical properties [18].

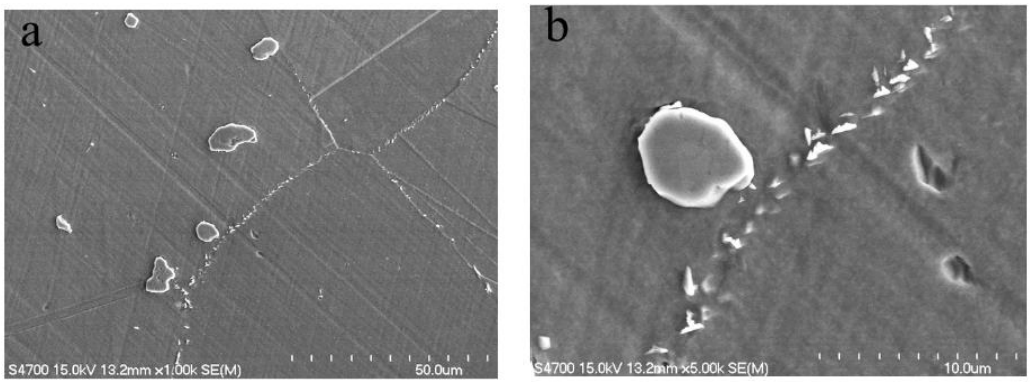

Figure 3.3 : Carbides and δ phase precipitated at grain boundary of Inconel 718 after solid solution and aging heat at 955°C for 3.5 hour **(a)** Magnification 1000X **(b)** Magnification 5000X [21].

3.2 Heat Treatment Characteristics of Inconel 718

The high temperature stregth of Inconel 718 is arised from stable FCC matrix combined with precipitation strengthening [23]. Inconel 718 is an age hardenable alloy. Alloying elements such as Al, Ti and Nb have limited solubility in the austenite matrix, and the solubility is dramatically reduced with reducing temperature; thus finely distributed precipitates can be initiated in the matrix from a supersaturated solid solution during heat treatment [14]. In this case, the coherent intermetallic compounds including gamma prime (γ') Ni_3(Al,Ti,Nb) and gamma double prime (γ") Ni_3Nb precipitates which in turn inhibit the dislocations movement and increase the strength of material. There are four major factors affecting the precipitation hardening efficiency

- Coherency strain between the matrix (γ) and the precipitates (γ' and γ") resulting from lattice parameters difference
- Antiphase- boundary (APB) energy in the presence of ordered precipitates (γ' and γ"). The APB energy is referring the energy required for the dislocations to cut through the ordered precipitates
- Volume fraction of precipitates (γ' and γ")
- Size of particles

Heat treatment needs to be performed controlledly to assure that adequate precipitation of gamma double prime (γ") instead of the δ (orthorombic) phase of the same Ni_3Nb composition. δ is in incoherent structure and adversely affect the

strength as long as available in large amounts. Due to lack of iron or at temperatures and times indicated in Time Temperature Transformation (TTT) diagram of Inconel 718 , the δ phase tranforms to gamma double prime (γ") phase.

Precipitation hardened alloys subjects to mechanical property changes adjacent to solvus temperature of the strengthening precipitate. Based on this fact, The mechanical properties of Inconel 718 reduces at about 700°C which is the solvus temperature of this alloy which can be seen in Figure 3.4.

Both solid solution and precipitation strengthening are the part of strengthening mechanism, therefore the heat treatment cycle of Inconel 718 is split into solid solution treatment and aging treatment [21].

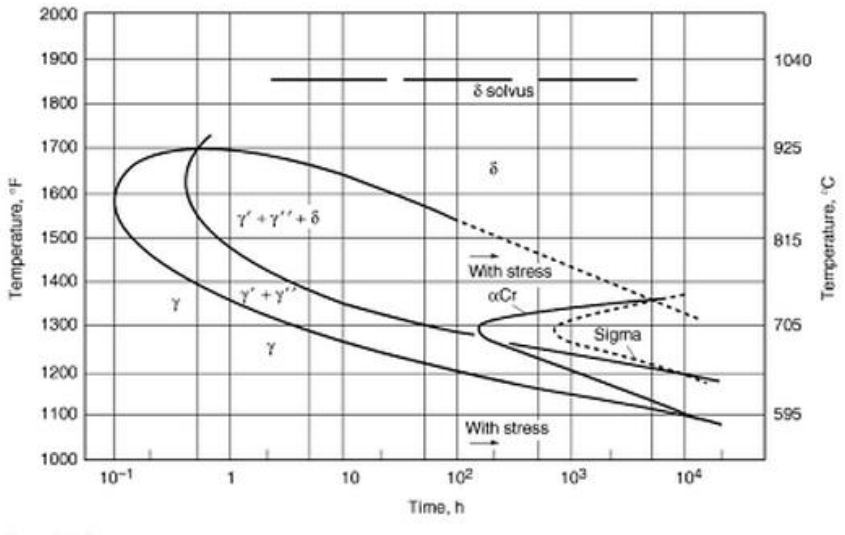

Figure 3.4 : TTT diagram of Inconel 718 [14,22].

Inconel 718 is usually undergone solution annealing and precipitation hardening (age hardening) heat treatments prior to use in most applications [10,22]. The temperature, time, and cooling rate may be modified upon the requirements of applications and desirable mechanical properties [14]. Inconel 718 is hardened by the precipitation of secondary phases (γ' and γ") into the metal matrix. In order to fulfill this phenomena, the aging compounds including aluminium, titanium and niobium shall be in solution with dissolving in matrix. When this aging constituents precipitate as different phases or are modified in some other form, desirable precipitation phases cannot be acquired. Therefore, solution heat treatment is the first step [22].

Two common heat treatments are specified for Inconel 718 :

i. Solution anneal at 925-1010 °C with subsequent rapid cooling, generally in water, then precipitation hardening at 718°C during 8 hours, furnace cool to 620°C, hold at that temperature for a total aging time of 18 hours with subsequent air cooling.

ii. Solution anneal at 1040 -1065 °C with subsequent rapid cooling, generally in water, then precipitation hardening at 760 °C during 10 hours, furnace cool to 650°C hold at that temperature for a total aging time of 20 hours with subsequent air cooling.

Other heat tretments are avaible for Inconel 718 desiged for oil and gas industry.

iii. Solution anneal at 1010-1035 °C and aged at 785°C for 6-8 hours and air cooled.

It is required for materials used in aerospace applications those having high tensile and fatigue strength as well as excellent stress-rupture characteristics [14]. Therefore, it is recommended to use a solution heat treatment below the δ solvus temperature (~1010°C) and a two-step aging heat tretment as described in first item above [14].

The highest room temperature integrity properties is achieved by the first heat treatment cycle. Moreover, due to introduction of fine grains, fatigue properties can be improved. The latter heat tretment cycle is preferred for improved impact strength, low temperature toughness and ductility. It is to be noted that this treatment can cause notch brittleness in stress rupture [14,22].

Taking into consideration the usage of Inconel 718 in the oil and gas industy, the high strength levels are not required unlike aerospace applications. Thus, the specified heat tretment is associated with higher fracture toughness, resistance to hydrogen embrittlement and stress corrosion cracking [14,22].

Selection of solution heat treatment temperatures rely on requested final properties. A higher solution temperature is selected in order to obtain better short-time tensile properties at elevated temperatures, improved fatigue resistance associated with finer grain size or improved resistance to notch rupture sensitivity [23]. The higher solution temperatures produce grain growth and dissolve more carbides [23].

The effect of the solution temperature and direct aging condition (without solution heat treatment) on mechanical properties of Inconel 718 is included in Table 3.2.

After conducting solution treatment for 1 hour at specified temperatures below except the first sample, all samples are air cooled and then aged at 720 °C for 8 hours, cool 55°C/h to 620°C, hold for 8 hours, air cool.

According to Table 3.2, the highest tensile strength is obtained with the direct aged condition with considerably lower stress rupture life. It is obvious that the lower solution temperatures result with better strength, wheras the higher solution temperatures up to 1010°C establish better stress rupture strength [14].

After aging, the resulting microstructure of Inconel 718 exhibits large grains that contain the principal aging phases (γ' and γ") and high concentration of carbides in the grain boundaries. It is to be noted that lower solution temperatures dissolves these precipitates without grain growth or significiant carbide solution [23].

Aging temperature and holding time are the significiant parameters during heat treatment. As an example; After solution heat treatment, the aging performed at 650°C contributes to structure with high impact energy and low strength, whereas the properties modified as decreasing impact energy and increasing yield strength rely on the aging temperature at 750°C [24].

Table 3.2 : Properties of Inconel 718 depending on solution heat treatment temperature [14].

Solution treatment	Yield Strength (MPa)	Tensile Strength (MPa)	Elongation%	Stress rupture @ 650°C with 690 MPa, life (h)
Direct aged	1330	1525	19	95
940°C	1240	1460	18	194
955°C	1180	1420	20	122
970 °C	1145	1405	23	218
980 °C	1172	1405	24	200
1010 °C	1185	1390	22	270
1040 °C	1165	1365	25	225

3.3 Weldability of Inconel 718

Inconel 718 is one of the earliest superalloy that has been introduced with its outstanding weldability either the age hardened or annealed condition among the other precipitation hardened superalloys [25]. Prior to the development of Inconel 718, the precipitation hardened nickel alloys which were strengthened by either Al and/or Ti addition encountered with a rapid precipitation of the hardening phase

during exposure to moderate temperatures [19]. Although the previous alloys can easily be welded in sheet metal thickness, they frequently face with the problem of strain-age cracking during welding or in the post weld aging stage. These cracks are generated in the heat affected zone (HAZ) of the weld joint. This is due to the fact that most of the nickel base superalloys constitute 3-5 % Al and Ti and are stregthened by $Ni_{3(}Al,Ti)$ phase. Since this phase precipitates rapidly and decrease the ductility, it induces cracks in HAZ during welding [25]. This rapid response led to difficulties in performing welding and repair without post weld heat treatment associated cracking, which has already been an issue for age-hardenable superalloys including Waspaloy, Rene 41, Inconel X750 and Udimet 700 [19].

Strain age cracking generally arises after welding or during aging heat treatment due to stresses induced (via welding residual stresses, precipitation reactions and fabrication processes) and surpass the material strength [19]. However, strain age cracking is not an issue for Inconel 718 providing that it contains low Al and/or Ti compounds as well as Nb introduction as the primary hardening constituent. The problem is resolved in Inconel 718 by means of delayed aging response associated with Nb addition. The age hardening response of Inconel 718 is shown in Figure 3.5.

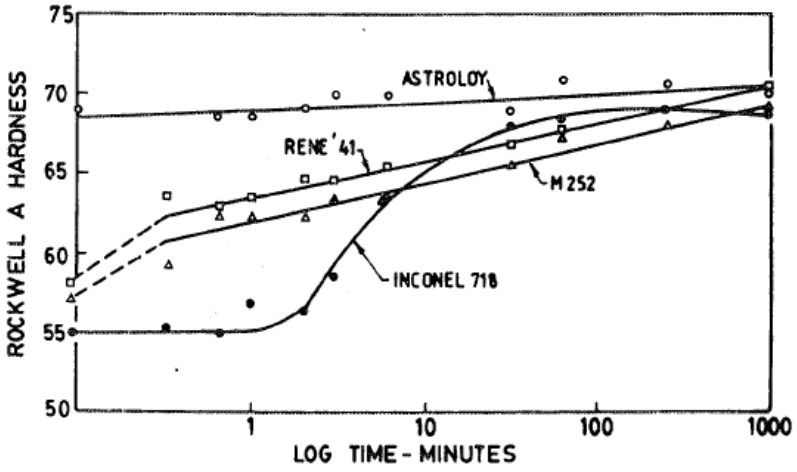

Figure 3.5 : Age-hardening response curve of Inconel 718 [25].

The addition of niobium leads to the formation of strengthening precipitate gamma double prime (γ") Ni_3(NbAlTi) which is different from gamma prime (γ') Ni_3(Al,Ti) in terms of morphology, composition and crystal structure. The sluggish age hardening behavior of gamma double prime (γ") enhances the resistance to strain age cracking by producing a relatively low strength and high ductility HAZ during the

aging. There is enough time for the alloy to reach the desired hardness level and facilitated stress to be relived or relaxed before hardening [19,25].

Welding of Inconel 718 usually performed by application of fusion welding processes such as Gas Tungsten Arc Welding (GTAW or TIG), electron beam (EB) and plasma welding techniques [19,25,26]. The welding procedures applicable to austenitic stainless steels also work for Inconel 718. However, this alloy can distort as much as carbon steels during welding due to their similar thermal expansion behavior [25]. Although weldability of Inconel 718 is quite better compared with other Ni-based superalloys, solidification cracking, HAZ liquation cracking and segregation are still issues associated with Inconel 718 welding.

Solidification Cracking

The reason for solidification cracking is related with the extended solidification range of this alloy. It is noted that Inconel 718 is prone to formation of low melting γ/Laves eutectic compound in the interdendritic interstices during welding [25]. Solidification cracking arises in the weld metal as seen in Figure 3.6 during the final stages of solidification, at a temperature adjacent to the solidus of the alloy. As the weld metal solidifies, the dominating non equilibirum conditions stimulate Nb segregation to dendrite interstice, and enlarge the alloy solidification range by terminating solidification with a γ/Laves eutectic. Cracking can occur due to the presence of this low melting eutectic liquid during the final stages of solidification in the weld metal [25].

Solidification cracking of austenitic materials is highly depend on the solidification temperature range and particularly the solidification incidents at grain boundaries and interdendritic regions [3]. This is also well established for alloys containing niobium (Nb) which stimulate the formation of NbC and Laves phase eutectics at about the last stages of solidifiction. It is to be highligthed that the Laves eutectic is more detrimental than the MC eutectic as it solidifies at a lower temperature and those enlarge the solification temperature range. The amount of these two phases is in fact related with the nominal composition of the alloy. The γ+Laves eutectic reaction can be avoided by varying the amount of carbon (C) which in turn decrease the sensitivity to solification cracking. The C/Nb ratio also have an effect on the amount and distribution of the γ+Laves eutectic. Moreover, it is determined that

grain structure morphology ifluence the sensitivity to solidification cracking as such material structure with equiaxed grains is less prone rather than columnar structure. This improvement is associated with better accomodation of strain, liquid feeding, healing of incipient cracks and lower concentration of impurity elements of equiaxed grains [3].

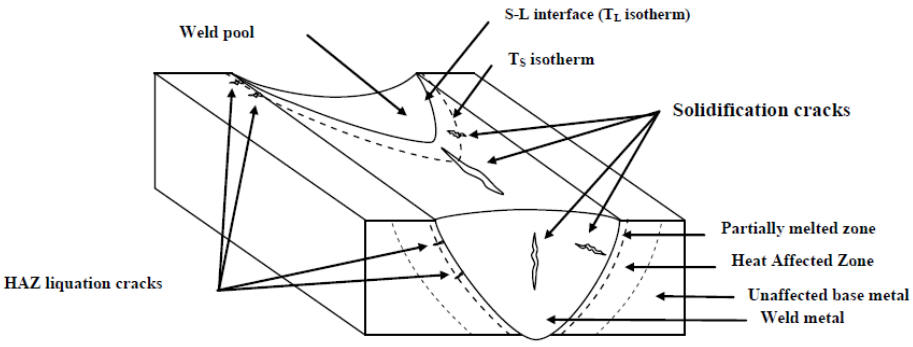

Figure 3.6 : Weld cracking scheme of Inconel 718 alloy [3].

HAZ Liquation Cracking

Liquation cracking is generally arises along the grain boundaries in the HAZ during either TIG or EB welding [3,25,27]. Nb containing austenitic alloys like Inconel 718 are more prone to liquation cracking. Solidification cracking can occur in fusion zone of Inconel 718 in specific conditions while liquation cracking in HAZ is always an issue for weld joints unless proper precautions taken [25]. Below in Figure 3.7 is an micrograph showing the liquation crakcs (microfissures) along the HAZ boundary of EB welded Inconel 718 alloy.

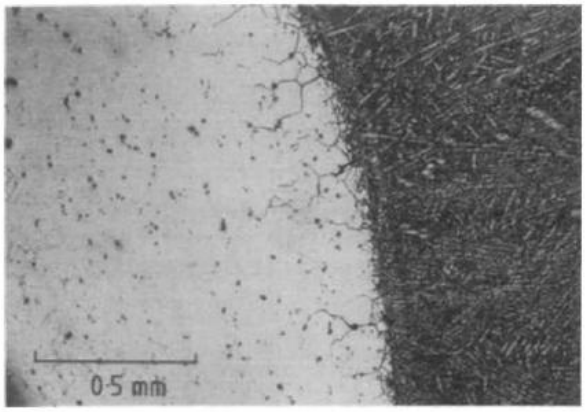

Figure 3.7 : Precipitation and microfissures on HAZ boundaries [28].

As seen in Figure 3.7, Microfissuring is associated with grain boundary tearing in the HAZ and usually cannot be detected prior to metallographic examination [27].

HAZ liquation cracking in precipitation hardened superalloys is because of the stresses induced by shrinkage during solidification and cooling in related with re-precipitation of secondary phases such as γ' phase during the cooling. Liquation of grain boundary constituents decreases the ductility dramatically and as a result very moderete stresses can lead to cracking [3].

During rapid heating by welding, second phase eutectic grain boundary precipitates such as γ/Laves or γ/NbC available in the HAZ of Inconel 718 do not have enough time to dissolve into the matrix. Since the temperatures easily exceed the eutectic temperatures of these grain boundary compounds in the HAZ, their dissolution in the matrix shall occur through liquation according to phase diagram. Thus, this type of liquation is defined as constitiuonal liquation. Constitutional liquation does not cover the actual melting of the particles in HAZ, in fact covers the liquation of the interface between γ matrix and these compounds. While Laves phase liquates at 1160 °C , the carbides liquate at higher temperatures. It is well established that cast alloy 718 exhibits zero ductility range on cooling than the wrought forms that is a measure of a greater weld HAZ intergranular cracking sensitivity [25].

The constitutional liquation of NbC is different than Laves in terms of the liquid associated with NbC is not molten carbide. As the carbide intend to dissolve into the matrix, through the back diffusion of the Nb and C, a Nb-Ni eutectic liquid initates. It is shown in Figure 3.8 how the intergranular cracking take place due to NbC liquation.

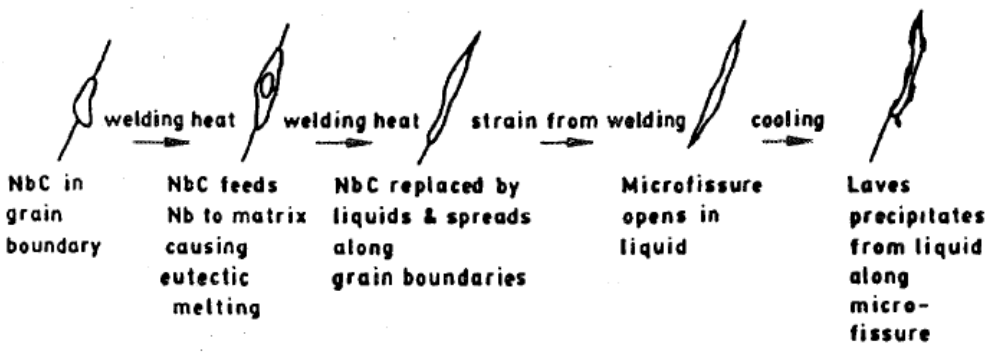

Figure 3.8 : Schematic illustration indicating the formation of intergranular HAZ cracks due to liquation of NbC particles [25].

It is also claimed that the intergranular cracking in Ni-base alloy is associated with the impurities such as phosphore (P) and sulfure (S) concentration and the grain size [25]. The effect of grain size on occurrence of these microfissures is given in Figure 3.9. According to the below graph, grain size of welded Inconel 718 shall be ASTM 5 or finer in order to avoid this problem.

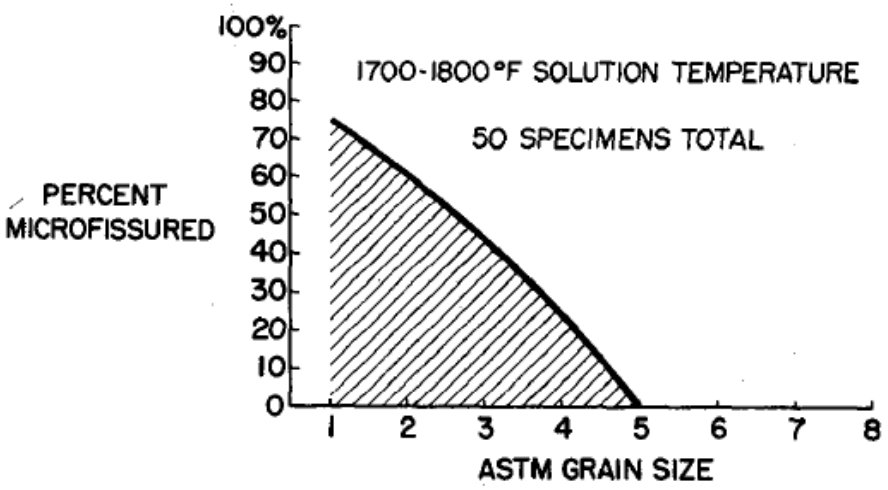

Figure 3.9 : Detected weld microfissures versus ASTM grain size of wrought Inconel 718 [27].

Microfissures has little impact on static mechanical properties such as tensile and stress-rupture strength, however it adversly affects the dynamic properties in particular fatigue strength **[27].** It is claimed that fatigue strength of fine grained parent material and welds are more or less equivalent, wheras coarse grained material and also welds are found to be weaker. As it is indicated in Figure 3.10, welds in coarse grained material is dramatically lost its fatigue strength with increasing cycles.

This cracking can be eliminated by reducing the heat input through high energy welding technique, minimizing weld restraint or limiting the stresses applied to the part and welding the material in the most proper heat treatment condition [3,26]. It is highligthed that a material in solution condition combined with fine grains is to be preferred to the same material with in aged condition with coarse grains considering resistance to HAZ liquation cracking [3,27].

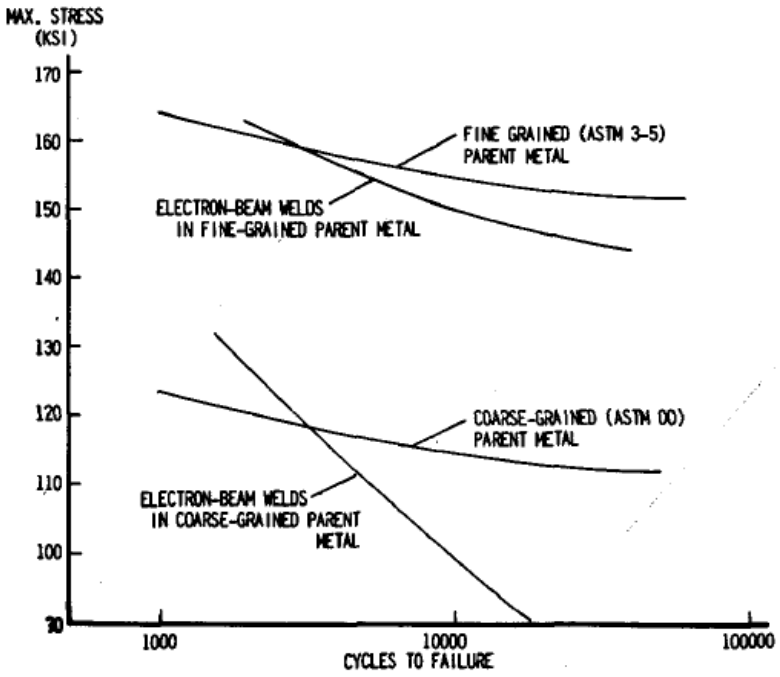

Figure 3.10 : Effect of grain size on low cycle fatigue strength of Inconel 718 [27].

Segragation

The weld metals generally solidify dendtritically. Even though the bulk weld metal composition is homogeneous, the dendritic structure can exhibit microsegregation which is characterized by a composition gradient between the cores and peripheries of individual dendrites. Microsegration takes place during non-equilibrium solidification of weldments. The solidification sequence of Inconel 718 including three phase transformation is shown in Figure 3.11. A carbide and Ni_2Nb intermetallic phase solidifies in the interdendritic spaces. It is to be noted that γ+Ni_2Nb eutectic crystallizes as a non equilibrium phase [29]. The cores of dendritic arms exhibit higher solidus temperature and constitute less solute than the interdendritic regions [30].

Inconel 718 is precipititation strengthened primarly by γ" in the form of Ni_3Nb. The sluggish ageing behavior of γ" precipitation is explained to contribute to the weldability in Section 3.3. However, niobium tends to segragate into interdendritic regions during the solidification process since niobium is a a high concentration refractory element, which consequently causes undesirable phases like Laves form in the welded structure [30].

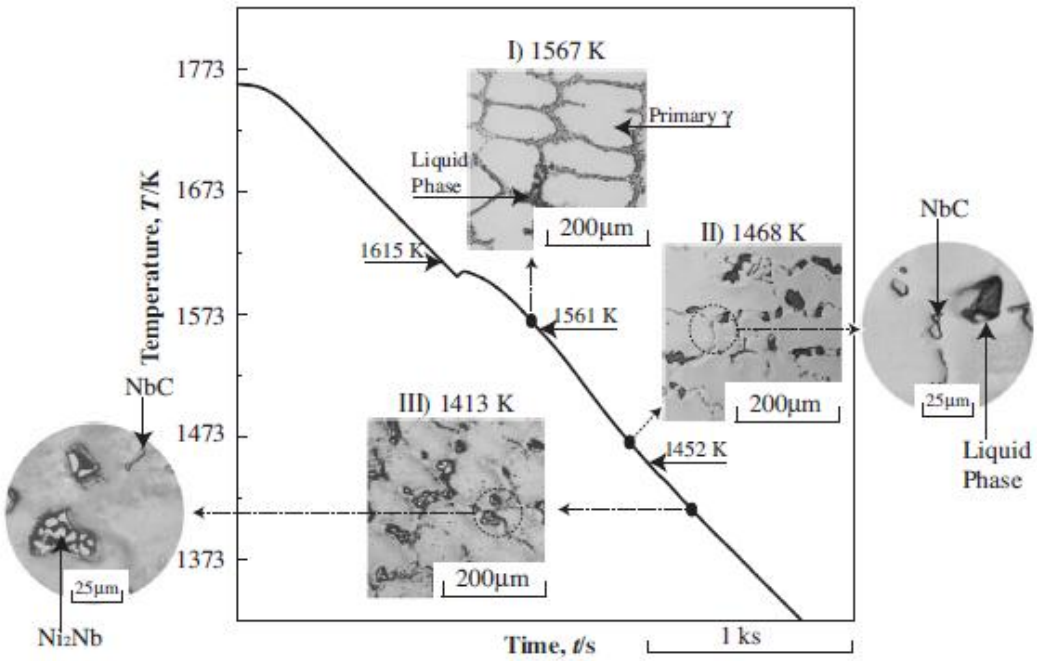

Figure 3.11 : Solidification sequence of Inconel 718 [29].

The introduction of Laves phase is common and unavoidable terminal solidification phase in weld metals due to microsegragation of alloying elements in particular those having high atomic diameter elements such as niobium, titanium and molybdenum etc. due to non-equlibrium solidification conditions present during welding. Laves is hexagonally close packed phase (HCP) in the form of $(Ni,Fe,Cr)_2(Nb,Mo$ and $Ti)$. It is required to constitute 10-30 % niobium concentration for the formation of Laves phase. It is claimed that interdendritic regions enriched by niobium, molybdenum, silicon and titanium consist of Laves phase according to quantitative microprobe analysis. These regions which in turn depleted in nickel, iron and chromium contents.

The solidification microstructure of Inconel 718 is shown in Figure 3.12. Dark area constituting some white massive phase and MC carbide can be distinguished between the dendrites. A SEM image with 3000X magnification of the dark area is also representing the plate-like phase as δ (Ni_3Nb) and the very fine precipitates surrounding the massive phase are γ" and γ'. Moreover, the massive phase may inlude two types of Laves phases such that Fe_2Nb and Cr_2Nb.

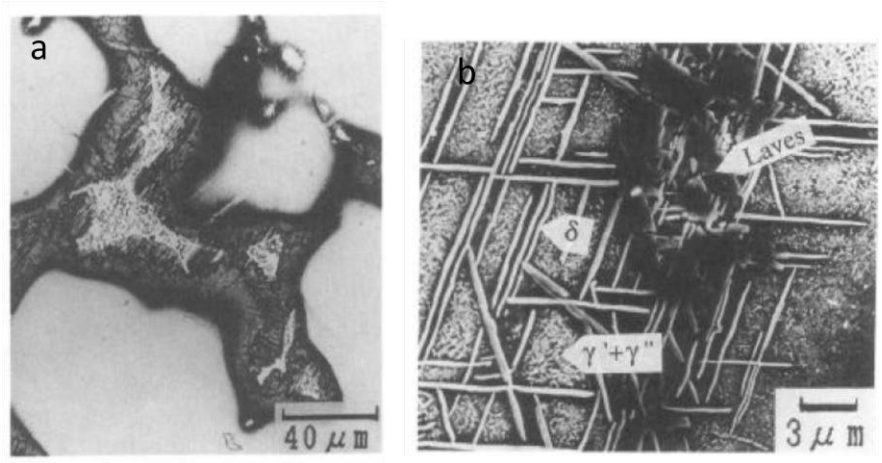

Figure 3.12 : Soldification microstructure of Inconel 718 **(a)** Magnification 300X **(b)** Magnification 3000X [31].

The formation of Laves phase in welded structures is unfavorable and detrimental. It is well established that the formation of Laves phase depleting the matrix of main alloying elements essential for hardening, introducing a weak-zone microstructure between the Laves phase and the matrix interface, acting as preferential sites for crack initiation and propagation due to its inherent brittle nature and adversely affecting the material properties, in particular ductility, fracture toghness, fatigue and creep rupture properties [19,30].

Introduction of Laves phase is due to segregation during weld solidification, hence it is imperative to minimize the segragation by control of heat input/cooling rate and usage of proper welding techniques. Furthermore, subsequent post weld heat treatment at effective temperatures contribute to reduce segragation through homogenization of the weld structure by redistributing of alloying elements [30].

It is recommeded to apply a welding technique which exhibit fast weld cooling rates, low weld heat inputs, heat extraction tecniques such as chilling blocks in tooling, steep thermal gradients, pulsing techniques, low niobium filler wires and electron beam oscillation techniques [30]. Once Laves phase is formed in weld metals, it is required to maintain the chemical composition more uniform by means of dissolving the brittle Laves phase and stimulating sufficient diffusion of niobium into the dendritic regions with performing solution/homogenization heat treatments. Solution/homogenization heat treatment is generally selected at temperatures between 925-1010 °C. It is to be noted that solution heat treatment above 1040 °C results in grain coarsening since the delta (δ) phase which controls grain size by

means of grain-boundary pinning mechanism, goes into solution at these temperatures. Consequently, fatigue and tensile strenghth properties of the base material is reduced. Higher solution heat treatment temperatures above 1063°C promotes HAZ cracking susceptibility, as well [30,32].

3.4 Weld Region Characteristics of Inconel 718

Localized heat input through an energy source and deposition of molten filler material is required for fusion welding process. The melting of the limited portion of metal, intermixing with filler material and solidifying (cooling) result in introduction of different microstructure to that base material. It is to be noted that mechanical properties across the weld joints vary due to the fact that base material adjacent to fusion zone is undergone different heating and cooling cycles as well as the weld and result in different microstructures in both weld (fusion zone) and the surrounding material (HAZ) [32].

Weld solidification exhibit similar characteristics to casting, however there are some major differences those of which the large temperature gradient across the melt and the dynamic nature of welding process, which contribute to the fact that solidification behavior is up on the welding speed. The metal adjacent to the fusion zone is undergone rapid heat treatment cycle which in turn promote various microstructures in zones schematized in Figure 3.13

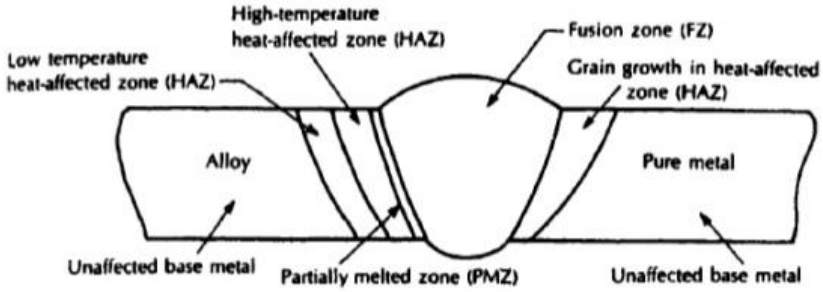

Figure 3.13 : Microstructural zones in fusion welding [33].

The different microstructures associates with the strength and toughness properties of the zones within weld joint [32].

In fusion welding, epitaxial solidification initially starts; hence, the initial crystal size of the weld metal is initiated directly from base metal. The alloys having a large solidification range due to constitutional supercooling exhibit difficulties to maintain

this planar front solidification. Therefore, planar growth transforms to cellular growth. Protrusions introduce and develop into long arms of cells which grow nearly parallel to the direction of maximum heat flow. It is to be noted that these elongated columnar grains are looking different in terms of size and shape rather than the base metal normally having equiaxed grains. The increased size of the columnar grains impact the strength of materials according to Hall-Pecth equation.

Once the temperature gradient decreases, the walls of primary cells become unstable since the cellular microstructure is only conditionally stable and thus generate secondry and tertiary arms resulting in a dendritic structure as schematized in Figure 3.14.

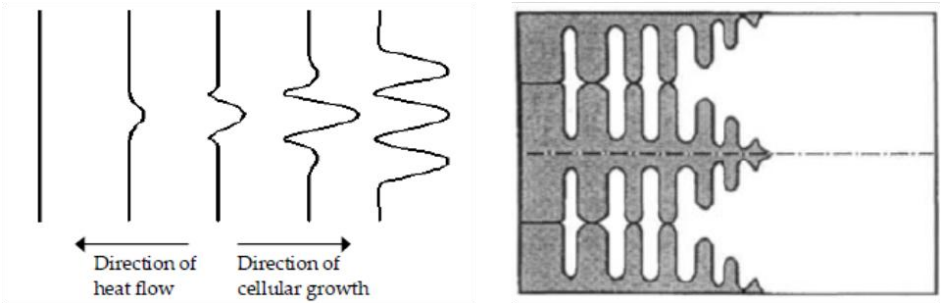

Figure 3.14 : Direction of cellular growth and columnar dendrites [32].

The zone instantly surrounding weld pool exhibit the peak temperature between solidus and liquidius. Thus, this area schematized in Figure 3.15 is undergone partial melting and called as the partially melted zone (PMZ).

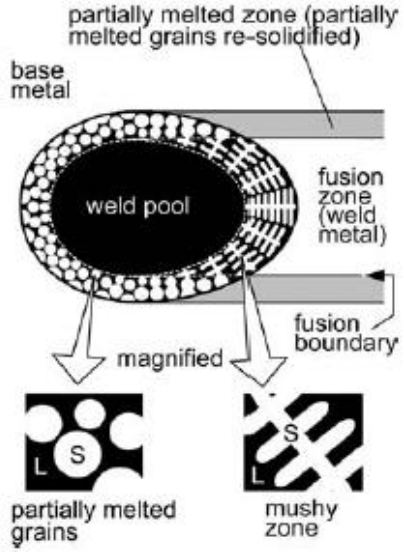

Figure 3.15 : Partially melted base metal grains around the weld pool of an alloy during welding [32].

Base material subjects to severe thermal cycles without melting in the region adjacent to the the fusion zone (FZ) that refers to Heat Affected Zone (HAZ). Hence, the microstructure and properties of this HAZ differentiates from base metal unsiderably. Considering Inconel 718 welds, there are two HAZ regions including coarse-grained and fine-grained HAZ as seen in micrograph in Figure 3.16. Grain growth is not an issue in the fine-grained HAZ directly adjacent to fusion zone due to grain boundary segregation and the subsequent pinning of the grains. However, the temperatures are relatively lower in the later case; grain growth is not avoided in this manner. The microstructure and morphology of different regions in the HAZ are determined by many factors including peak temperature of thermal cycling, heating rate, holding time at high temperature and subsequent cooling speed [34]. The HAZ is considered as the critical region for weld joints and susceptible sites to failure [32].

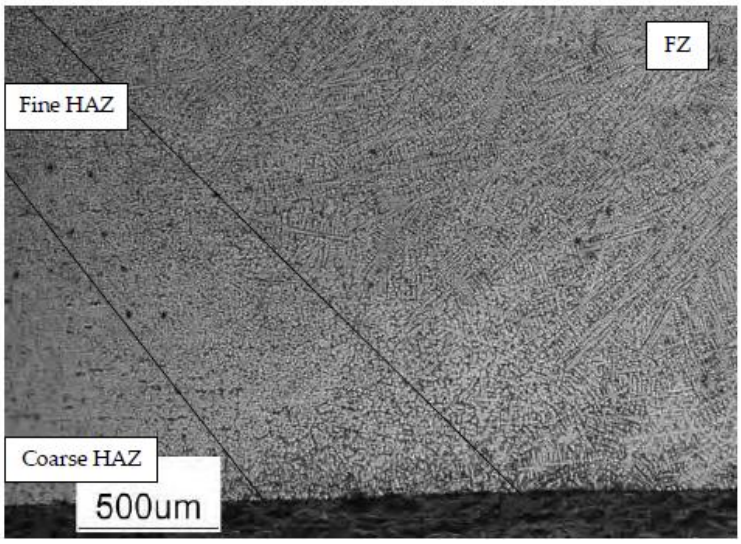

Figure 3.16 : Inconel 718 weld microstructal zones [32].

3.5 Fusion Welding Methods for Inconel 718

Successful fusion welding of high strength and high temperature resistant superalloys is required regarding economic manufacture of modern lightweight, high performance gas turbines [27].

Cobalt base superalloys can be welded by gas-metal arc (GMA) or gas tungsten arc (GTA) techniques without difficulty. However, proper heat treatments prior to welding are required to avoid hot cracking possibility [10]. Solid solution strengthened nickel and iron-nickel base alloys are also weldable by different fusion

welding techniques. The most frequent techniques to perform fusion welds can be listed as GTA, GMA and shielded metal arc (SMA) welding [10].

However, precipitation hardened iron-nickel and nickel based superalloys are less weldable and it is more difficult to weld them comparing with those solid solution strengthened superalloys [27]. Due to the introduction of gamma prime (γ') strengthening phase, these alloys are more prone to strain age cracking. As given in Figure 3.17, The tendency of a superalloy to strain age cracking increases with increasing amount of aluminium and titanium which is known as γ' formers [10]. Strain age cracking is generally an issue for highly restrained or high residual stresses induced weldments. It is to be noted that cracking is associated with stress, precipitation strengthening and in particular existence and volumetric contentration of γ' [10].

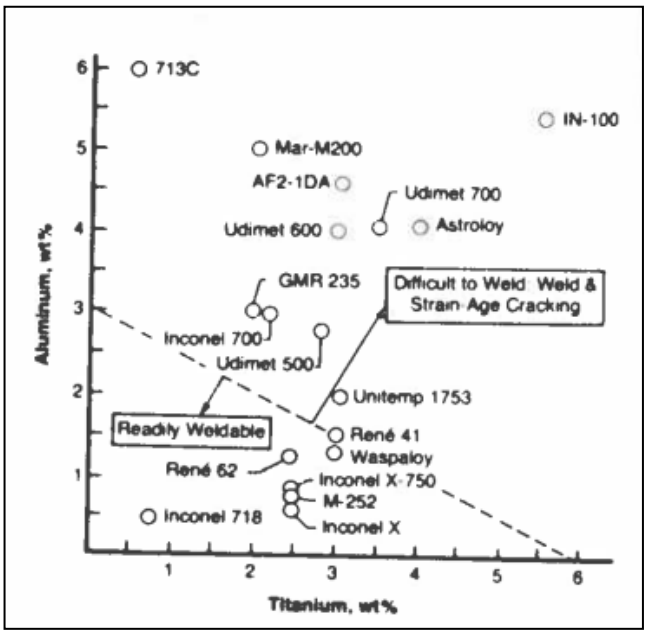

Figure 3.17 : Weldability diagram for some γ' strengthened nickel and iron-nickel base superalloys, indicating the affect of aluminium and titanium content [10].

Precipitation hardenable superalloys have been welded by GMA (Gas Metal Arc), GTA (Gas Tungsten Arc), EB (Electron Beam), laser and PA (plasma arc) processes [10]. In welding superalloys, it is to be noted that these alloys consist of high contents of reactive elements that can be readily oxidized to generate films or inclusions those adversely affect the weld joint quality. Hence, the main process requirement of welding superalloys is that they shall be clean prior to welding and welded in inert gas atmosphere, which in turn implies the available welding

processes to gas tungsten arc welding (GTAW) with or without filler material, gas metal arc welding and electron beam welding. While welding with GTAW and gas metal arc welding, root side of the weld joint also need to be protected by inert gas as well as face side due to oxidation equally damage. Considering filler materials, the common practice in welding superalloys is to use a weaker, more ductile austenitic filler metal than the base material in order to eliminate weld cracking. However, filler material having the same composition with base material can be preferred for maximum joint strength. Filler materials are usually excluded for EBM. It is to be noted that weld joint efficiency up to %75-90 is achieved with applying the weaker and dissimilar filler material, wheras %85-100 joint efficiency can be achieved with using no filler material or parent metal filler material. However, it depends on the base material dilution and weld reinforcement build up. Superalloys like Inconel 718 shall be welded in solution condition and subjected to subsequent heat treatment to provide high joint efficiencies [27]. Both electron beam welding (EBW) and gas tungsten arc welding (GTAW) are the two equally important fusion-joining methods employed for fabrication of aerospace parts and assemblies [30,32].

Electron Beam Welding (EB)

Electron beam welding (EBW) is a fusion welding process which melts and joins metals via heating them with an beam of high velocity electrons [35]. This process is generally performed under vacuum conditions (10^{-3} to 10^{-6} torr) [3]. The electron beam welding machine as seen in Figure 3.18 consists of three main components such that beam generation, beam manipulation and forming and working chamber.

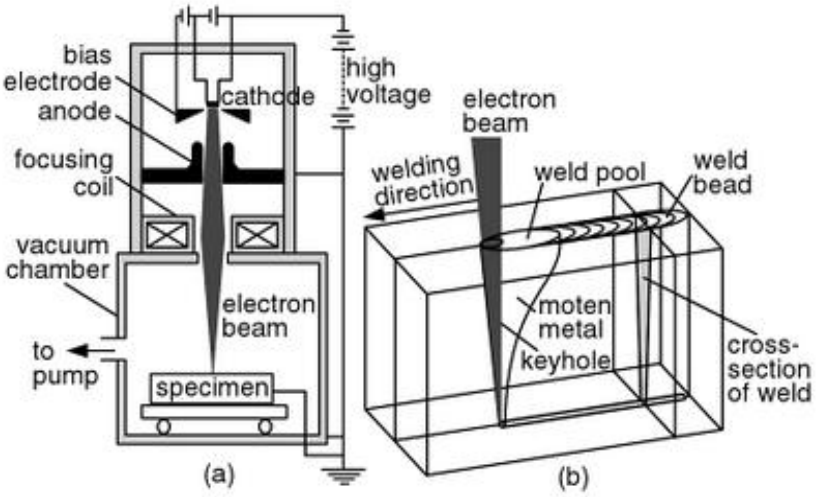

Figure 3.18 : Electron beam welding **(a)** Process **(b)** Keyhole [35].

The generation of electrons occurs at the cathode flament. As the cathode of the electron beam gun has been heated under vacuum, it emits electrons by thermal emission. These electrons are accelarated by means of the electric field between a negatively charged bias electrode and the anode. The electrons are focused by electromagnetic coils as they pass the small hole in the anode and at last directed onto workpiece [3]. The approximate beam currents and voltages is said to be 50-1000 mA and 30-175kV, respectivelty. An electron beam can vaporize the metal and generate a vapor hole during welding which is clarified as keyhole in Figure 3.18b.

Full penetration keyholing can be achieved even in thick workpieces with regards to high power density in EBW. Joints performed by multiple-pass arc welding can be welded with EBW in a single pass at high welding speed. Based on this fact, the total heat input per unit length of the weld is much lower comparing with that in arc welding, which in turn assure very narrow HAZ and negligible distortion. The fine beam size requires precise fit-up of the joint and alignment of the joint with the gun [35].

Reactive and refractory elements can be welded under vacuum without air contamination. Furthermore, dissimilar metals can be welded with this tecnique since rapid cooling in EBW hinder the introduction of coarse and brittle intermetallic phases. However, materials including high-vapor-pressure constituents like Mg alloys and Pb containing alloys are not suitable for EBW since there is risk to contaminate vacuum system by evaporation of these elements [35].

It is to be noted that the cost for implementation of this equipment is very high. It is also time consuming to prepare required vacuum conditions and X-ray shielding. To eliminate these concerns, medium vacuum (10^{-3}-25 torr) EBW and nonvacuum (1atm) EBW have been developed for industrial use. However, the weld quality is decreased accordingly with reduced vacuum levels [3,35].

Tungsten Inert Gas Welding (TIG or GTAW)

Gas tungsten arc welding (GTAW) is also known as tungsten inert gas welding (TIG) is a method, which melts and joints metals by heating them with an arc introduced between a nonconsumable tungsten electrode and the workpiece [35]. The arc is initiated by high voltage, high frequency pulses or by touching the electrode to the workpiece.

There are four main components of TIG welding system including DC/AC power source to provide the welding current, welding torch (air or water cooled) with tungsten electrode and gas nozzle, inert shielding gas for preventing the molten weld pool contamination from open atmosphere and controls for moving the welding torch depending on the mode of operation (manual, semi-automatic and automatic). Figure 3.19 represents the principal elements of TIG welding [35].

The shielding gas goes through the torch body and is guided by a nozzle toward the weld pool to prevent air contamination. Protection from the air is much better in GTAW since an inert gas such as argon and helium or a mixture of gases is usually apllied as the shielding gas toward the weld pool. However, in some cases a noninert gas such as hydrogen or nitrogen may be added in small amounts to the shielding gas mixture [35].

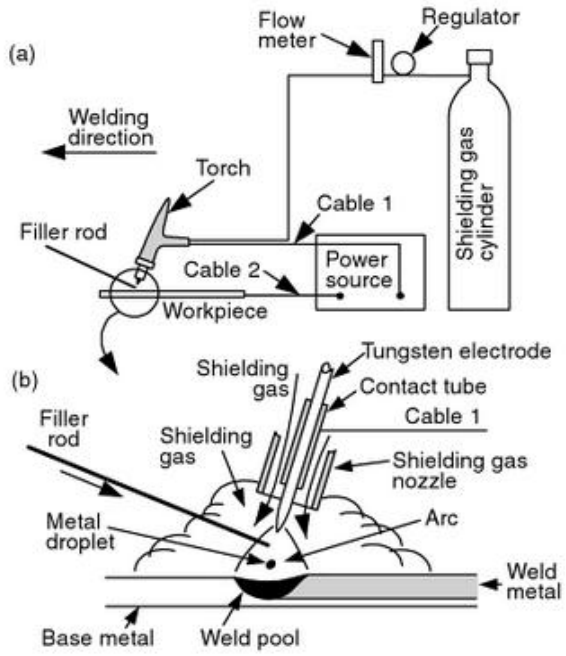

Figure 3.19 : Gas tungsten arc welding **(a)** Overall process **(b)** Welding area enlarged [35].

Melting temperature of tungsten is about 3422 °C, which is nearly twice times higher than the melting temperatures of welded materials. The higher melting point of tungsten contributes to initiate the arc without causing the electrode melting [32,36]. Tungsten maintains its stability during welding operation, that is why GTAW is defined as non-consumable electrode process.

TIG welding is principally used in aircraft industry and the process was developed on the early 1940's [36]. The main advantage of TIG welding is to producing high precision, pure welds which shows high resistance to corrosion and cracking over long time periods [32]. This promotes the usage of TIG welding for critical welding operations like sealing spent nuclear fuel canisters prior to burial. TIG welding cause no slag and no spatter formation because both are contained by the inert gas that shields the weld pool and make TIG welding process relatively clean and time-efficient process [32].

Maximum quality is achieved as long as all equipment and materials engaged in process being free form oil, moisture, dirt and other impurities. Those mentioned uncleanliness cause weld porosity which in turn decrease the weld strength and joint quality [32]. Thus, removal of oil and grease shall be performed by using alcohol or similar solvents.

The concentrated nature of the TIG is another key point of the process. Welds of great srength and quality can be made with thin materials, light materials, dissimilar materials, in most available metals and all with minimal distortion. However, TIG welding has an disadvantage that the low heat input due to low welding current or high welding speed can cause limited penetration. Indicating a reverse situation, too much heat input causes the weld bead to grow in width while burn-through and spatter increase [32].

Manual GTAW is generally considered the most difficult of all the welding processes performed in industry due to require great care and skill to control the amount of current used and avoid contact between the electrode and the metal while assuring a short arc length. Autogenous GTAW without filler material is used in thin square edged sections up to 2 mm, wheras V and X type edge preparations are required for thicker sections. In the later case, introduction of filer material is needed [35]. Even though thin sections can be welded without filler material (in other words autogenous welds), unlike other welding processes, GTAW normally requires feeding a filler wire into the weld area and introducing the welding torch simultaneoulsy. This unpracticle and difficult application can be overcome by automating the movement of torch and feeding of filler wire [32]. Hence, it can be used for precision welding in nuclear and aircraft industries. Aircraft frames and engine casings are a few examples of TIG welding applications.

Control of weld bead shape is significiant in terms of direct effect on the mechanical properties of welds. Therefore, it is to be noted that selection of process parameters is essential. The major process parameters can be listed as arc voltage (arc length), polarity, welding current, welding speed, filler wire feed rate and shielding gas composition and flow rate as grouped in Figure 3.20 [37].

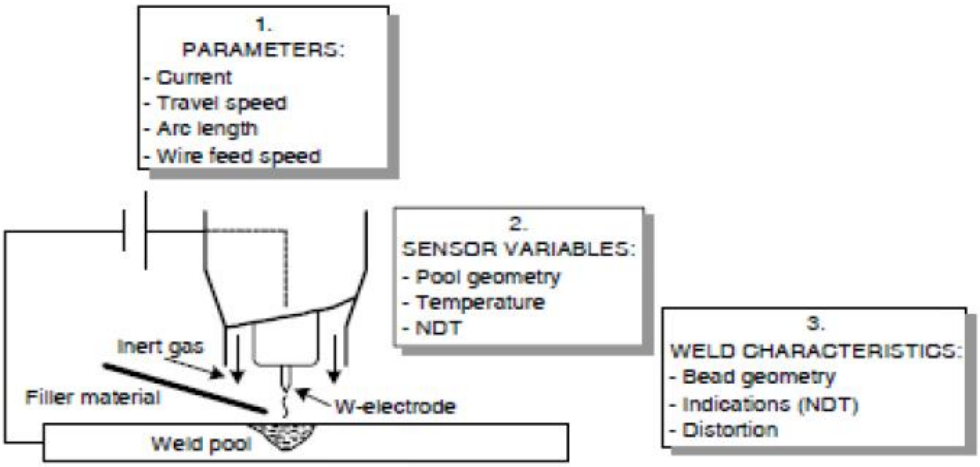

Figure 3.20 : TIG welding process with its parameters [38].

4. EXPERIMENTAL METHODS

4.1 Material

The material used in this study is Inconel 718 alloy with two different nominal thickness of 2 and 3.2 mm. AMS 5596 grade Inconel 718 alloy was supplied as solution heat treated condition (950 °C to 990°C). The chemical composition of the material is presented in Table 4.1

Table 4.1 : Chemical composition of AMS 5596 Inconel 718 alloy.

% Wt Composition of Inconel 718	**Ni**	**Fe**	**Cr**	**Mo**	**Nb+Ta**
	53.40	18.70	18.10	3.04	4.99
	Ti	**Al**	**Nb**	**Co**	**C**
	0.99	0.56	4.99	0.34	0.049

Figure 4.1 exhibits the microstructure of the materials as received condition. The microstructure of the base material in solution heat treated condition constitutes fine equiaxed austenitic grains.

Figure 4.1 : The microstructure of as received Inconel 718 alloys (100X).

The long sheets of Inconel 718 was cut-off by guillotine shear along the rolling direction to prepare specimens being welded as seen in Figure 4.2.

Figure 4.2 : Size of specimens being welded.

4.2 Welding Process

During the study, TIG welding of specimens was performed by Jetline external longitudional seam weld machine as seen in Figure 4.3. Argon is used as shielding gas within the system and filler wire is selected as AMS 5832 grade Inconel 718.

Figure 4.3 : Jetline external longitudinal seam weld machine.

The size of the specimens for weld preparation and subsequent heat treatment were arranged in a manner that at least four tensile specimens and a slice for metallurgical examination can be extracted. Table 4.2 summarizes the experimental plan to determine the effects of post weld heat treatment on the TIG welded joints.

Table 4.2 : Welded-specimen plan.

Thickness	Dimension (widthxlength)	PWHT
3.2 mm	185x200 mm	-
3.2 mm	185x200 mm	Aging
3.2 mm	185x200 mm	Solution+Aging
2 mm	150x250 mm	-
2 mm	300x250 mm	Aging
2 mm	300x250 mm	Solution+Aging

Square butt weld joint design and single V-groove butt weld joint design employed for 2 and 3.2 mm thick specimens, respectively. Each specimen were cleaned with acetone to remove dirt and grease to avoid weld contamination. Prior to welding, specimens were tack-welded to create desired butt joints between two sheet parts being welded together as seen in Figure 4.4. The weldings were done perpendicular to the rolling direction of the specimens.

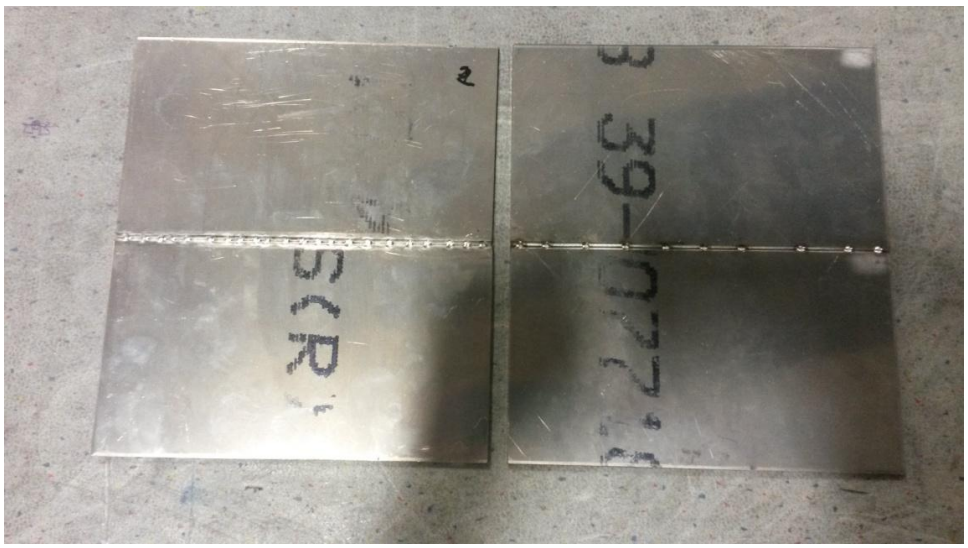

Figure 4.4 : Tack welded parts.

Three coupons from 3.2 mm and three coupons from 2 mm thick sheet were TIG welded with using an external longitudinal seam weld machine as seen in Figure 4.3. Depending on the specimen thickness, fixed paramaters used for welding during this study. Considering 2 mm thick specimens, the current and voltage were selected as

90 Amps and 9 Volts, respectively. The specimens were welded with 7 IPM (inch per minute) welding speed as well as 8 IPM (inch per minute) filler feed rate. On the other hand, the current and voltage applied as 120 Amps and 9.5 Volts to 3.2 mm thick specimens. Their welding speed was selected as 4.5 IPM (inch per minute) and filler feed rate was 16 IPM (inch per minute). Both grup of specimens welded under the shielding gas atmosphere using ultra high purity argon (99.999 %) on top surface of the workpiece and simultaneously bottom surface with a flow rate of 30 CFH (cubic feet per hour) and 35 CFH (cubic feet per hour), respectively. Pre-flow shielding gas was applied approximately 5 seconds prior to striking the arc to assure that the weld area is fully covered. Below in Table 4.3 summarizes the process paramaters applied during TIG welding. TIG welding environment is shown in Figure 4.5.

Table 4.3 : Process paramaters of TIG welding dependent on thickness.

Parameter	Thickness: 2 mm	Thickness: 3.2 mm
Filler wire	AMS 5832 Inconel 718	AMS 5832 Inconel 718
Filer feed rate	8 IPM	16 IPM
Shielding gas type	Argon	Argon
Gas flow rate	30 CFH	30 CFH
Backing gas	35 CFH	35 CFH
Current	DC	DC
Amperage	90A	120A
Voltage	9V	9.5V
Travel speed	7 IPM	4.5 IPM

.

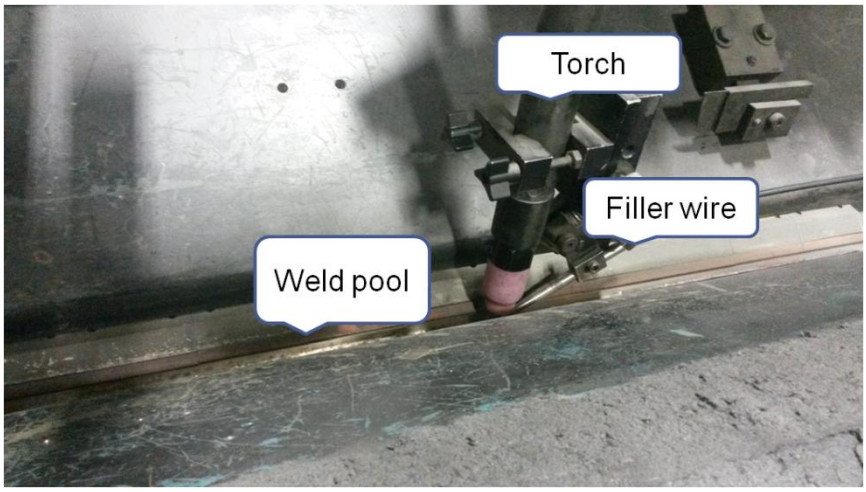

Figure 4.5 : TIG Welding environment.

Thoriated tunsgten electrodes were avaiable in welding equipment. Filler wire has the composition of Al 0.5%, B 0.004%, C 0.05%, Cb+Ta 1.25 % max, Co 1 % max, Cr 18%, Cu 0.30% max, Fe 19 %, Mn 0.35% max, Mo 3%, Ni 53%, Ti 0.9%, Rem. 0.40 % max.

Start and end coupons attached to the edge of the sheet samples in order to avoid unstable welding conditions occuring at the start and the end as shown in Figure 4.6.

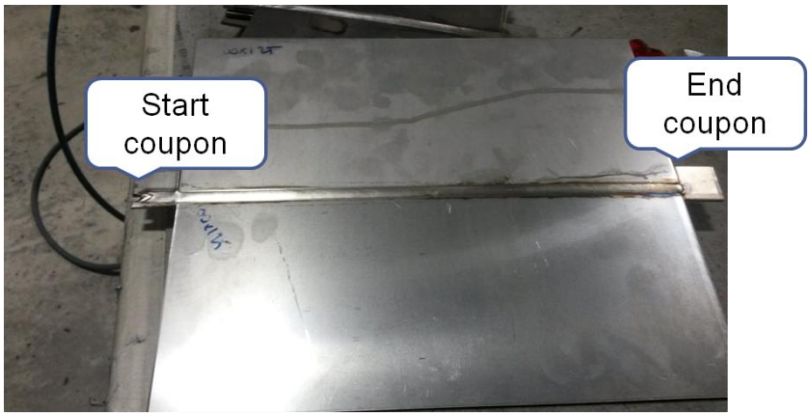

Figure 4.6 : Welded specimen with start and end coupons.

Welded specimens were qualified with %100 X-Ray radiography and dye penetrant test as schematized in Figure 4.7. Weld joints were inspected visually to assure that full penetration and fusion is maintained. FPI (Fluorescent Penetrant Inspection) was performed in case of any flaws open to surface. Fluorescent (Type I), post emulsifiable dye penetrant (Method D) with Level II sensitivity and Form a dry powder developer employed. All parts passed the FPI inspection with no indication observed. At last, the welded specimens subjected to radiographic inspection to ensure the quality of weld joint. There is no internal defects reported based on X-ray films. The weld qualities were guaranteed via NDT techniques. It is to be noted that sound welds readily achieved by joint design and selected TIG weld paramaters. There is no cracks, pores, lack of penetration, lack of fusion and heavy oxidation on weld area.

Theoratical heat input was calculated according to approaches in literature. Heat input generally refers to $Q_{nominal}$ or EI considering arc welding, and the term heat input per unit length of weld refers to the ratio $Q_{nominal}/V$ or EI/V, where V is the welding speed, E is the constant voltage and I is the constant current [35].

The heat source efficiency (η) can be defined as $Q/Q_{nominal.}$ The power supplied from the heat source is not %100 transferred to the workpiece, a portion of the power is also lost to the surroundings. Heat source efficieny of TIG welding process is suggested to be 0,6-0,8 in literature [35]. The average heat source efficiency is estimated as 0,7 for the following heat input calculations.

Heat input per unit length for 2 mm thick specimens is calculated as 192 J/mm and for 3.2 mm thick specimens calculated as 419 J/mm according to the constant voltage and current as well as travel speed given in Table 4.3.

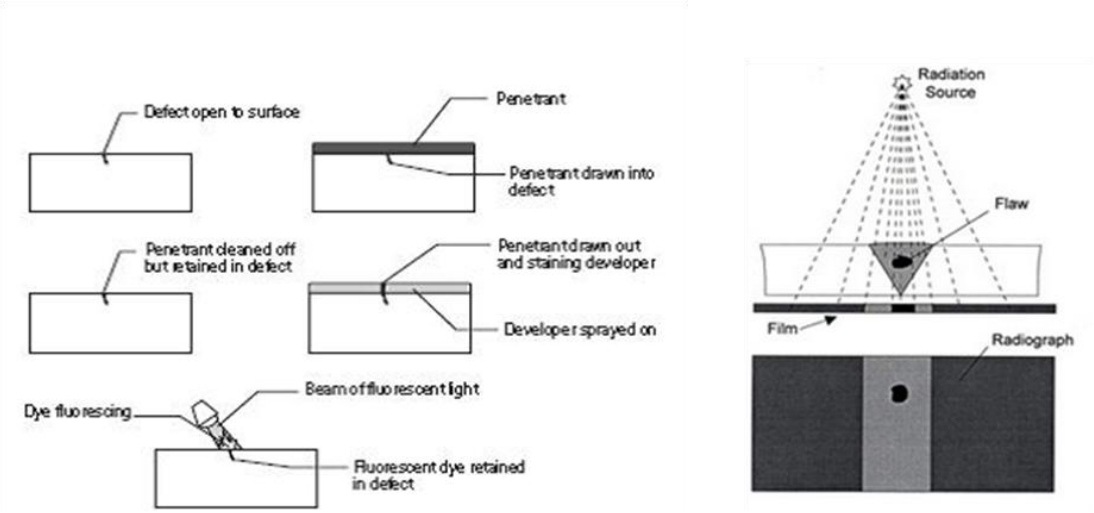

Figure 4.7 : FPI and X-Ray Methods [39].

4.3 Heat Treatment

Heat treatment of welded and non welded specimens performed in vacuum furnaces. It is required for materials used in aerospace applications those having high tensile and fatigue strength as well as excellent stress-rupture characteristics Therefore, it is recommended to use a solution heat treatment below the δ solvus temperature (~ 1010°C) and a two-step aging heat tretment [14]. According to the information gathered from literature, solution heat treatment temperature has been selected as 980±10°C and two-step aging heat reatment applied for hardening. Figure 4.8 illustrates the heat treatment cycles.

As described in Table 4.4, specimens together undergone two different post weld heat treatment cycles. Non welded specimens involved to study in order to compare base material properties with weld joint as a result of same heat treatment cycles.

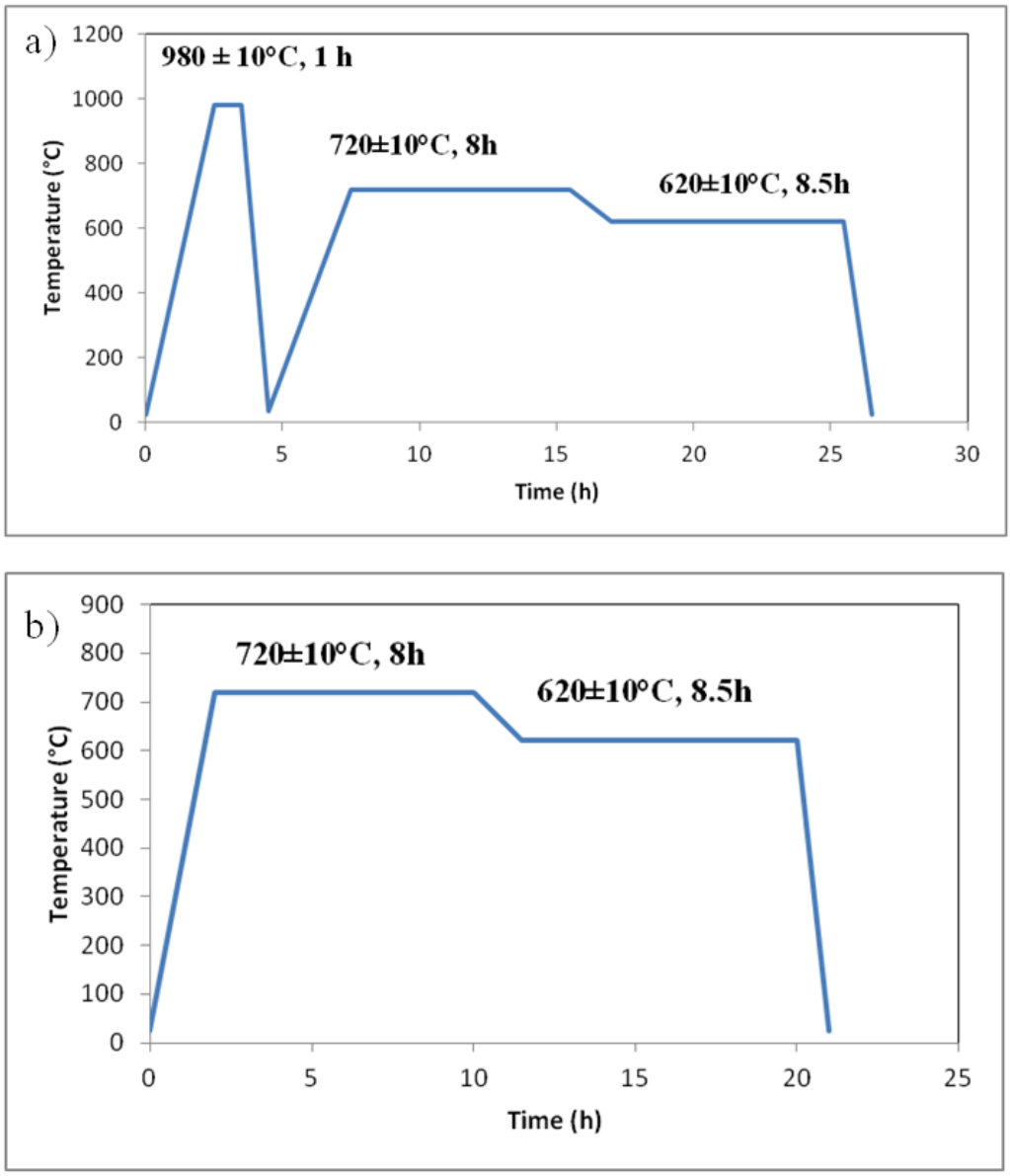

Figure 4.8 : Heat treatment schemes **(a)** Solution+age **(b)** Direct age.

Table 4.4 : Heat treatment plan of welded and non-welded specimens.

Thickness	Specimen Type	Dimension (widthxlength)	Heat Treatment
3.2 mm	welded	185x200 mm	aging
3.2 mm	welded	185x200 mm	solution+aging
3.2 mm	base material	45x100 mm	aging
3.2 mm	base material	45x100 mm	solution+aging
2 mm	welded	300x250 mm	aging
2 mm	welded	300x250 mm	solution+aging
2 mm	base material	150x125 mm	aging
2 mm	base material	150x125mm	solution+aging

4.4 Weld Characterization

4.4.1 Preparation of metallurgical samples

Prior to characterization of weld structure, each weld jont was sectioned transverse to the welding direction by using Discotom-100 model (Struers) abrasive cut-off machine. After cutting, slices was hot mounted in bakalite by using a hydrolic specimen mounting press (CitoPress-10 Struers). Mechanical polishing was performed using 180, 240, 320, 400, 600 and 800 grit silicon carbide grinding papers. Final polish was achieved with diamond solution. Two different etchans with swab etch tecnique was used to reveal the microstructure under microscopy. The firsrt etchant calls Shantz's Reagent and contains Ferric Chloride Hexahydrate (%11-12), acetic acid (%18-20), hydrochloric acid (%44-46), sulfuric acid (%3-4), nitric acid (%3-4) and deionized water (%18-20). The second one composed of hydrochloric acid (%95) and hyrogen peroxide (%5) and employed for some heat treatedspecimens.

4.4.2 Optical microscopy

Microstructural examination was performed using an Eclipse MA200 model (Nikon) inverted metallurgical microscope equipped with Clemex camera and Clemex digital imaging software. Fusion zone, heat affected zone and base material microstructures of welded specimens were determined. The effects of heat treatment on the microstructure of both welded and non welded specimens were examined via optical microscopy.

4.4.3 Scanning electron microscopy (SEM)

Microstructure was also observed using a 15kV HITACHI TM 1000 SEM (seen in Figure 4.9) with backscattered electrons. It shall be noted that higher magnifications providing by SEM result in detecting smaller particles.

4.4.4 XRD analysis

Identification of phases on both weld and base metal was done by using X-Ray diffraction method (XRD). The equipment used during this study as shown in Figure 4.10 is GBC-Emma model and in particular Mo Kα (λ= 0,7093 Å) radiation with 40mA and 40kV paramaters applied.

Figure 4.9 : SEM.

Figure 4.10 : XRD equipment.

4.5 Microhardness Test

The Vickers microindentation hardness was employed for each welded specimens along the middle thicknes using a 422D model (Innovatest) Vickers microhardness machine. The testing load was selected as 200 g. The dwell time of 15s and indentation spacing of 0.2 mm was applied.

4.6 Tensile Testing

Geometry of welded tensile testing samples were determined according to BS EN ISO 4136:2012 Destructive test on weld in metallic materials-Transverse tensile test. In this standard, dimensions are specified depending on the thickness of the plate. Therefore, two different tensile testing geometry was determined regarding 2 and 3.2 mm thick welded sheets. Figure 4.11 and 4.12 represents the test geometries used during this study.

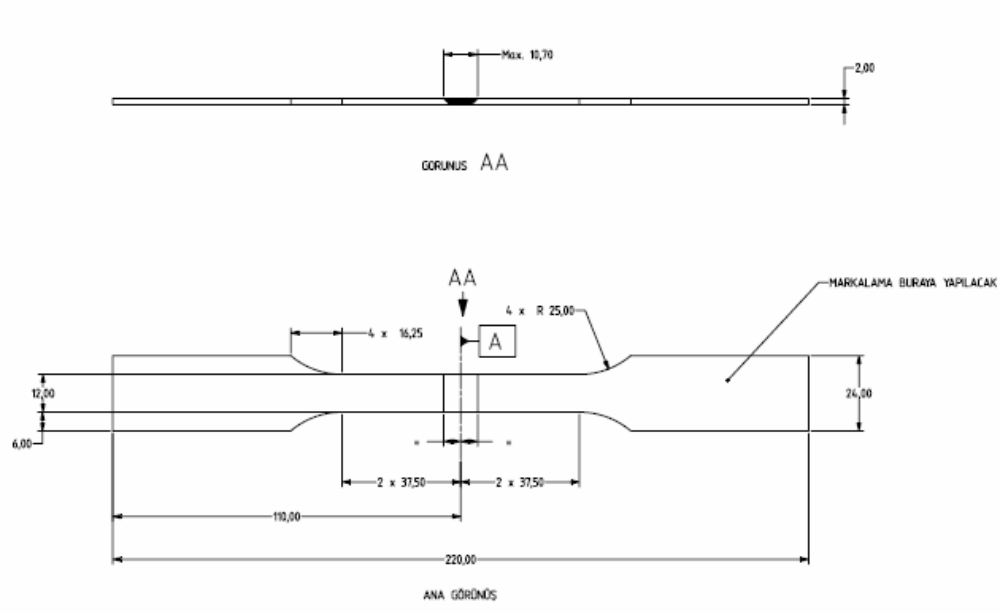

Figure 4.11 : Representative test geometry for 2 mm thick material.

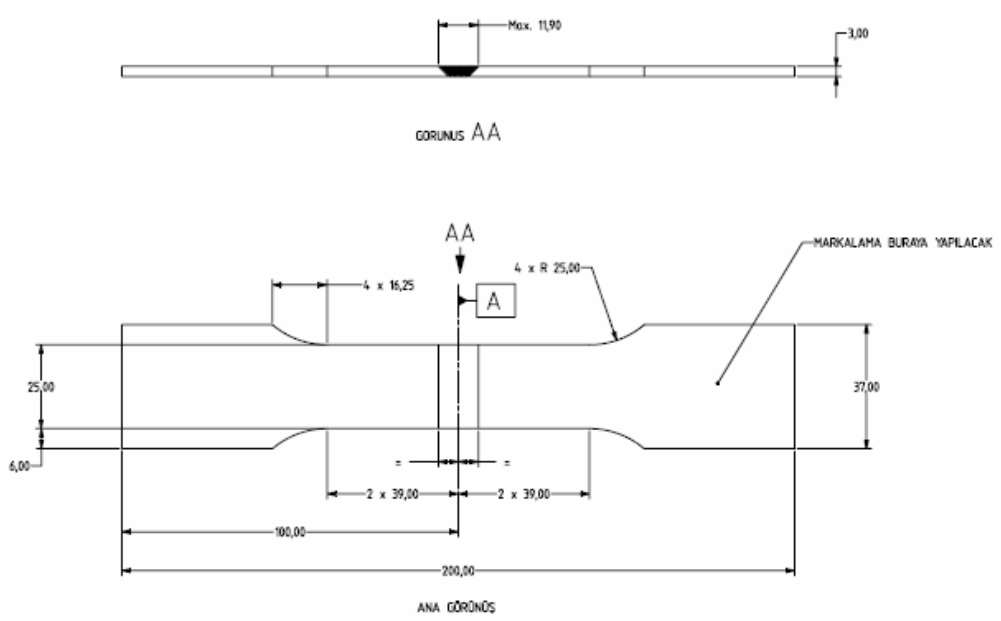

Figure 4.12 : Representitive test geometry for 3,2 mm thick material.

For each weld and post weld heat treatment combination, 4 specimens were machined by CNC milling as represented in Figure 4.14.

Tensile load was applied to test specimen taken transversely from the welded joint. The welds were done perpendicular to rolling direction. The tensile specimens were tested at room temperature using a 25 ton machine as seen in Figure 4.13. The cross-head speed was fixed at 3 mm/min.

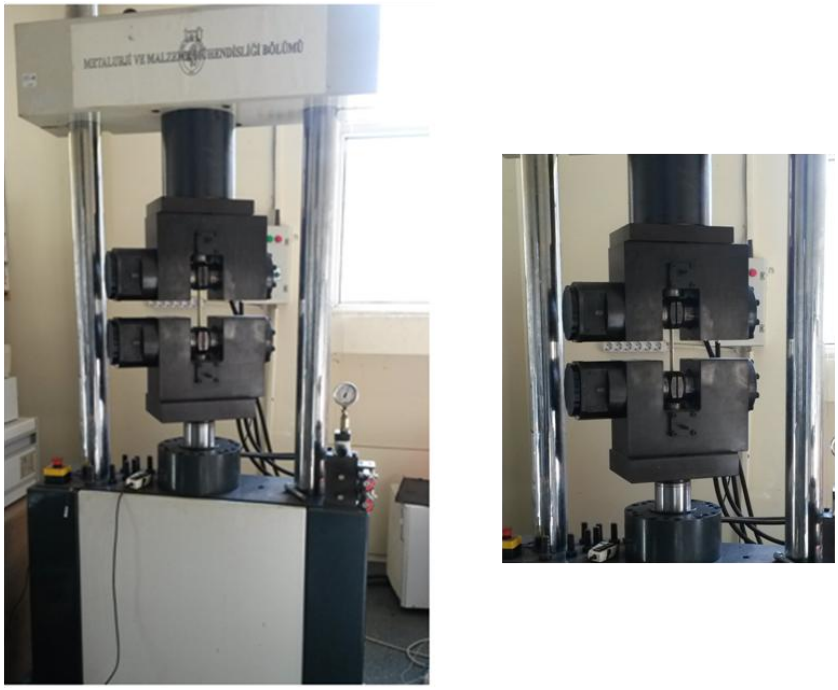

Figure 4.13 : Dartec Tensile testing machine.

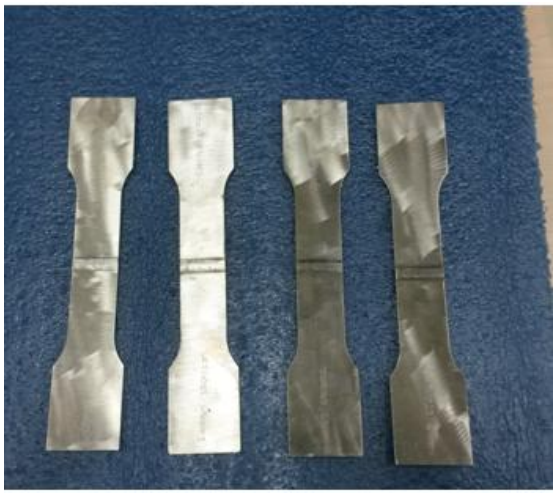

Figure 4.14 : Welded tensile specimens per ISO 4136.

Geometry of base material (non-welded) tensile test specimens were determined according to ASTM E8M - Standard Test Methods for Tension Testing of Metallic

Materials. Sub-size specimens referenced in this standard were machined by CNC milling. The sub-size specimens were tested at room temperature using a 100kN machine as seen in Figure 4.15. The cross-head speed was fixed at 3mm/min.

Figure 4.15: Shimadzu tensile testing machine.

After tensile testing, the fracture surface of tensile tested specimens were examined by using SMZ100 Model Nikon stereomicroscope. The features observed during this examination compared with the following genaral macroscopic appearance of ductile and brittle fractures.

Below characteristics are generally common for ductile fractures [40].

- A considerable amount of plastic deformation prior to the fracture.
- Shear lips are revealed at the fracture termination areas.
- The appearance of fracture surface may be fibrous or may have a matte or sliky texture associated with the material type.
- The cross section at the fracture is usually decreased by necking.
- Crack growth is relatively low.

Below characteristics are generally common for brittle fractures [42].

- Little or no appearent plastic defomation prior the failure.
- The fracture surface is usually flat and normal to the loading direction and to the part surface.
- The appearance of fracture surface may be granular or crystalline and facets may be observed.
- Chevron patterns may be visible.
- Rapid crack growth leads to catastrophic failures.

5. RESULTS AND DISCUSSIONS

5.1 The Microstucture of Base Materials

The Inconel 718 sheets were supplied in solution condition. The as-received microstructure of the base material taken with an optical microscope exhibit typical austenitic matrix with equiaxed grains as seen in Figure 5.1a and 5.2a. The γ grains are a FCC nickel base austenitic continuous phase with solid solution elements such as Co,Cr, Mo and W [19]. The grain size measurement was conducted according to ASTM E112-Standard Test Methods for Determining Average Grain Size specification. Heyn Lineal Intercept Procedure was applied in a way that straight lines with known length were drawn to count the number of grains intercepted. Mean linear intercept length was calculated using equation 5.1.

Mean linear intercept length = Length of test line/Number of intercepts **(5.1)**

As indicated in Table 5.1, corresponding ASTM grain size numbers (G) to calculated mean linear intercept length were obtained using the conversion matrix given in ASTM E 112. It can be stated from Table 5.1 that post weld heat treatments did not resulted in remarkable grain size change. Additionaly, The 2 mm thick sheets in all conditions have sligthly finer grains.

Table 5.1 : Average grain size numbers of 2 mm and 3,2 mm thick Inconel 718 sheets in as-received, direct aged and solution+aged states.

Thickness of sheet	2 mm	3,2 mm
As received	9,5	9
Direct Aged	9,5	9
Solution (980°C)+Aged	9,5	9

Microstructural examination of base material in as received condition also performed under scanning electron microscope (SEM). SEM studies revealed the particular form secondary phases in the microstructure indicated in Figure 5.1b and 5.2b. As previously mentioned in section 3.1, those secondary phases are suggested to be MC type carbides. Carbon in the structure forms these MC type carbides with contribution of Ti or Nb [18].

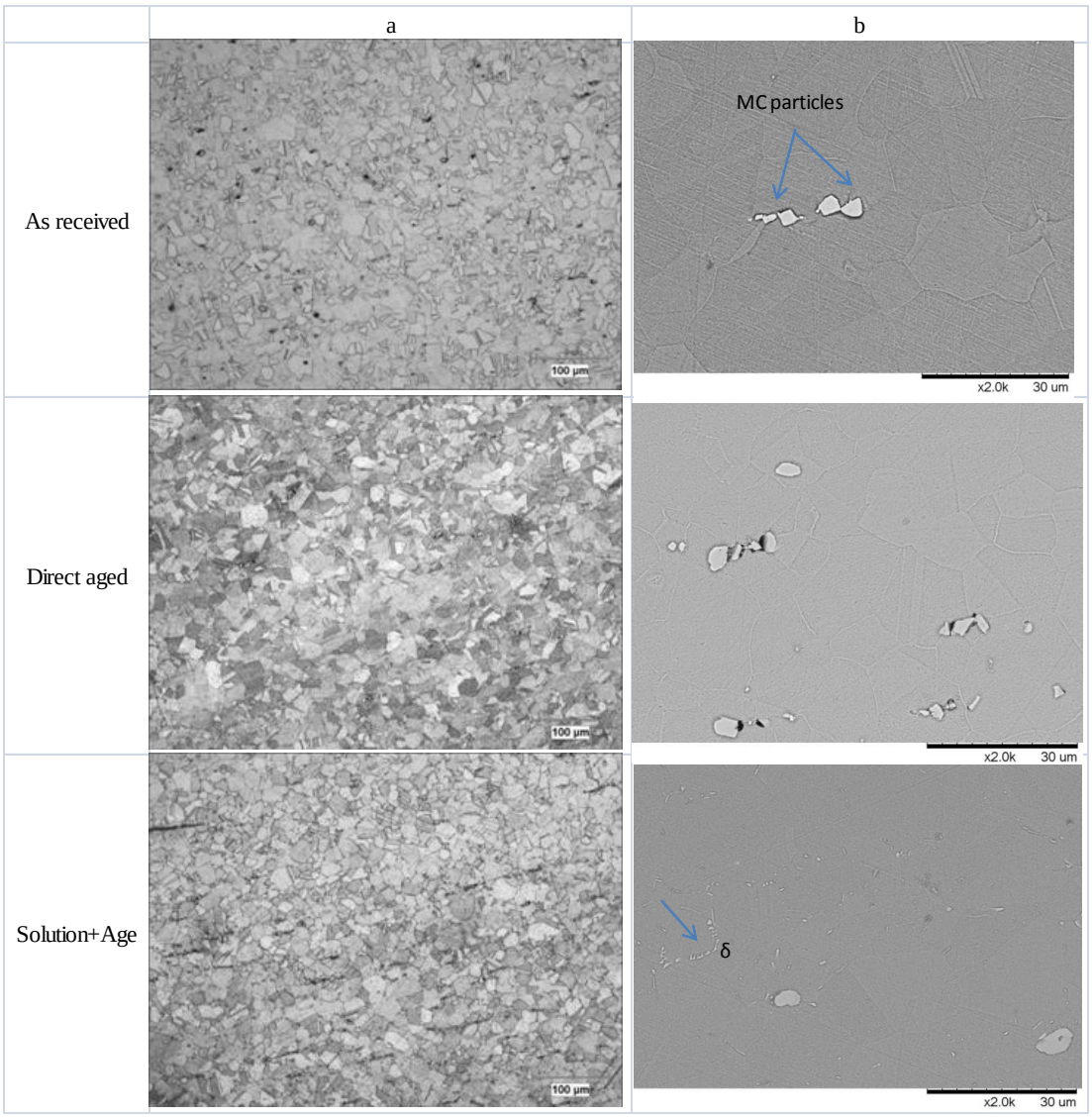

Figure 5.1 : Microstructure of the base material (2 mm) in different heat treatment conditions **(a)** Magnification 200X **(b)** Magnification 2000X.

The solution heat treatment at 980°C seems not to dissolve the carbides. However, formation of different needle-like phase at grain boundaries was observed indicating in Figure 5.1b and 5.2b. The needle-like phase is suggested to be delta (δ) in literature. As explained in section 3.1, Gamma double prime (γ") phase is metastable and under the long time exposure to temperatures higher than 650°C, it can tranform to delta (δ) phase in the form of Ni_3Nb. However, those particles were not detected during XRD analysis as seen in Figure 5.3. It is thought to be due to their lower volume fraction.

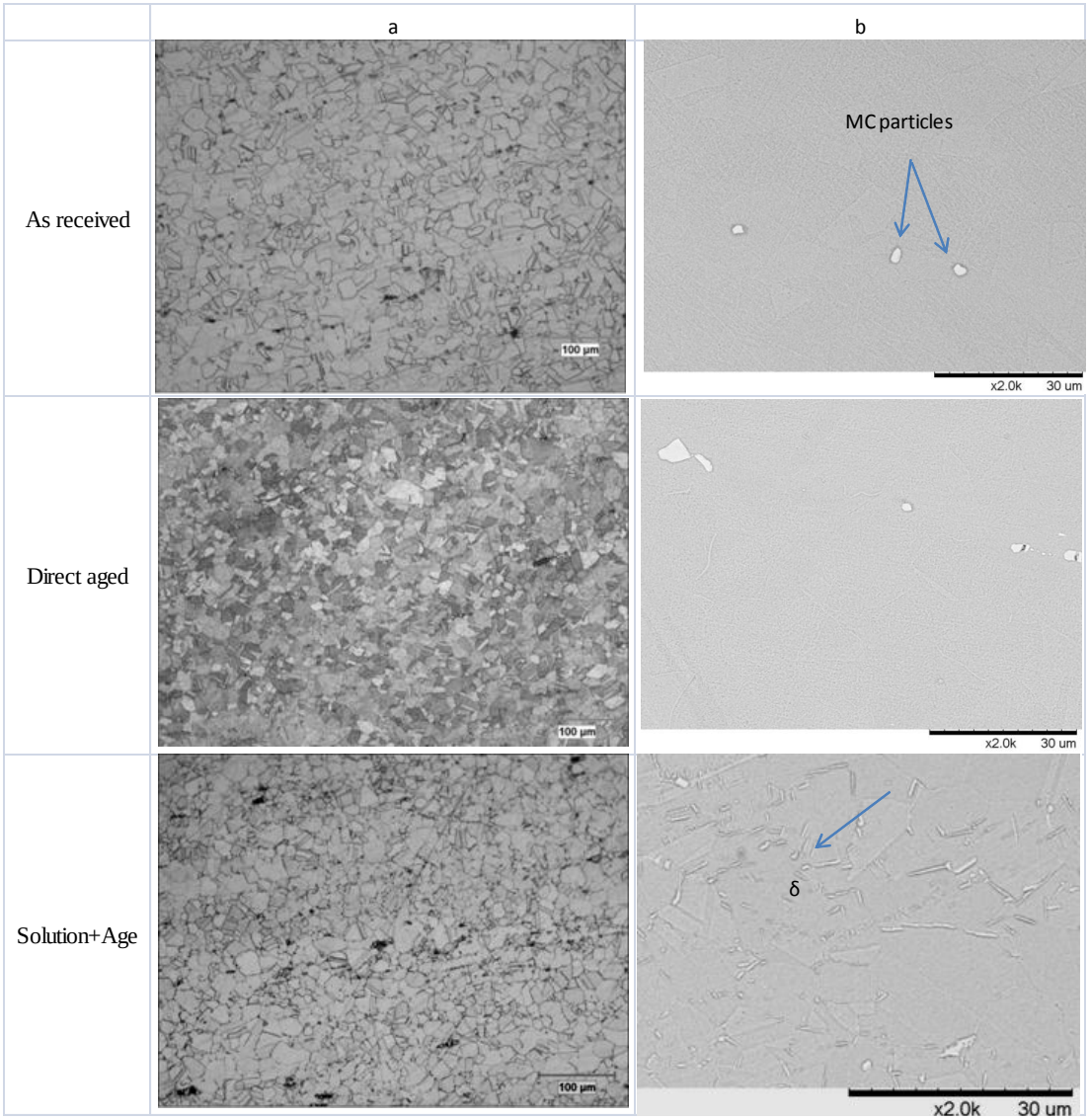

Figure 5.2 : Microstructure of the base material (3,2 mm) in different heat treatment conditions **(a)** magnification 200X **(b)** magnification 2000X.

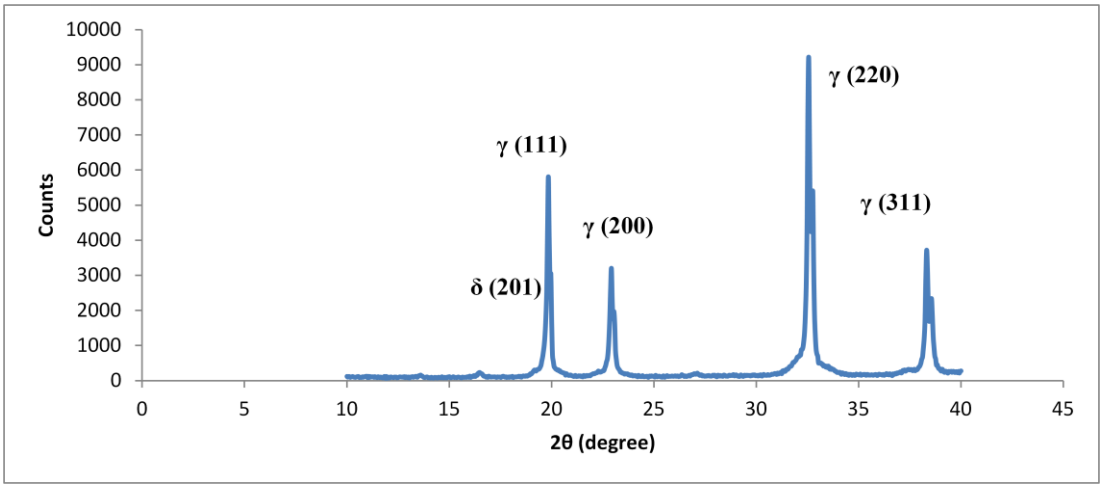

Figure 5.3 : XRD pattern of solution and aged Inconel 718 sample.

Hardness measurements were conducted along the mid-tickness of specimens. Below Table 5.2 summarizes the average hardness values of samples in different heat treatment conditions.

Table 5.2 : Average hardness ($HV_{0,2}$) values of Inconel 718 samples in different PWHT conditions.

Thickness(mm)	PWHT	Average hardness ($HV_{0,2}$)
2	-	232,7 ± 6,6
2	aging	484,6 ± 11,1
2	solution+aging	477,4± 11,9
3,2	-	238,4 ± 9,0
3,2	aging	475,1 ± 13,4
3,2	solution+aging	474,2 ± 13,5

According to Table 5.2, aging and solution+aging heat treatments resulted in nearly 100% increase of hardness levels. In addition, there is no remarkable change on hardness levels in between specimens subjected to different heat treatments. In literature, this hardness increase attributed to precipitation of gamma prime (γ') and gamma double prime (γ") phases. As mentioned in Section 3.2, Inconel 718 is hardened by the precipitation of secondary phases (γ' and γ") into the metal matrix. However, XRD analysis in this study could not detect these precipitates due to their lower volume fraction.

5.2 Structural Features of Weld Regions

5.2.1 Macrostructural examinations

Figure 5.4 represents the macrostructure of butt welded joints of 2 and 3.2 mm thick specimens under different heat treatment conditions. The weld pool shape is developed by the amount of heat transfer from the heat source to the base metal, the travel speed, the nature of fluid flow in the weld pool and the cooling rate. An elliptical weld pool forms at low heat input and slow travel speeds, wheras more elongated, shifting from elliptical to teardrop shaped weld pool results at high heat inputs and high travel speeds [35]. The resultant weld pool geometries given in Figure 5.4a and 5.4b are similar to those elliptical and teardrop shape, respectively which is consistent with their heat inputs per unit length calculated in Section 4.2. Heat input per unit length for 2 mm thick specimens is 192 J/mm and for 3.2 mm thick specimens is 419 J/mm.

It can be stated that weld joints are free from porosities, undercuts, inclusions, lack of fusion and lack of penetration which was also confirmed by NDT (FPI and X-Ray) inspections.

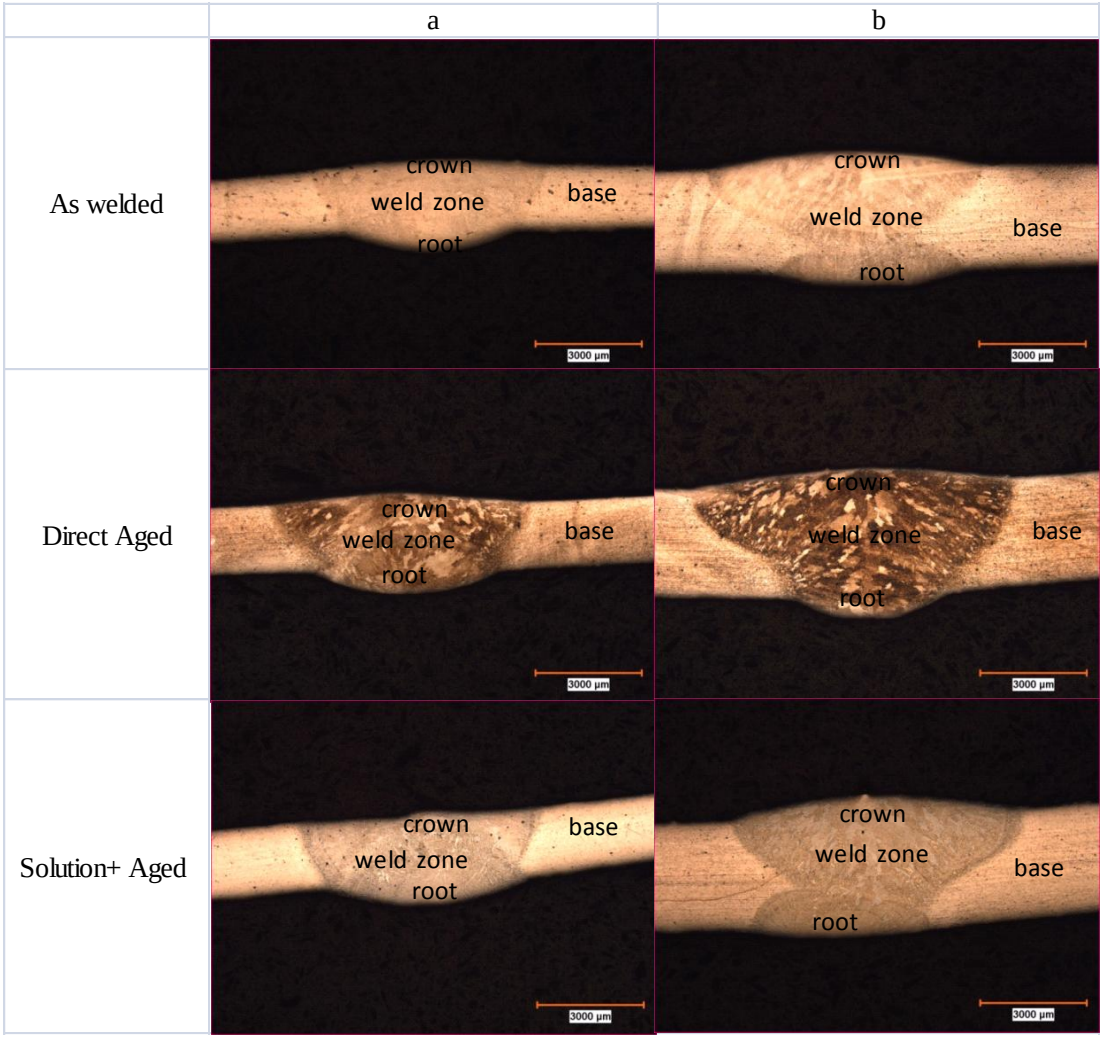

Figure 5.4 : Cross section macrophotos of TIG welded Inconel 718 alloy in different heat treatment conditions with **(a)** 2 mm **(b)** 3,2 mm base material thickness.

Table 5.3 represents the weld bead sizes of different specimens. As it can be seen, the weld crown width increases with increasing heat input asscociated with base material thickness.

Table 5.3 : Average weld bead sizes of specimens.

	Weld Crown Width (mm)	
PWHT	**t:2mm**	**t:3,2 mm**
As welded	6,6	7,8
Direct Aged	7,1	9,1
Solution+ Aged	7,1	8,4

5.2.2 Microstructural examinations

As Welded Specimens (No PWHT)

This group of specimens examined as welded condition with no subsequent heat treatment. During the solidification of an alloy the S/L interface and the mode of solidification can be planar, cellular or dendritic based on the solidification condition and the material nature [35]. Inconel 718 solidifies in a dendritic mode. The dendrites extend from the fusion zone boundary to the weld center [19]. Figure 5.5 represents the microstructure of weld transverse section as welded condition with no subsequent heat treatment. The dendrites in the weld fusion zone is appeared to be equiaxed while columnar dendrites seen close to the fusion boundary. There are some coarse equiaxed dendrites in weld center while modifying to be finer towards the root side due to rapid cooling.

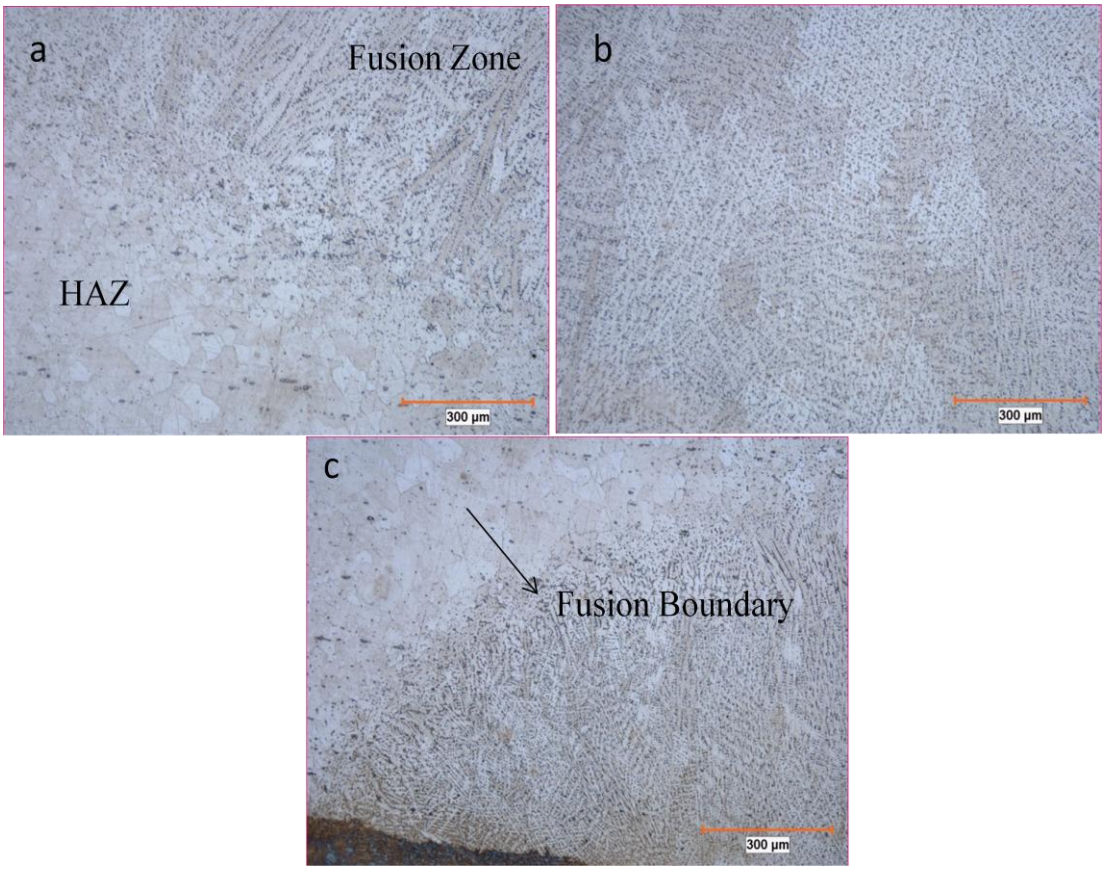

Figure 5.5 : Microstructure of weld transverse section as welded condition **(a)**Fusion zone and HAZ **(b)** Equiaxed dendrites in the weld interior **(c)** Columnar dendrites adjacent to the fusion boundary and very fine equiaxed dendrites in fusion zone at root side.

Figure 5.6 represents the solidification mode variances from planar to cellular, to columnar dendritic and to equiaxed dendritic according to the increase in degree of

constitutional supercooling. The region where columnar or equiaxed dendrites and the liquid phase exist together is named the mushy zone. It is to be noted that a a very high degree of constitutional supercooling, the mushy zone can be widen that makes easier for equiaxed dendrites to nucleate rather than for columnar dendrites to extend along the mushy zone [35].

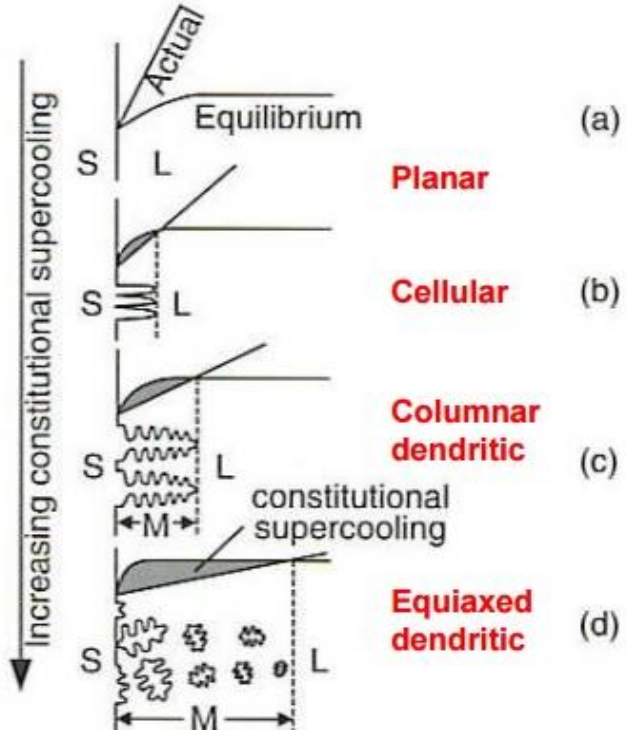

Figure 5.6 : Effect of constitutional supercooling on solidification mode **(a)** planar **(b)** cellular **(c)** columnar dendritic **(d)** equiaxed dendritic (S, L and M refers to solid, liquid and mushy zone).

The effect of temperature gradient G and the growth rate R on the solidification microstructure of alloys is schematized in Figure 5.7. The ratio G/R determines the mode of solidification wheras the the product GR determines the size of the solidification structure [35].

As seen in Figure 5.5, the weld microstructure changes from the fusion boundary to the middle of fusion zone such that columnar to equiaxed dendrites. The growth rate is less along the fusion boundary rather than the fusion zone. Maximum temperature is expected to be in the weld centerline and then decrease towards the fusion boundary. Thus, temperature gradient is highest at at the fusion boundary and less at the weld center.

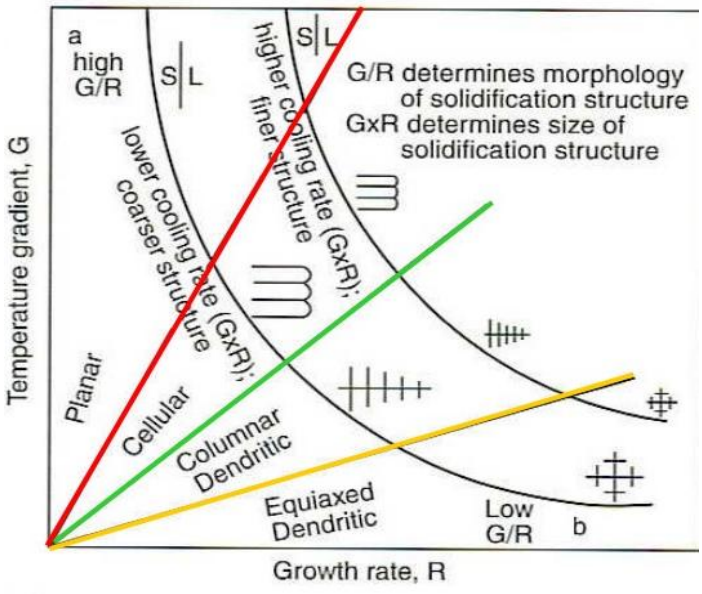

Figure 5.7 : Effect of temperature gradient G and growth rate R on the morphology and size of the solidification microstructure [35].

HAZ is located in the region adjacent to the fusion boundary and subjects to high tempearatures without melting. However, the microstructure influences from these thermal cycles and differ from base material in terms of microstructure. As given in Figure 5.8, HAZ region consists of different subzones. There are two HAZ regions including coarse grained HAZ and fine grained HAZ regarding Inconel 718 welds [32].

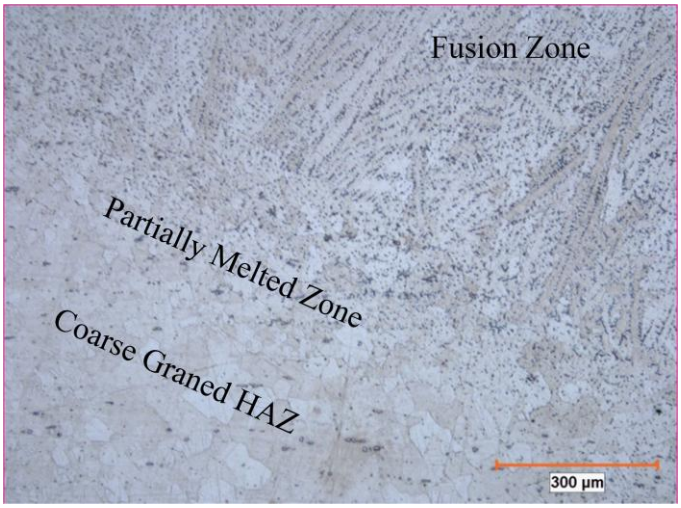

Figure 5.8 : Microstructure of weld transverse section indicatig PMZ and coarse-grained HAZ.

The average coarse grained HAZ width of as-welded specimens measured as 0,47 and 0,57 mm for 2 and 3,2 mm thick specimens, respectively. It can be thought that

HAZ width depend on the heat input per unit length. Grain growth is not an issue for fine-grained region directly adjacent to the fusion boundary due to grain boundary segragation and the subsequent pinning of the grains. However, grain growth cannot be limited via these mechanisms as the temperature is lower in the latter subzone [32]. The fine grained HAZ could also be referred to as Partially Melted Zone (PMZ) due to incipient melting/liquation of the grain boundaries [32].

At higher magnifications during SEM studies, irregular-shaped particle form secondary phase observed in interdendritic regions in Figure 5.9a. As mentioned in Section 3.3, it is suggested to be Laves particles. The formation of Laves phase is due to to microsegragation of high atomic diameter alloying elements such as niobium, titanium and molybdenum under the non-equilibrium solidification conditions during welding. The form of Laves phase is introduced as $(Ni,Fe,Cr)_2(Nb,Mo,Ti)$ and differ from other phases in Inconel 718 material system with its high niobium concentration. Laves phase appeared to be white in SEM secondary images due to higher emission of electrons from Laves phase [19].

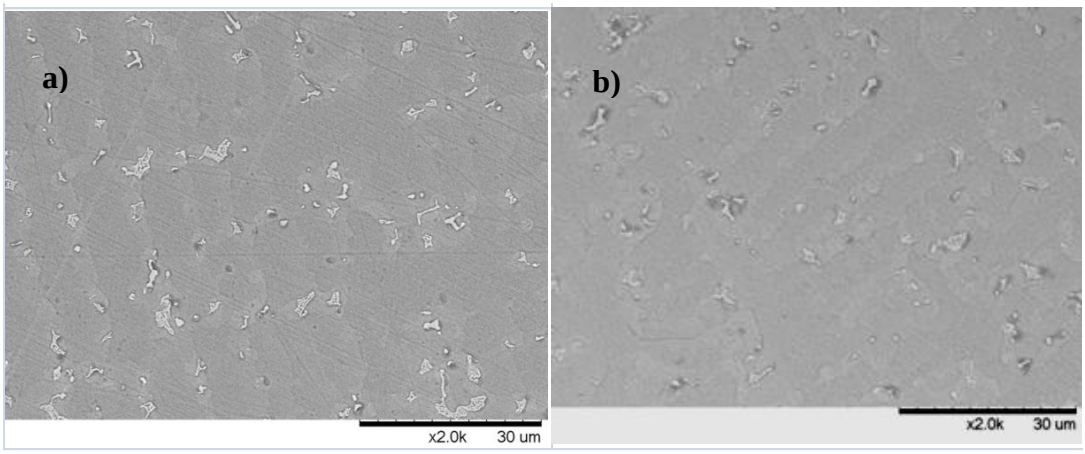

Figure 5.9 : SEM microstructure of the weld fusion zone for as-welded condition **(a)** 2mm thick specimens **(b)** 3,2 mm thick specimens.

In addition, spot analysis by utilizing SEM equipped EDS (Energy Dispersive Spectrometer) performed to evalute weight % of elements inside these secondary particles. At least three different particles and two analysis per particle were done for repetitive results. According to results below in Figure 5.10, The secondary particles were found to be rich in Nb, Ti, Mo and lean in Ni, Fe and Cr compared to the the base material composition. As it is explained in Section 3.3, formation of Laves phase requires Nb concentration in between 10%-30% [30,41]. The Nb concentration of the particle inside the 2 and 3,2 mm thick specimens were found as 29,24 % and

27,98%, respectively. Nb concentration of Laves phase is dependent on solidification condition which affects the extent of Nb segragation [41].

	2 mm	3,2 mm
SEM (5000X)	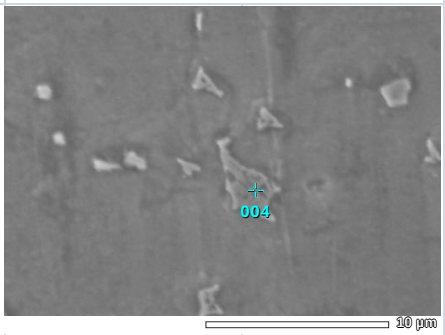	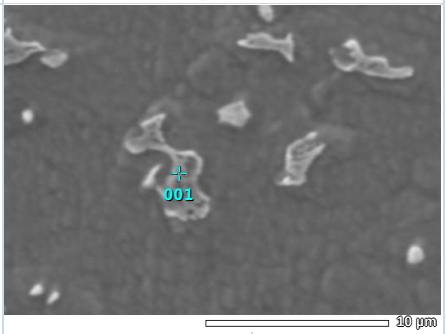
EDS (spot analysis)	Element / Wt. % / At. Ni 39,07 43,35 Nb 29,24 20,50 Cr 12,41 15,55 Fe 12,11 14,13 Mo 5,32 3,61 Mn 0,10 0,12 Ti 1,39 1,90 Al 0,35 0,84	Element / Wt. % / At. Ni 40,70 45,23 Nb 27,98 19,65 Cr 12,41 15,57 Fe 10,73 12,54 Mo 6,30 4,29 Mn 0,08 0,09 Ti 1,64 2,24 Al 0,16 0,39

Figure 5.10 : SEM energy dispersive microanalysis of fusion zone.

Post-weld Heat Treated Specimens

a)Direct aged

This group of specimens subjected to direct aging after welding explained before in section 4.3. As seen in Figure 5.11, the microstructure of direct aged specimens also reveals the equiaxed dendritic structure at fusion zone with partially melted zone adjacent to fusion boundary and coarse grained HAZ near unaffected base material.

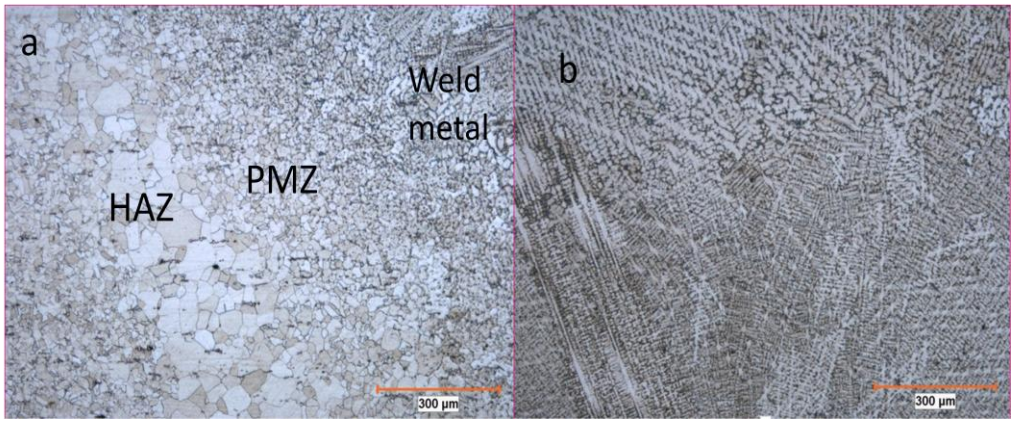

Figure 5.11 : Microstructure of weld transverse section welded and post weld direct aged condition **(a)** Fusion boundary and HAZ **(b)** Equiaxed dendrites in the weld interior.

The coarse grained HAZ width was measured 0,35 and 0,45 mm for 2 and 3,2 mm thick specimens, respectively. It is consistent with their heat inputs per unit length. It can be thought that direct aging heat treatment did not modify the weld microstructure based on microstructures in Figure 5.11. Microstructure in direct aging condition was similar to those in as-welded condition in terms of subzones, but slightly different in terms of HAZ widths.

At higher magnifications during SEM studies, bright etching irregular-shaped secondary particles were also observed in the interdendritic regions as shown in Figure 5.12. As mentioned in Section 3.3, it is suggested to be Laves particles.

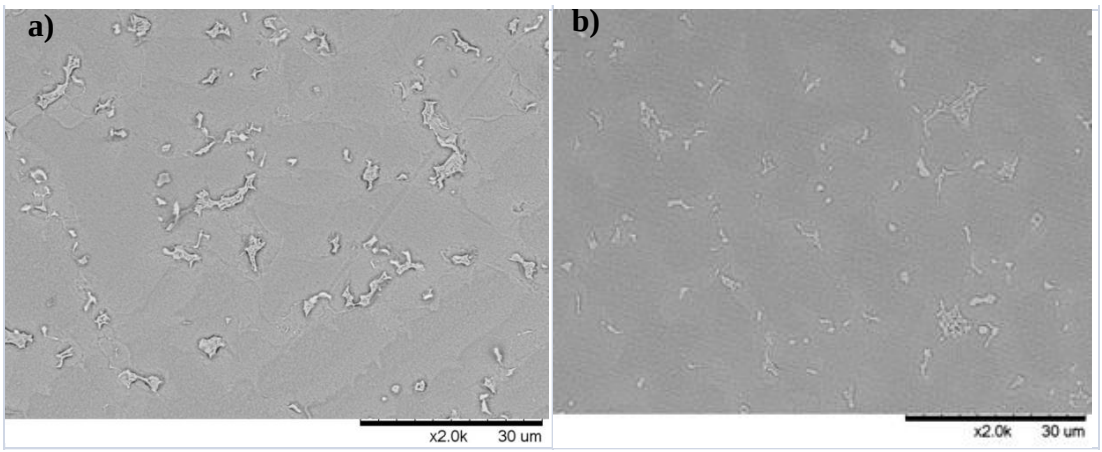

Figure 5.12 : SEM microstructure of the weld fusion zone for direct aged condition **(a)** 2mm thick specimens **(b)** 3,2 mm thick specimens.

In addition, spot analysis by utilizing SEM equipped EDS (Energy Dispersive Spectrometer) performed to evalute % weight of elements inside these secondary particles. At least three different particles and two analysis per particle were done for repetitive results. According to results below in Figure 5.13, the secondary particles were found to be rich in Nb, Ti, Mo and lean in Ni, Fe and Cr compared to the the base material composition. The Nb concentration of particles inside 2 and 3,2 mm thick specimens were obtained as 25,08% and 27,74%, respectively. The Nb concentration of Laves particles are comparable with the ones in as-welded condition. It can be interpreted that post weld direct aging heat treatment did not modify the Laves phase.

	2 mm	3,2 mm
SEM (5000X)	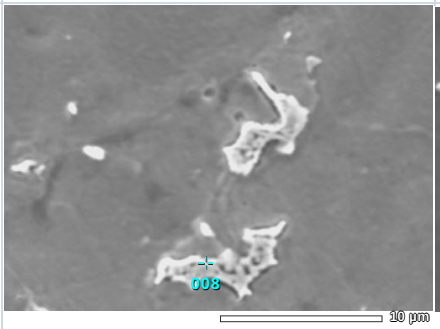	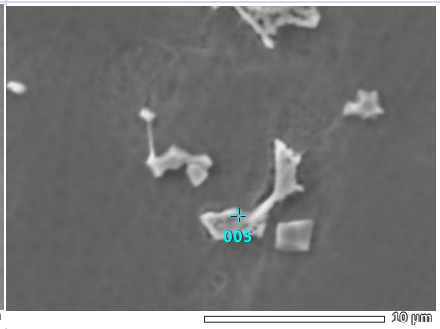
EDS (spot analysis)	Element / Wt. % / At. Ni 41,33 45,19 Nb 25,08 17,32 Cr 13,76 16,99 Fe 12,01 13,81 Mo 5,79 3,87 Mn 0,32 0,38 Ti 1,55 2,07 Al 0,16 0,37	Element / Wt. % / At. Ni 37,30 41,48 Nb 27,74 19,50 Cr 13,78 17,30 Fe 12,10 14,15 Mo 7,13 4,85 Mn 0,22 0,26 Ti 1,63 2,22 Al 0,10 0,24

Figure 5.13 : SEM energy dispersive microanalysis of fusion zone.

b)Solution Treated and Aged

This group of specimens subjected to solution heat treatment (980°C) and aging after welding explained before in section 4.3. As seen in Figure 5.14, the microstructure of solution treated at 980°C and aged specimens also reveals the equiaxed dendritic structure at fusion zone with partially melted zone adjacent to fusion boundary and coarse grained HAZ near unaffected base material.

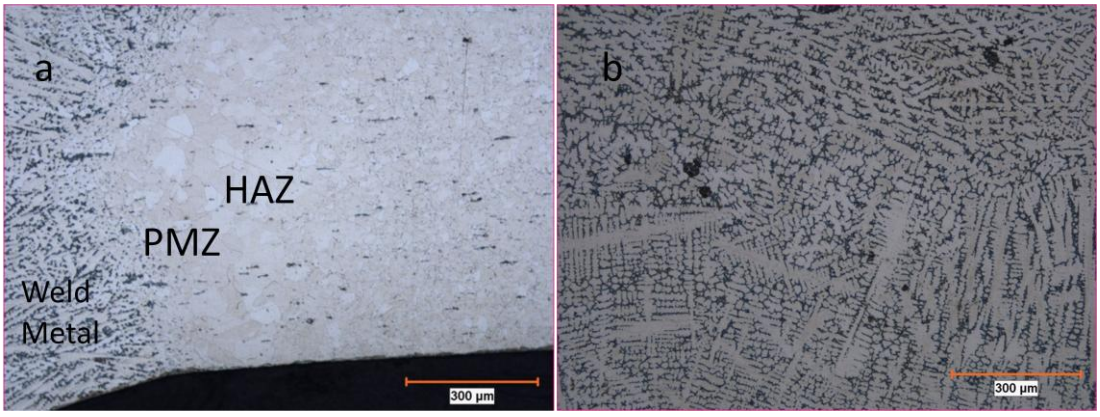

Figure 5.14 : Microstructure of weld transverse section welded and post weld solution and aging HT condition **(a)** Fusion boundary and HAZ **(b)** Equiaxed dendrites in the weld interior.

The coarse grained HAZ width was measured 0,28 and 0,37 mm for 2 and 3,2 mm thick specimens, respectively. It is consistent with their heat inputs per unit length. It

can be thought that solution heat treatment at 980 °C and aging did not alter the weld microstructure based on microstructures in Figure 5.14. Microstructure in solution and aged condition was similar to those in as-welded condition in terms of subzones, but slightly different in terms of HAZ widths.

At higher magnifications during SEM studies, bright etching irregular-shaped secondary particles with precipitated needle-like particles around them were observed in the interdendritic regions as shown in Figure 5.15. As mentioned in Section 3.3, irregular shaped secondary particles are suggested to be Laves phase. Moreover, the needle-like phase around Laves particles is suggested to be delta in literature [41]. The delta phase is an equilibrium Ni_3Nb precipitate which requires 6-8% Nb and precipitates in between 860-995°C [41].

According to SEM images in Figure 5.15, It can be interpreted that solution heat treatment at 980 °C and then aging resulted in partially dissolution of Laves particles and precipitation of needle-like δ phase around the Laves particles in interdendritic regions. In addition, spot analysis by utilizing SEM equipped EDS (Energy Dispersive Spectrometer) performed to evalute % weight of elements inside these secondary particles. At least three different particles and two analysis per particle were done for repetitive results. The Nb concentration of particles inside 2 and 3,2 mm thick specimens were found as 27,92% and 24,40%, respectively as seen in Figure 5.16. This is consistent with SEM images that the undissolved Laves phase still exist in many of the delta clusters in the fusion zone.

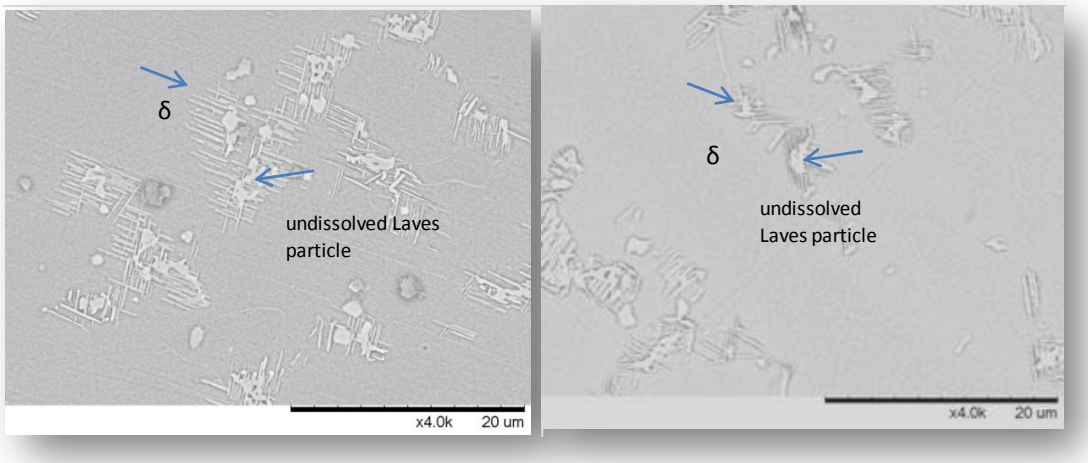

Figure 5.15 : SEM microstructure of the weld fusion zone for solution+aged condition **(a)** 2mm thick specimens **(b)** 3,2 mm thick specimens.

As explained in literature, Post-weld solution heat treatments performed at delta formation temperature range, delta phase precipitates in regions of moderate Nb concentration around the Laves particles. Since Laves dissolution take place at the same time during the heat treatment, some amount of Nb released into surroundings which provides more Nb for delta precipitation [41].

	2 mm	3,2 mm
SEM (5000X)	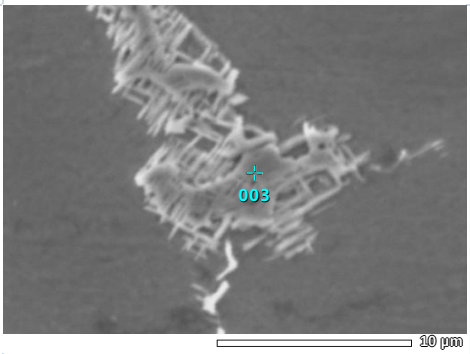	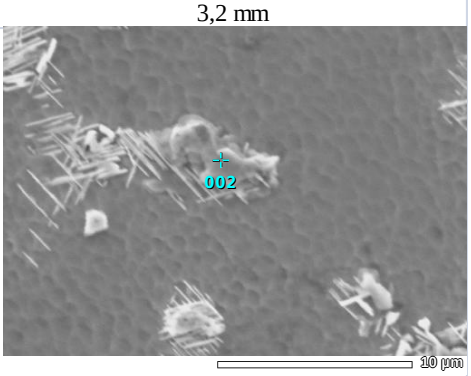
EDS (spot analysis)	Element / Wt. % / At. Ni 44,71 50,47 Nb 27,92 19,92 Cr 8,73 11,13 Fe 7,98 9,48 Mo 8,41 5,81 Mn 0,10 0,12 Ti 2,04 2,83 Al 0,10 0,25	Element / Wt. % / At. Ni 42,03 46,12 Nb 24,40 16,92 Cr 11,99 14,85 Fe 10,77 12,42 Mo 7,88 5,29 Mn 0,50 0,58 Ti 1,94 2,61 Al 0,50 1,20

Figure 5.16 : SEM energy dispersive microanalysis of fusion zone.

5.3 Microhardness

The Vickers microhardness ($HV_{0,2}$) measurements were performed along the mid-thickness of welded specimens with 0,2 mm indentation spacing. The average results of hardness test in three different zones namely fusion zone, heat affected zone and base material along the middle thickness of the cross section in as-welded and post weld heat treated condition were represented in Table 5.4. The hardness distribution through the section is also included in Appendix A.

The fusion zone and HAZ hardness in as-welded condition considering both thickness is similar to that base material hardness in same heat treatment condition. Comparable hardness values in fusion zone, HAZ and base material in as-welded condition are explained in literature that precipitation of γ" and γ'did not occur during weld metal cooling [41].

Table 5.4 : Average results of microhardness measurements.

Average hardness results (HV 0,2)				
Thickness(mm)	**PWHT**	**FZ**	**HAZ**	**BM**
3,2	-	241,7± 7,7	243,1± 4,4	238,4 ± 9,0
3,2	solution+age	452,4 ± 19,4	474,2 ± 15,6	474,2 ± 13,5
3,2	aging	422,4 ± 17,5	465,5 ± 17,9	475,1 ± 13,4
2	-	224,6 ± 4,2	228,7 ± 4,7	232,7 ± 6,6
2	solution+age	448,8± 15,5	476,7± 13,5	477,4± 11,9
2	aging	444,5 ± 16,8	479,7 ± 12,0	484,6 ± 11,1

The base material in solution treated condition (as-received) considering both thickness has average hardness values of ≈230-240 HV. The PWHT cycles that is either solution+age or direct aging heat treatment made the hardness values increase up to twice of the base material's such that ≈470-480 HV as seen in Table 5.4. It can be stated that post weld heat treatments have resulted in significiant increase in the hardness levels in all three zones. As mentioned in Section 3.1, the hardness increase is due to precipitation of γ"(gamma double prime) and γ'(gamma prime) phases.

Fusion zone hardness is approximatey %5 lower than HAZ and base material hardness for all post weld heat treated specimens. This difference between weld metal and base material after PWHT is attributed to the amount of γ" precipitation in literature [41].

Formation of Laves phase in fusion zone deplates the Nb content in the structure which in turn decreases the amount of principal strengthening phase (γ") precipitation.

HAZ hardness and base material hardness is comparable all conditions. It can be thought that HAZ did not suffer any undesirable microstructural changes.

5.4 Tensile Properties

Room temperature tensile tests of welded specimens were performed in servohydraulic universal tensile testing machine which was shown in Figure 3.14. In addition, base material tensile tests in exactly same heat treatment condition were conducted for comparison. As seen in Table 5.5 and Table 5.6, tensile specimens were examined after test for the failure locations.

One off four tensile specimens in the as welded condition having 2mm thickness and one off four tensile specimens in the 980°C solution treated and aged condition having 3,2 mm thickness were fractured in the fusion zone. All other tensile specimens were fractured in the base material (BM). It should be noted that no failure at the fusion zone has been detected for the direct aged samples regardless of the thickness

Table 5.5 : Welded tensile test specimens with failure locations.

PWHT	Thickness: 2 mm	Failure location
As-welded		Fusion zone
		BM
		BM
		BM
Solution+Age		BM
		BM
		BM
		BM
Direct age		BM
		BM
		BM
		BM

PWHT	Thickness: 3,2 mm	Failure location
As-welded		BM
		BM
		BM
		BM

Solution+Age	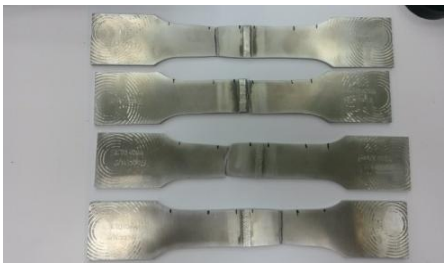	BM
		Fusion zone
		BM
		BM
Direct age		BM
		BM
		BM
		BM

To investigate fracture surfaces of specimens failed in fusion zone, below pictures in Figure 5.17 acquired with stereomicroscope. The deformation seems to initiate from surface through the section.

The reason for surface initiation of fracture can be associated with the geometry of the weld crown. It was already confirmed with X-ray inpections that there is no internal defects in the weld regions. Possible initiation regions are shown by arrows in below Figure 5.17.

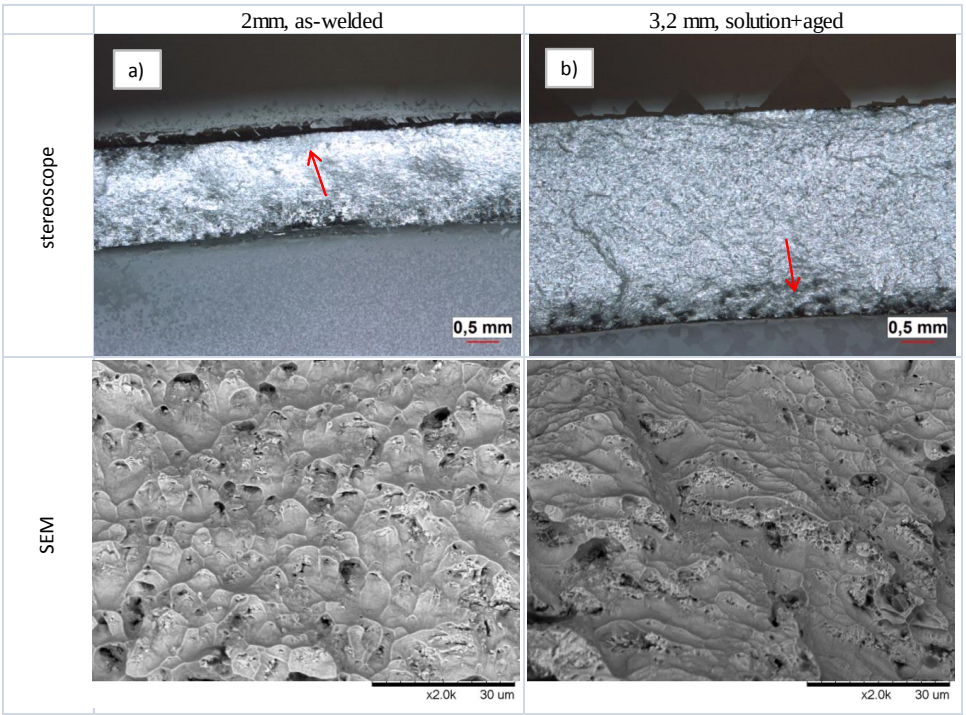

Figure 5.17 : Fracture surface macrophotos and SEM images **(a)** As-welded, 2mm thick specimen **(b)** Solution+aged, 3,2 mm thick specimen.

Cross sections of specimens failed in fusion zone further examined microscopically for weld region and fracture characteristics. Figure 5.18 represents the weld cross section condition of 2 mm specimen failed from fusion zone. As seen in Figure 5.18, The fracture section represents the characteristics of ductile intergranular fracture with dimple morphology. In addition, It is revealed that matrix and secondary particles (Laves phase) separated from interface. The possible reasons have been thought that matrix deforms easily as it is softer than the secondary particles in structure while the hard secondary particles cannot deform as much as with matrix. Thus leads to interface separation detected in SEM image. This also explained in literature that The presence of Laves particles inside the dimples on fracture surface shows that microvoids were initiated at the Laves/matrix interface [41].

Figure 5.19 represents the weld cross section condition of 3,12 mm thick specimen failed from fusion zone. As seen in Figure 5.19, The fracture section represents the characteristics of brittle intergranular fracture. The matrix in solution heat treated and aged condition is harder and could not deform easily. This is the possible reason of intergranular brittle fracture taken place preferentially through the secondary particles (Laves and delta phase) at grain boundaries.

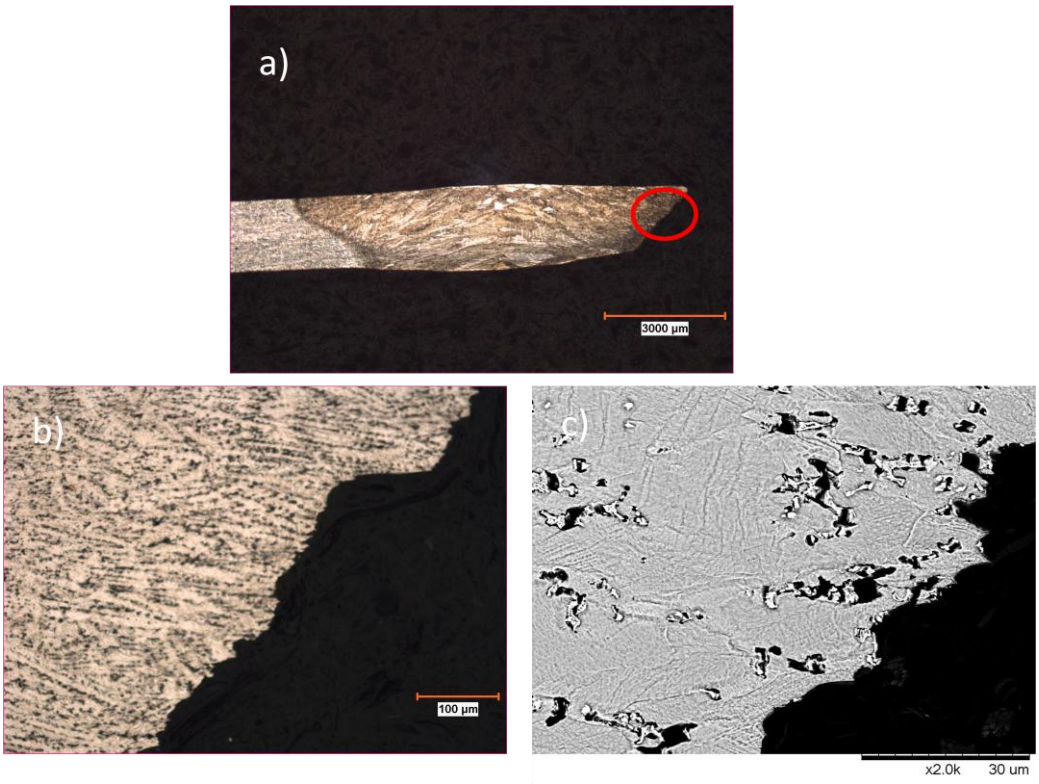

Figure 5.18 : Cross sections of weld region after tensile testing **(a)** and **(b)** Micrographs at 20X and 200X **(c)** SEM image at 2000X.

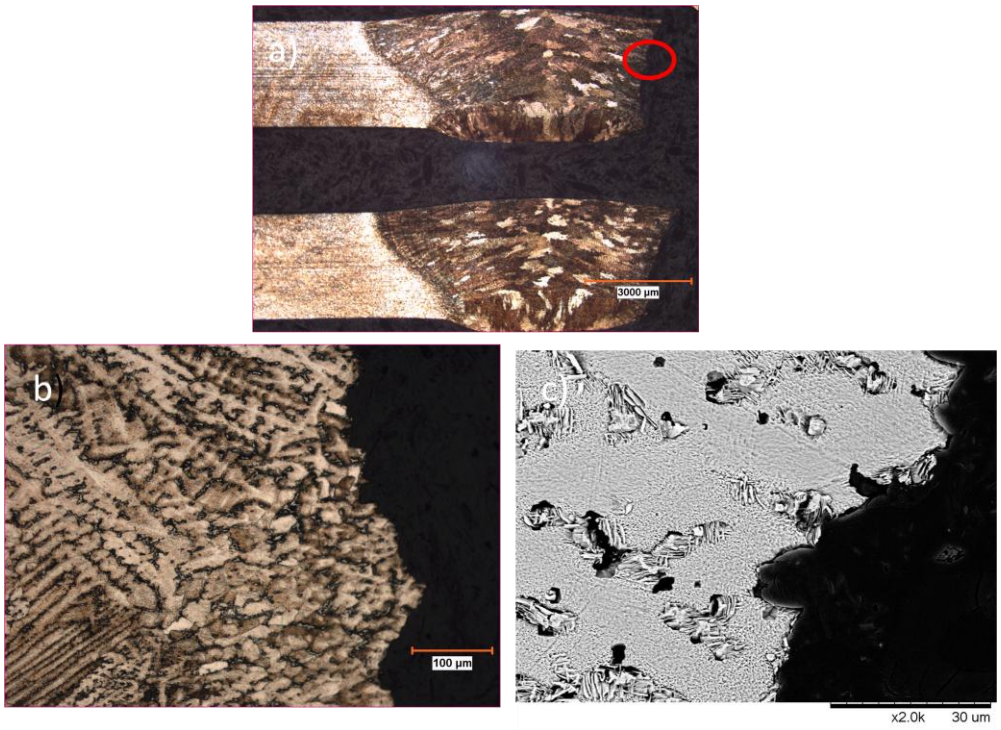

Figure 5.19 : Cross sections of weld region after tensile testing **(a)** and **(b)** Micrographs at 20X and 200X **(c)** Taken by SEM at 2000X.

As explanined in literature, the amount and morphology of Laves phase significantly influence the fracture process: the lower amount and fine, discrete particle morphology of Laves phase better than higher amount and coarse interconnected particle morphology [41].

The tensile test results of all welded and base material specimens evaluated and following results obtained:

- Both post-weld heat treatments increased the yield strength up to 150%, UTS up to 60% wheres decreased the ductility down to 140%.
- The yield strength and ductility of solution+aged and direct aged welded specimens are almost in the same range. The differences between yield strength and ductlity are found to be lower than 5%. However, almost identical tensile strength values were obtained from the solution+aged and direct aged specimens.

When the mechanical properties of welded samples and original samples are compared, following conclusions can be made.

- For 2 mm thick sheets : The difference of yield strength, tensile strength and ductility in same heat treatment conditions are lower than 5%. It is negligible.
- For 3,2 mm thick sheets : The difference of yield strength and ductility in same heat treatment conditions is more than 10%, whereas tensile strength is lower than 5%.

Due to the difference between two group (having different thickness) in terms of degradation of tensile properties, weld cross sections have been microscopically checked after welding. The sampler micrographs are attached in Appendix B. The width of weld crown found to be elongated about 10% for the 3,2 mm thick specimens while no remarkable elongation for 2 mm thick specimens was identified.

The observations indicate that deformation was started from fusion zone where hardness is lowe than the base material. This is consistent with inferior tensile properties (10% reduction in yield point) of welded 3,2 mm specimens compared to base material in same heat treatment conditions.

However, fusion zone deformation is not an issue for 2mm thick specimens having no weld crown elongation. Thefore, it is suggested that deformation

started from any region away from fusion zone so that almost identical yield points were obtained with original samples and welded samples.

6. CONCLUSIONS

This study investigated the effects of post-weld heat treatment on the microstructure and mechanical properties of TIG welded 2 and 3,2 mm thick Inconel 718 sheets.

The main conlusions include :

- Solution heat treatment at 980±10°C resulted in formation of needle-like delta (δ) phase at grain boundaries of Inconel 718.
- Sound welds readily achieved by joint design and selected TIG weld paramaters for both thickness.
- The resultant weld pool geometry of 2 mm thick specimen was similar to elliptical shape while weld pool geometry of 3,2 mm thick specimen was elongated shifting from elliptical to teardrop shape which are consistent with their heat inputs per unit length.
- Microstructure of weld transverse section consist of dendritic form fusion zone, HAZ and unaffected base material. HAZ includes two subzones namely coarse grained HAZ and partially melted zone (PMZ).
- The width of weld crown and HAZ increased with increasing heat input.
- It was observed during SEM studies that Laves phase was formed in fusion zone due to segregation of niobium during solidification. The high niobium concentration (up to 25%) in Laves particles was confirmed with EDS analysis.
- Post weld aging heat treatment did not dissolve the Laves phase. However, solution heat treatment at 980±10°C partially dissolve the Laves phase and results in precipitation of delta (δ) phase around Laves particles.
- Post weld heat treatmant increased the hardness levels of all three zones namely fusion zone, HAZ and base material. The hardness levels are identical

in HAZ and base material while fusion zone found to be approximately 5% softer.

- Comparable hardness values in fusion zone, HAZ and base material in as-welded condition could reflect that precipitation of γ" and γ'did not occur during weld metal cooling.
- Fusion zone hardness is lower than HAZ and base material hardness for all post weld heat treated specimens. This difference between weld metal and base material after PWHT can be attributed to the amount of γ" precipitation.
- Tensile testing was performed to original samples and welded samples. Two samples as-welded (2 mm thick sheet) and solution+aged (3,2 mm thick sheet) conditions fractured from fusion zone during tensile testing. Fracture regions were further examined and found that microvoids were initiated at the Laves/matrix interface.
- It is obtained that both post-weld heat treatments increased the yield strength up to 150%, ultimate tensile strength up to 60% wheras decreased the ductility down to 140%.
- The yield strength and ductility of solution+aged and direct aged welded specimens are almost in the same range. The differences between yield strength and ductility are found to be lower than 5%. However, almost identical ultimate tensile strength values were obtained from the solution+aged and direct aged specimens.
- When the mechanical properties of welded samples and original samples in 2 mm thick samples are compared, It was concluded that the difference of yield strength, tensile strength and ductility in same heat treatment conditions are negligible. Deformation was started from any region away from fusion zone so that almost identical yield points were obtained with original samples and welded samples.
- When the mechanical properties of welded samples and original samples in 3,2 mm thick samples are compared, It was concluded that the difference of yield strength and ductility in same heat treatment conditions is more than 10%, while tensile strength is lower than 5%. Deformation was started from

fusion zone where hardness is lower than the base material. This is consistent with inferior tensile properties (10% reduction in yield point) compared to base material.

REFERENCES

[1] Gustafsson, D. (2012). High Temperature Fatigue Crack Propagation Behavior of Inconel 718 (Doctoral dissertation). Retrieved from Linköping Studies in Science and Technology. (No. 1487)

[2] Pollock, T. M., and Tin, S. (2006). Nickel-Based Superalloys for Advanced Turbine Engines: Chemistry, Microstructure, and Properties. *Journal of Propulsion and Power*, Vol. ***122***, no. 2, pp. 361-374.

[3] Andersson, J. (2011). Weldability of Precipitation Hardening Superalloys – Influence of Microstructure, PhD Thesis, Chalmers University of Technology, Göteborg, Sweden.

[4] Donachie, M. J., and Donachie S, J. (2002). *Superalloys- A Technical Guide, Second Edition,* ASM International.

[5] Thomas, A., El-Wahabi, M., Cabrera, J. M., Prado, J. M. (2006). High temperature deformation of Inconel 718. *Journal of Materials Processing Technology*, *177*, 469-472.

[6] Fisk, M., and Lundback, A. (2012). Simulation and validation of repair welding and heat treatment of an alloy718 plate, *Finite Elements in Analysis and Design*, 58, 66-73.

[7] De, A. (2012). Trends in Joining Aerospace Materials, *4th Indo-American Frontiers of Engineering Symposium*, Bethesda, Maryland, USA, March 1-3.

[8] Gao, P., Zhang, K., Zhang, B., Jiang, S., Zhang, B. (2011). Microstructures and high temperature mechanical properties of electron beam welded Inconel 718 superalloy thick plate. *Transactions of Nonferrous Metals Society of China*, *21*, 315-322.

[9] Odabaşı, A., Ünlü, N., Göller, G., Eruslu, M. N. (2010). A Study on Laser Beam Welding (LBW) Technique: Effect of Heat Input on the Microstructural Evolution of Superalloy Inconel 718. *The Minerals, Metals & Materials Society and ASM International*, Vol. ***41A***, 2357-2365 doi:10.1007/s11661-010-0319-y.

[10] Davis, J. R. (1997). *Heat-Resistant Materials*, ASM Specialty Handbook.

[11] Zhang, S., and Zhao, D. (2013). *Aerospace Materials Handbook*, CRC Press, Taylor &Francis Group**.**

[12] Hassey, P. (2010). ATI Mission Critical Metallics Presentation, Retrieved from http://www.sec.gov/Archives/edgar/data/814250/000095012310110284/l41250exv99w1.htm

[13] Davis, J. R. (1998). *Metals Handbook Desk Edition*, Second Edition, ASM International.

[14] Geddes, B., Leon, H., Huang, X. (2010). *Superalloys: Alloying and Performance*, ASM International.

[15] Bhadeshia, H. K. D. H., (n.d)**.** Superalloys, University of Cambridge, Retrieved from http://www.msm.cam.ac.uk./phase-trans/2003/nickel.html

[16] Radavich, J. F., (1989). The Physical Metallurgy of Cast and Wrought Alloy 718, Superalloy 718-Metallurgy and Applications, Edited by E.A.Loria, P 229-240.

[17] Campo, E., Turco, C., Catena, V. (1985). The correlation between heat treatment, structure and mechanical characteristics in Inconel 718, *Metallurgical Science and Technology,* Vol.3[1], 16-21.

[18] Chamanfar, A., Sarrat, L., Jahazi, M., Asadi, M., Weck, A., Koul, A.K. (2013). Microstructural characteristics of forged and heat treated Inconel-718 disks, *Materials and Design, 52*, 791-800.

[19] Cao, X., Rivaux, B., Jahazi, M., Cuddy, J., Birur, A. (2009). Effect of pre- and post-weld heat treatment on metallurgical and tensile properties of Inconel 718 alloy butt joints welded using 4 kW Nd:YAG laser, *J Mater Sci, 44*, 4557–4571, doi: 10.1007/s10853-009-3691-5.

[20] Xin, Y., Xueming, H., Yixiong, W., Songnian, L., (2015). Precipitates in coarse-grained heat-affected zone of Ni-based 718 superalloy produced by tungsten inert gas welding, *Journal of Materials Processing Technology, 217*, 13-20.

[21] Kuo, C. M., Yang, Y. T., Bor, H. Y., Wei, C. N., Tai, C. C. (2008). Aging effects on the microstructure and creep behavior of Inconel 718 superalloy, *Materials Science and Engineering A 510-511*, 289-294.

[22] Url-1 <*http://www.specialmetals.com/products/inconelalloy718.php*>, date retrieved: 22.03.2014.

[23] Chandler, H. (2006). *Heat Treater's Guide-Practices and Procedures for Nonferrous Alloys*, ASM International.

[24] Klopp, W. D., (1995). Nickel Base Alloys:IN-718, Aerospace Structural Metals Handbook, USA.

[25] Muralidharan, B. G., Shankar, V., Gill, T. P. S. (1996). Weldability of Inconel 718- A Review, *Indira Gandhi Centre for Atomic Reseacrh Technical Report*, **IGC-175**, Kalpakkam, India.

[26] Agilan, M., Venkateswaran, T., Sivakumar, D., Pant, B. (2014). Effect of Heat Input on Microstructure and Mechnical Properties of Inconel-718 EB Welds, *Procedia Materials Science, 5,* 656-662.

[27] Hoppin, G. S., and Yount, R. E. (1969). Fusion Welding of Age-Hardenable Superalloys, *International Automotive Engineering Congress*, Detroit, Michigan, USA.

[28] Vincent, R. (1985). Precipitation Around Welds In The Nickel-Base Superalloy, Inconel 718, *Acta Metallurgica,* Vol. ***33***, No.7, pp. 1205-1216.

[29] Kang, S. H., Deguchi, Y., Yamamoto, K., Ogi, K., Shirai, M. (2004). Solidification Process and Behavior of Alloying Elements in Ni-Based Superalloy Inconel718, *Materials Transections*, Vol. ***45***, No. 8, pp. 2728-2733.

[30] Radhakrishna, C. H., and Rao, K. (1997). The formation and control of Laves phase in superalloy 718 welds, *Journal of Materials Science*, *32,* 1977-1984.

[31] Murata, Y., Morinaga, M., Yukawa, N., Ogawa, H., Kato, M. (1994). Solidification Structures of Inconel 718 With Microalloying Elements, Superalloys 718, 625, 706 and Various Derivatives, Edited by E.A Loria, P 81-88.

[32] Tanner, D. W. J. (2009). Life Assessment of Welded Inconel 718 At High Temperature (Doctoral Dissertation), The University of Nottingham, England.

[33] Paul, J. (2014). Casting, Forming, Welding. Indian Institute of Technology, Kharagpur, India.

[34] Wang, Q., Sun, D. L., Na, Y., Zhou, Y., Han, X. L., Wang, J. (2011). Effects of TIG Welding Parameters on Morphology and Mechanical Properties of Welded Joint of Ni-base Superalloy, *Procedia Engineering*, 10, pp. 37-41.

[35] Kou, S. (2003). *Welding Metallurgy, Second Edition*, Wiley-Interscience, A John Wiley & Sons, Inc., Publication.

[36] Jeffus, L., (1999). *The Essential Welder: Gas Tungsten Metal Arc Welding*, pp.1-3, 1st edition, December 15, 1999**.**

[37] Hussain, K. A., Lateef, A., Javed, M., Pramesh, T. (2010). Influence of Welding Speed on Tensile Strength of Welded Joint in TIG Welding Process, International Journal of Applied Engineering Research, Volume. ***1***, No. 3, pp. 518-527.

[38] Sicard, P., and Levine, M. (1988). "*An approach to an expert robot welding system*", IEEE Transactions

[39] Url-2 <*http:// www.globalspec.com/learnmore/test_measurement/ nondestructive_test_equipment/ndt_supplies_accessories*>, date retrieved: 01.02.2015.

[40] Liu, A. F. (2005). *Mechnanics and Mechanisms of Fracture: An Introduction***,** ASM International, chapter 2.

[41] Ram, G. D. J., Reddy, A.. V., Rao, K. P., Reddy, G. M., Sundar J. K. S. (2005). Microstructure and Tensile Properties of Inconel 718 Pulsed Nd-YAG Laser Welds, *Journal of Materials Processing Technology*, *167*, 73-82.

APPENDICES

APPENDIX A : Hardness distribution of welded specimens in different PWHT cycles.

APPENDIX B : Weld macrostructures after tensile testing.

APPENDIX A

Table A.1: Hardness distribution of welded specimens subjected no PWHT **a)** thickness : 2mm **b)** thickness : 3,2mm.

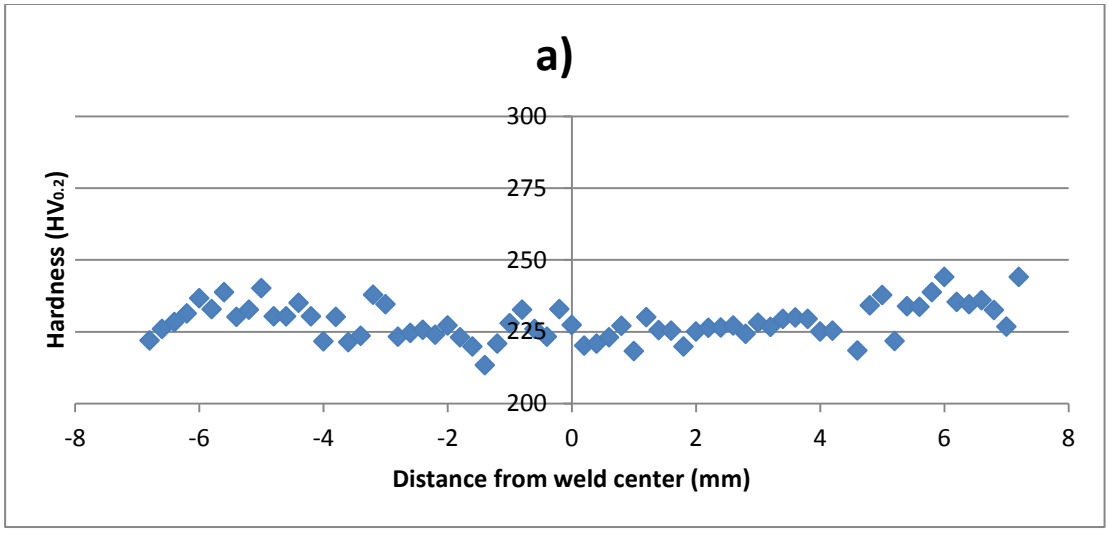

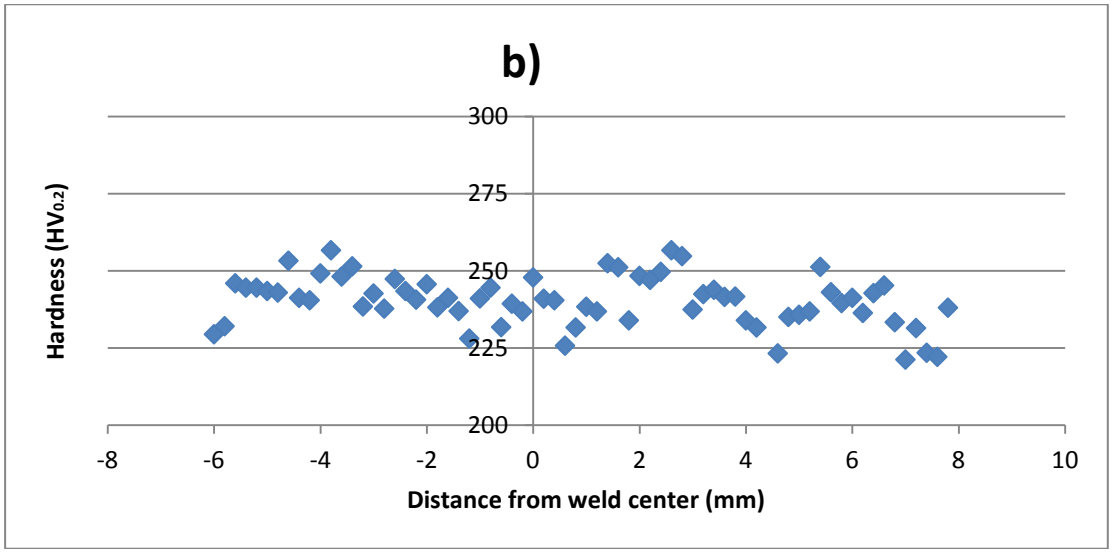

Table A.2 : Hardness distribution of welded specimens subjected to post weld solution+aging heat treatment **a)** thickness : 2 mm **b)** thickness : 3,2 mm.

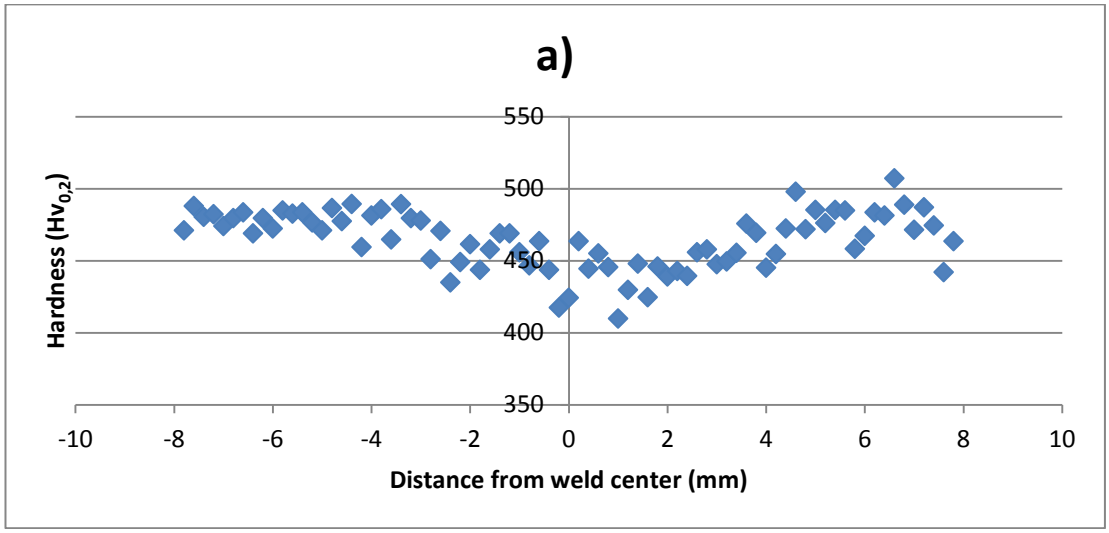

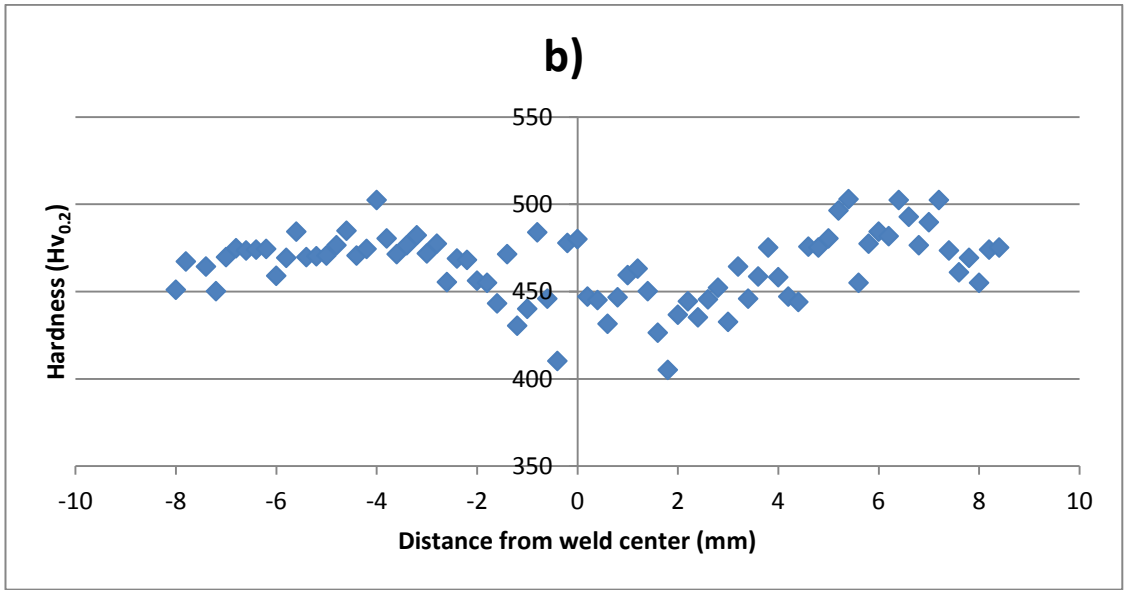

Table A.3 : Hardness distribution of welded specimens subjected to post weld direct aging heat treatment **a)** thickness : 2 mm **b)** thickness : 3,2 mm.

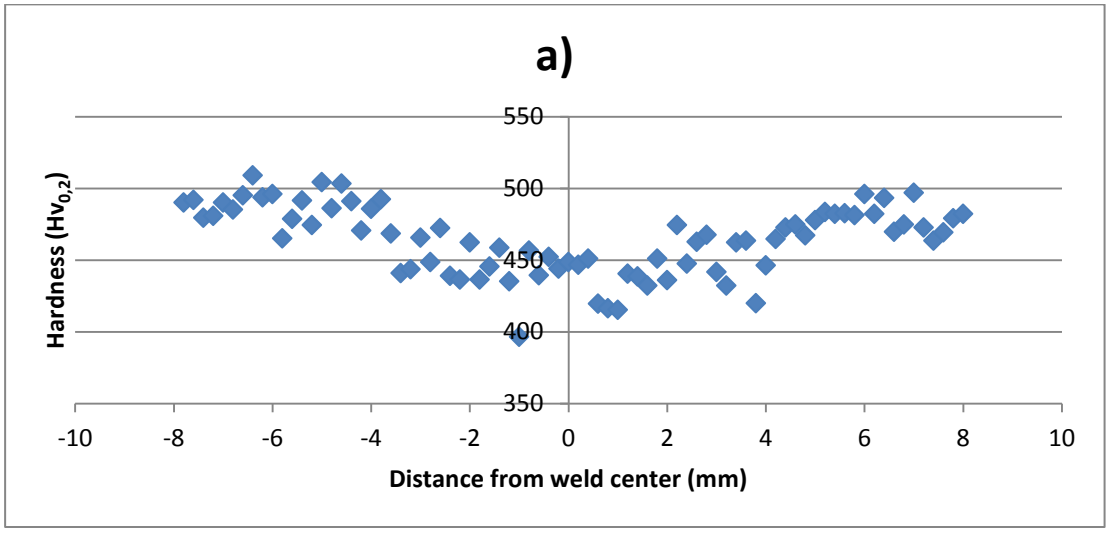

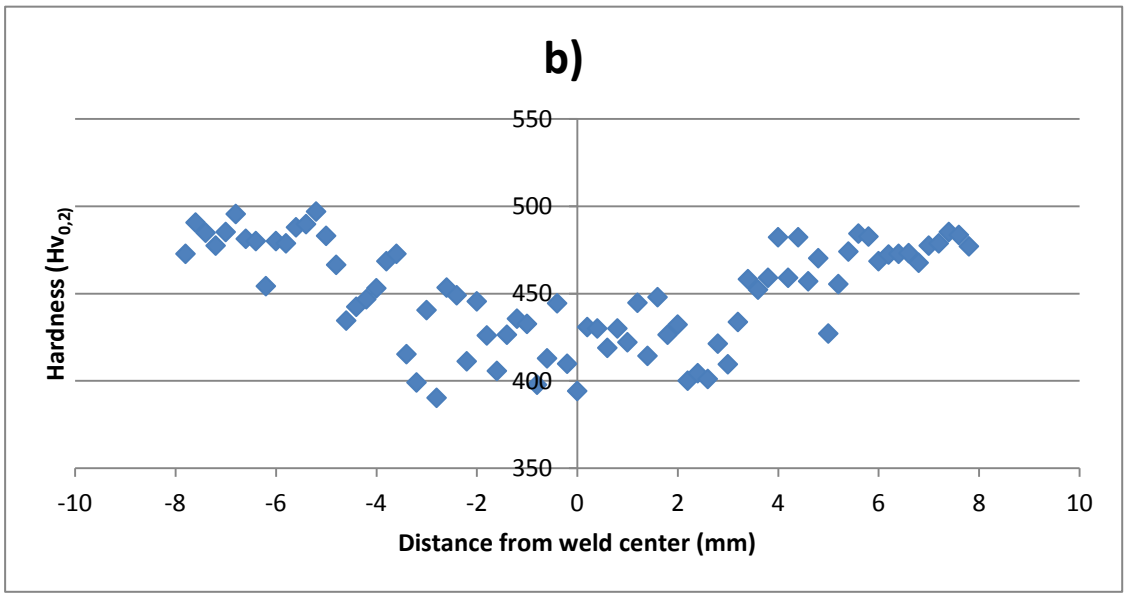

APPENDIX B

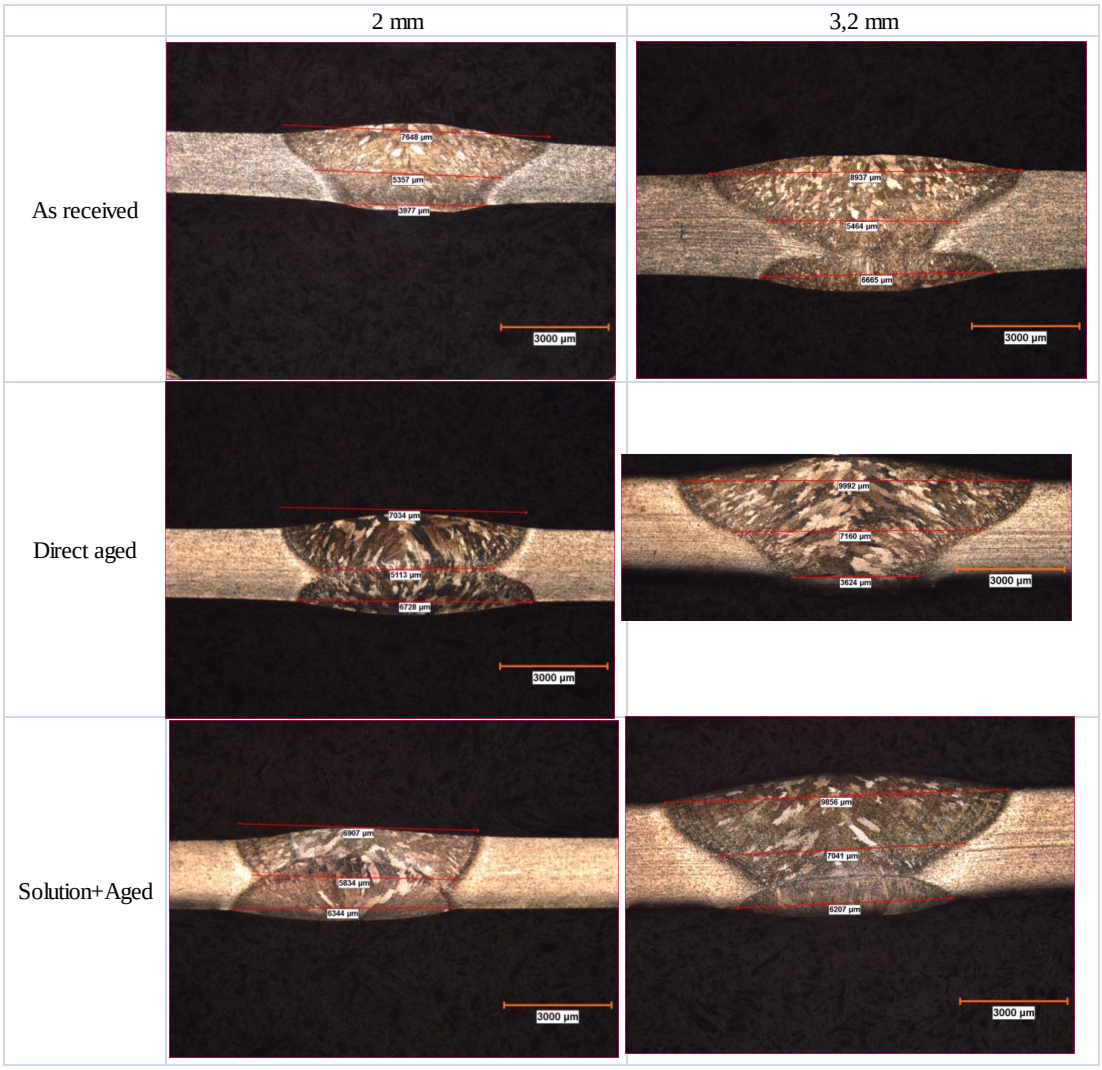

Figure B.1 : Weld macrostructures after tensile testing.

CURRICULUM VITAE

Name Surname: Ece Canan KOŞMAZ

Place and Date of Birth: İstanbul- 29.10.1990

E-Mail: ecekosmaz@hotmail.com

B.Sc.: ITU- Metallurgical and Materials Engineering